https://www.mdc-berlin.de/de/veroeffentlichungstypen/clinical-journal-club

Als gemeinsame Einrichtung von MDC und Charité fördert das Experimental and Clinical Research Center die Zusammenarbeit zwischen Grundlagenwissenschaftlern und klinischen Forschern. Hier werden neue Ansätze für Diagnose, Prävention und Therapie von Herz-Kreislauf- und Stoffwechselerkrankungen, Krebs sowie neurologischen Erkrankungen entwickelt und zeitnah am Patienten eingesetzt. Sie sind eingeladen, uns beizutreten. Bewerben Sie sich!

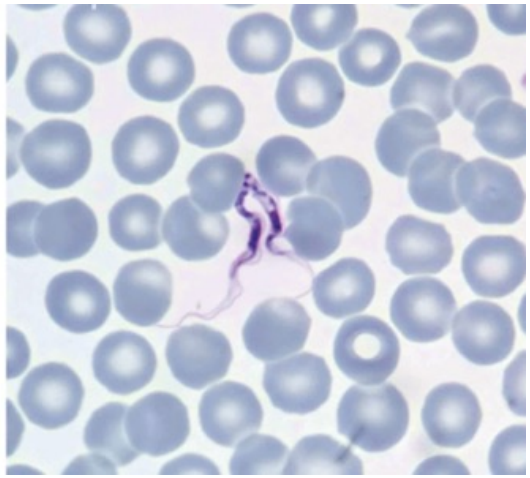

A 34-year-old man presented to the emergency department a week after returning from a safari in Zimbabwe with a 4-day history of fever and generalized weakness. On physical examination, a crusted, tender lesion on the crown of the head was noted. The parietal scalp was shaved with the patient's permission, revealing a 4 cm by 4 cm ulceration. A peripheral-blood smear is also shown. What is the most likely diagnosis?

→

Cutaneous leishmaniasis
Loaiasis
Mansonellosis
Onchocerciasis
Trypanosomiasis

Als Wächterlymphknoten
bezeichnet man die im Lymphabflussgebiet
eines Primärtumors liegenden Lymphknoten, die im Falle
einer lymphogenen Metastasierung zuerst betroffen sind. Die
Identifikation und Entfernung der Wächterlymphknoten hat
sich im Rahmen des operativen Tumormanagements
des Mammakarzinoms, des malignen Melanoms und
des Prostatakarzinoms etabliert. Bei Tumorfreiheit der
Wächterlymphknoten kann auf eine Tumorfreiheit der
nachgeschalteten Lymphknotenstationen geschlossen und auf
eine ausgedehnte Lymphonodektomie verzichtet werden.
Aus diesem Grunde werden die
Wächterlymphknoten präoperativ durch radioaktive Tracer
(i.d.R. Technetium) markiert, die intra- oder subkutan in das
Lymphabstromgebiet des Primärtumors injiziert werden. Diese
können mittels Gamma-Kamera (Wächterlymphknoten-
Szintigraphie) oder einer intraoperativ einsetzbaren Gamma-
Sonde detektiert werden.

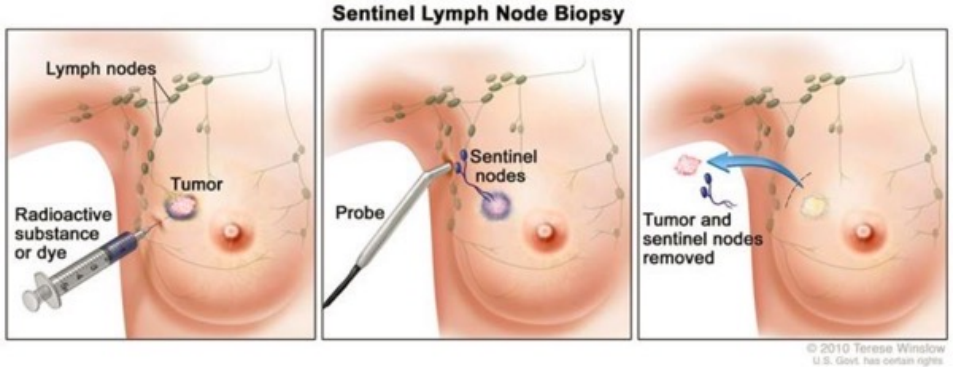

Sentinel-Lymph-Node Biopsy Alone or with Lymphadenectomy in Cervical Cancer

Limited data are available on survival outcomes after sentinel-lymph-node biopsy alone as compared with lymphadenectomy in cervical cancer.

In this multicenter, randomized, noninferiority trial, we enrolled patients with cervical cancer that was stage IA1 (with lymphovascular invasion), IA2, IB1, or IIA1 according to 2009 International Federation of Gynecology and Obstetrics criteria. Sentinel-lymph-node biopsy was performed at the time of surgery and was followed by examination of frozen sections. Patients who had negative sentinel lymph nodes were intraoperatively assigned in a 1:1 ratio not to undergo pelvic lymphadenectomy (the biopsy-only group) or to undergo lymphadenectomy (the lymphadenectomy group). All the patients underwent hysterectomy, and adjuvant therapy was provided according to a unified protocol. The primary end point was disease-free survival at 3 years, with a prespecified noninferiority margin of 5 percentage points in the upper limit of the confidence interval for the difference between the lymphadenectomy group and the biopsy-only group. Secondary end points included retroperitoneal nodal recurrence, cancer-specific survival, and surgical complications.

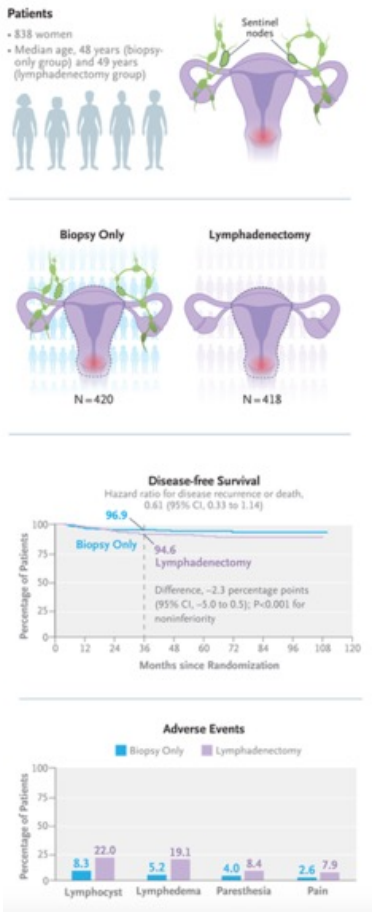

Despite its century-long application, pelvic lymphadenectomy has inherent limitations. It prolongs operative duration and carries risks, including vascular and neural injury, lymphedema, lymphocyst, venous thromboembolism, and surgery-related death. Furthermore, lymphadenectomy may be overtreatment, because the majority of early-stage cases are free of node metastasis. Dissecting nonmetastatic nodes offers no clear therapeutic benefit and may compromise the anatomical foundation for immunosurveillance.

Sentinel-lymph-node biopsy is a less invasive approach aimed at precisely dissecting the nodes that carry the highest risk of metastasis. The use of sentinel-lymph-node biopsy allows for the omission of extensive lymphadenectomy when sentinel lymph nodes are normal, which reduces complications from surgery. Over the past decades, numerous studies have validated the diagnostic accuracy of sentinel-lymph-node biopsy in cervical cancer. Favorable prognoses and decreased complications were also observed in patients exempted from lymphadenectomy after sentinel-lymph-node biopsy.

Inclusion and Exclusion Criteria

Eligible participants were women 18 to 65 years of age with histologically confirmed squamous-cell carcinoma, adenocarcinoma, or adenosquamous carcinoma that was classified as stage IA1 (with lymphovascular invasion), IA2, IB1, or IIA1 according to the International Federation of Gynecology and Obstetrics (FIGO) 2009 criteria.

Randomization and Treatment Procedures

All the patients underwent sentinel-lymph-node mapping at the time of surgery without restrictions on tracers or surgical approaches. Patients who had no sentinel lymph nodes detected or who had nodes that were obviously metastatic were excluded at screening and did not undergo randomization. All harvested sentinel lymph nodes were subjected to frozen-section assessment, with at least two different levels examined per node; subsequently, patients were assigned to the PHENIX-I (node-negative) cohort or the PHENIX-II (node-positive) cohort according to sentinel-lymph-node status. We report here the results for the PHENIX-I cohort only. In each cohort, patients were intraoperatively assigned in a 1:1 ratio to omit lymphadenectomy (the biopsy-only group) or to undergo bilateral pelvic lymphadenectomy (the lymphadenectomy group). Side-specific lymphadenectomy was performed in the case of unilateral sentinel-lymph-node detection. All the patients underwent radical hysterectomy, except for those with stage IA1 cancer, who underwent simple hysterectomy. Paraaortic lymphadenectomy was not required, and preservation of ovaries was optional.

End Points

The primary end point was 3-year disease-free survival, which was defined as survival free from disease recurrence or death from cervical cancer. Key secondary end points were retroperitoneal nodal recurrence and cancer-specific survival.

Characteristic	Biopsy Only (N=420)	Lymphadenectomy (N=418)
Age		
Median — yr	48	49
<50 yr — no. (%)	224 (53.3)	226 (54.1)
≥50 yr — no. (%)	196 (46.7)	192 (45.9)
ECOG performance-status score — no. (%)†		
0	397 (94.5)	392 (93.8)
1	23 (5.5)	26 (6.2)
Body-mass index‡	23.4±3.0	23.3±3.2
Histologic type — no. (%)		
Squamous-cell carcinoma	307 (73.1)	303 (72.5)
Adenocarcinoma	99 (23.6)	102 (24.4)
Adenosquamous carcinoma	9 (2.1)	8 (1.9)
Other§	5 (1.2)	5 (1.2)
Histologic grade — no. (%)		
G1	34 (8.1)	40 (9.6)
G2	197 (46.9)	192 (45.9)
G3	124 (29.5)	121 (28.9)
Not assessable	65 (15.5)	65 (15.6)
FIGO 2009 stage — no. (%)¶		
IA1 with LVSI	2 (0.5)	3 (0.7)
IA2	18 (4.3)	24 (5.7)
IB1	355 (84.5)	346 (82.8)
IIA1	45 (10.7)	45 (10.8)
Tumor size — no. (%)‖		
<2 cm	252 (60.0)	246 (58.9)
≥2 cm	168 (40.0)	172 (41.1)
Tracer type — no. (%)		
Methylene blue	355 (84.5)	357 (85.4)
Indocyanine green	62 (14.8)	58 (13.9)
Nanocarbon	3 (0.7)	3 (0.7)
Surgical approach — no. (%)		
Open	157 (37.4)	165 (39.5)
Laparoscopic	263 (62.6)	253 (60.5)
Preservation of ovaries — no. (%)		
Yes	141 (33.6)	136 (32.5)
No	279 (66.4)	282 (67.5)

Event	Intention-to-Treat Population		Per-Protocol Population	
	Biopsy Only (N=420)	Lymphadenectomy (N=418)	Biopsy Only (N=389)	Lymphadenectomy (N=394)
	number (percent)			
Recurrence*				
Any	16 (3.8)	26 (6.2)	10 (2.6)	21 (5.3)
Vaginal stump	7 (1.7)	4 (1.0)	5 (1.3)	4 (1.0)
Retroperitoneal nodal	0	9 (2.2)	0	8 (2.0)
Pelvic	0	3 (0.7)	0	2 (0.5)
Paraaortic	0	1 (0.2)	0	1 (0.3)
Both	0	5 (1.2)	0	5 (1.3)
Pelvic, non–vaginal stump	0	10 (2.4)	0	9 (2.3)
Abdominal	0	3 (0.7)	0	3 (0.8)
Distant site	9 (2.1)	17 (4.1)	5 (1.3)	14 (3.6)
Multiple sites†	0	10 (2.4)	0	10 (2.5)
Data missing	0	1 (0.2)	0	1 (0.3)
Death from cervical cancer	6 (1.4)	16 (3.8)	4 (1.0)	12 (3.0)
Death from other causes‡	3 (0.7)	1 (0.2)	3 (0.8)	1 (0.3)
Death from any cause	9 (2.1)	17 (4.1)	7 (1.8)	13 (3.3)

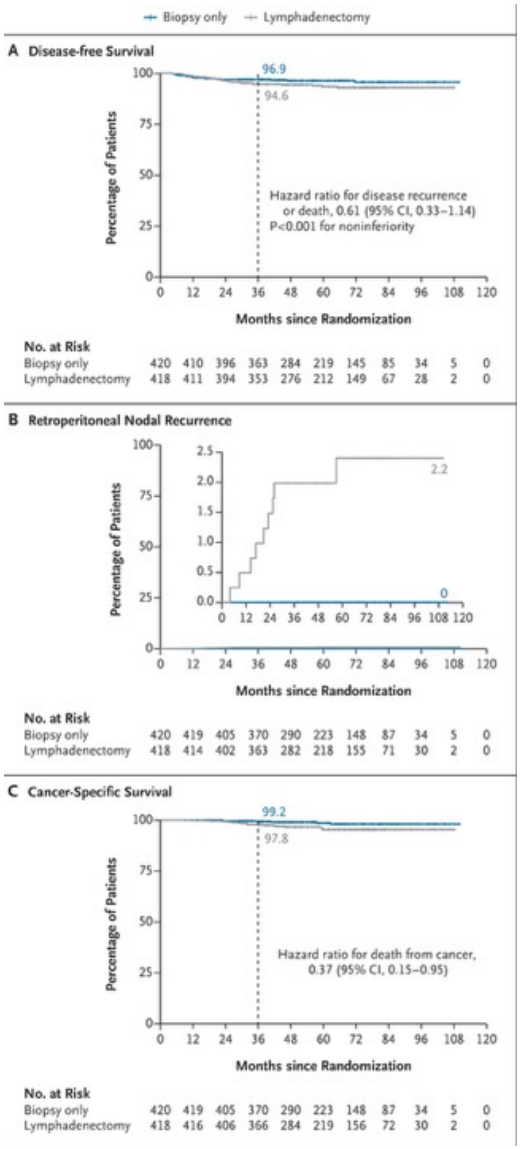

Event	Biopsy Only (N=420)	Lymphadenectomy (N=418)	P Value
	number (percent)		
Any adverse event	244 (58.1)	298 (71.3)	<0.001
Fever	62 (14.8)	78 (18.7)	0.13
Pain	11 (2.6)	33 (7.9)	0.001
Infection†	18 (4.3)	31 (7.4)	0.05
Anemia	68 (16.2)	64 (15.3)	0.73
Hypoalbuminemia	27 (6.4)	54 (12.9)	0.001
Lymphocyst‡	35 (8.3)	92 (22.0)	<0.001
Lymphedema§	22 (5.2)	80 (19.1)	<0.001
Paresthesia§	17 (4.0)	35 (8.4)	0.009
Urinary retention§	31 (7.4)	32 (7.7)	0.88
Urinary incontinence§	20 (4.8)	16 (3.8)	0.51
Constipation§	34 (8.1)	34 (8.1)	0.98
Deep-vein thrombosis‡	10 (2.4)	15 (3.6)	0.30
Intestinal obstruction¶	6 (1.4)	11 (2.6)	0.22
Ureteral fistula¶	6 (1.4)	2 (0.5)	0.29
Ureterectasis‡	1 (0.2)	7 (1.7)	0.04
Myocardial infarction¶	0	1 (0.2)	0.50
Atrial fibrillation¶	1 (0.2)	0	1.00
Vault bleeding¶	2 (0.5)	0	0.50
Vault rupture¶	0	1 (0.2)	0.50

Subgroup	No. of Patients	Biopsy Only	Lymphadenectomy
		no. of patients with events/total no.	
Overall	838	16/420	26/418
Body-mass index			
<25	617	13/311	18/306
≥25	221	3/109	8/112
FIGO 2009 stage			
IA1–IB1	748	13/375	23/373
IIA1	90	3/45	3/45
Pathological type			
Squamous-cell carcinoma	610	7/307	15/303
Nonsquamous-cell carcinoma	228	9/113	11/115
Histologic grade			
1 or 2	463	8/231	11/232
3 or not assessable	375	8/189	15/186
Tumor size at baseline			
<2 cm	501	8/253	15/248
≥2 cm	337	8/167	11/170
Tumor size after surgery			
<2 cm	505	9/254	15/251
≥2 cm	333	7/166	11/167
Surgical approach			
Open	322	8/157	7/165
Laparoscopic	516	8/263	19/253
Sensitivity analysis			
Bilateral mapping	694	13/354	23/340
No protocol violations or deviations	699	6/333	20/366
No adjuvant radiotherapy	555	9/274	10/281

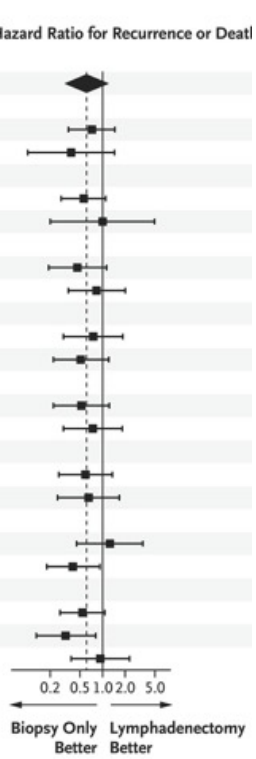

Subgroup Analyses of the Primary End Point.

All prespecified subgroup analyses were conducted in the intention-to-treat population with univariate Cox proportional-hazards models. The vertical dashed line indicates the hazard ratio for the overall population. Sensitivity analyses were conducted in patients with bilateral sentinel-lymph-node detection (bilateral mapping), in patients without protocol violations or deviations, and in patients who did not receive adjuvant radiotherapy. Body-mass index is the weight in kilograms divided by the square of the height in meters. FIGO denotes International Federation of Gynecology and Obstetrics.

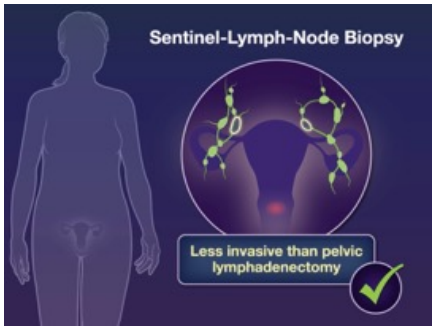
Sentinel-Lymph-Node Biopsy
Less invasive than pelvic lymphadenectomy

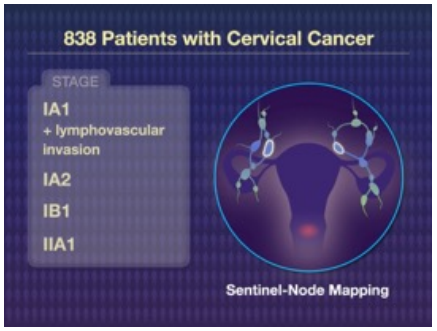
838 Patients with Cervical Cancer
STAGE
IA1
+ lymphovascular invasion
IA2
IB1
IIA1
Sentinel-Node Mapping

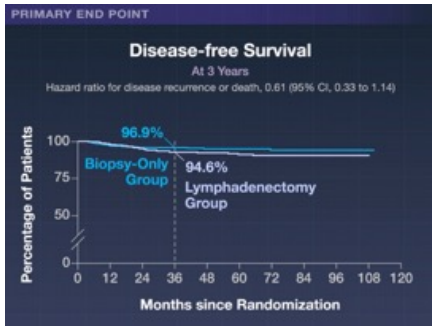
PRIMARY END POINT
Disease-free Survival
At 3 Years
Hazard ratio for disease recurrence or death, 0.61 (95% CI, 0.33 to 1.14)
96.9%
Biopsy-Only Group
94.6%
Lymphadenectomy Group
Percentage of Patients
Months since Randomization

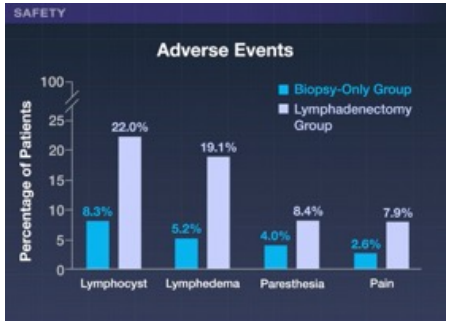
SAFETY
Adverse Events
Biopsy-Only Group
Lymphadenectomy Group
Percentage of Patients
8.3%
22.0%
5.2%
19.1%
4.0%
8.4%
2.6%
7.9%
Lymphocyst
Lymphedema
Paresthesia
Pain

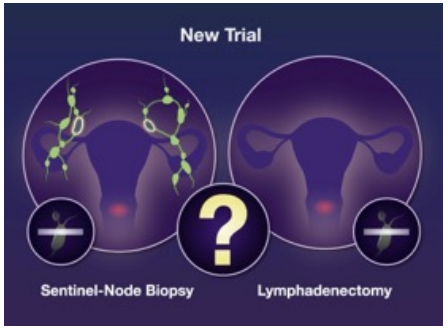
New Trial
Sentinel-Node Biopsy
Lymphadenectomy

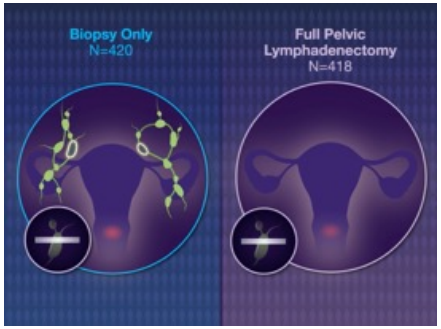
Biopsy Only
N=420
Full Pelvic Lymphadenectomy
N=418

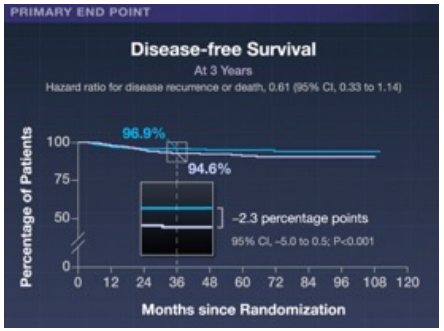
PRIMARY END POINT
Disease-free Survival
At 3 Years
Hazard ratio for disease recurrence or death, 0.61 (95% CI, 0.33 to 1.14)
96.9%
94.6%
–2.3 percentage points
95% CI, –5.0 to 0.5; P<0.001
Percentage of Patients
Months since Randomization

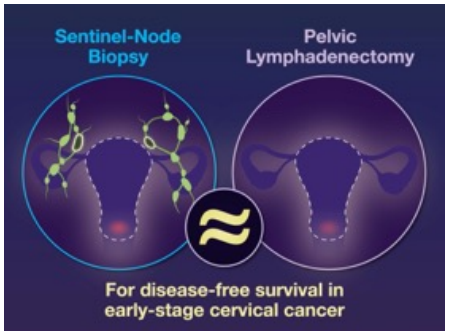
Sentinel-Node Biopsy
Pelvic Lymphadenectomy
For disease-free survival in early-stage cervical cancer

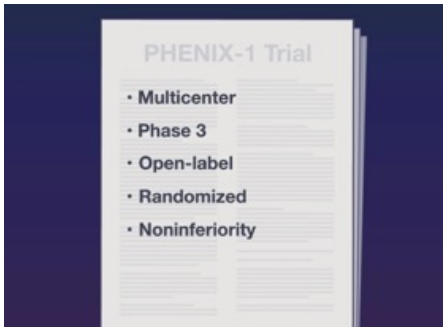
PHENIX-1 Trial
• Multicenter
• Phase 3
• Open-label
• Randomized
• Noninferiority

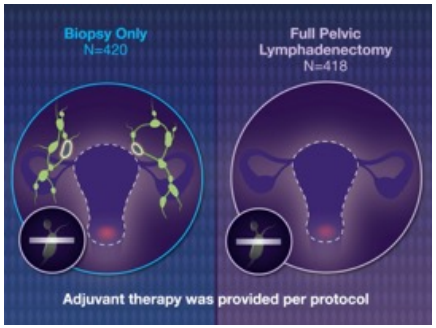
Biopsy Only
N=420
Full Pelvic Lymphadenectomy
N=418
Adjuvant therapy was provided per protocol

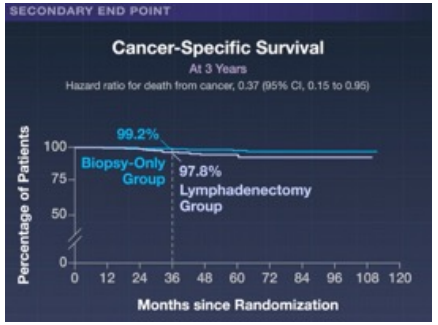
SECONDARY END POINT
Cancer-Specific Survival
At 3 Years
Hazard ratio for death from cancer, 0.37 (95% CI, 0.15 to 0.95)
99.2%
Biopsy-Only Group
97.8%
Lymphadenectomy Group
Percentage of Patients
Months since Randomization

Telitacicept ist ein Medikament zur Behandlung verschiedener Autoimmunerkrankungen, das bereits in China für systemischen Lupus erythematodes (SLE) zugelassen ist. Es handelt sich um ein Fusionsprotein, das die Proteine BLyS und APRIL hemmt und dadurch B-Zellen-Reaktionen unterdrückt. Es wird auch in klinischen Studien für andere Krankheiten wie rheumatoide Arthritis und Myasthenia gravis untersucht und hat bei IgA-Nephropathie positive Ergebnisse gezeigt.

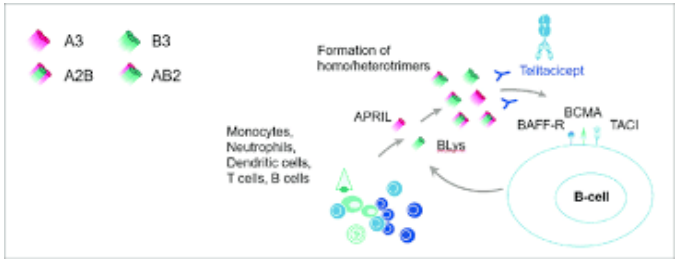

Wirkungsweise

- Telitacicept ist ein Fusionsprotein, das die Funktionen der beiden Proteine B-Lymphozyten-Stimulator (BLyS) und APRIL (a proliferation-inducing ligand) blockiert.
- Es bindet an die Liganden BLyS und APRIL, wodurch die Zell-Zell-Interaktion mit deren Rezeptoren auf der Zelloberfläche unterbrochen wird.
- Diese Blockade hemmt die Proliferation und Reifung von B-Lymphozyten und unterdrückt so die Immunantwort.

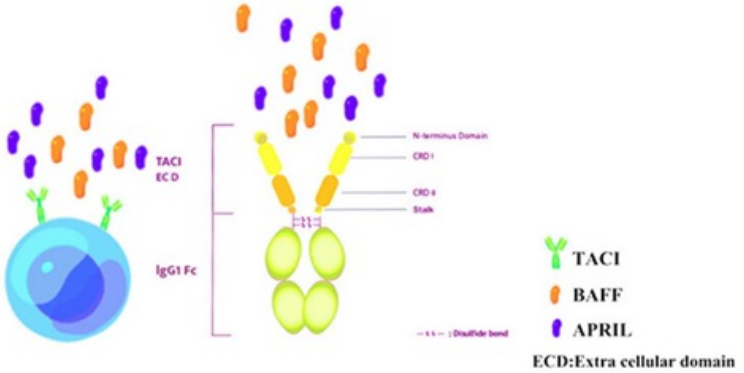

A Phase 3 Trial of Telitacicept for Systemic Lupus Erythematosus

Telitacicept, a new dual inhibitor of the cytokines B-lymphocyte stimulator (BLyS) and APRIL (a proliferation-inducing ligand), showed efficacy in adults with active systemic lupus erythematosus (SLE) in a phase 2b trial when added to standard therapy.

We conducted a phase 3 trial in China in which participants with active SLE were randomly assigned (in a 1:1 ratio) to receive telitacicept (160 mg) or placebo subcutaneously once weekly for 52 weeks, in addition to standard therapy. The primary end point at week 52 was a response on the modified SLE Responder Index 4 (SRI-4), with a response on this composite measure defined as a reduction of at least 4 points in the Safety of Estrogens in Lupus Erythematosus National Assessment–Systemic Lupus Erythematosus Disease Activity Index (SELENA-SLEDAI) score (ranging from 0 to 105, with higher scores indicating greater disease activity), no new disease activity as measured on the British Isles Lupus Assessment Group index, and no worsening in the Physician's Global Assessment score.

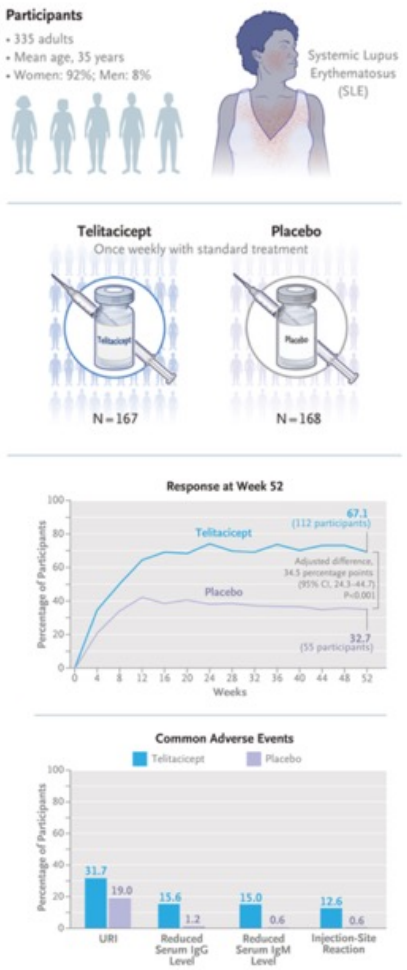

B lymphocytes play a central role in the pathogenesis of SLE. B-lymphocyte stimulator (BLyS) is a key regulator of B-cell differentiation, maturation, function, and survival. Increased BLyS levels are observed in patients with autoimmune disorders, including SLE, and the relevance of this cytokine as a therapeutic target in patients with SLE was shown by successful trials of belimumab, a monoclonal antibody that binds and neutralizes BLyS. However, many patients with SLE do not have a response or have only a partial response to belimumab. The cytokine known as APRIL (a proliferation-inducing ligand) also affects differentiation and maturation of B lymphocytes, and levels of APRIL have been found to be higher in patients with SLE than in patients with rheumatoid arthritis and healthy volunteers. The current trial tested the hypothesis that inhibition of both BLyS and APRIL may be a useful approach to treating SLE.

Telitacicept is a fusion protein of the IgG Fc fragment and the extracellular domain of the TACI (transmembrane activator and calcium-modulator and cyclophilin-ligand interactor) receptor that binds both BLyS and APRIL, inhibiting their interactions with several B-cell receptors. The pharmacokinetics and pharmacodynamics of telitacicept were studied in Chinese patients with SLE, and preliminary data suggested beneficial effects. A phase 2b trial showed efficacy and an acceptable side-effect profile at a range of doses. Here, we report efficacy and safety results of a phase 3 trial of telitacicept at a dose of 160 mg weekly as compared with placebo in Chinese persons with active SLE.

Randomization and Procedures

Eligible persons were randomly assigned in a 1:1 ratio to receive telitacicept (160 mg) or placebo subcutaneously, once weekly for 52 weeks, added to stable, standard therapy. Randomization was stratified according to baseline scores of 9 or less or more than 9 on the Safety of Estrogens in Lupus Erythematosus National Assessment–Systemic Lupus Erythematosus Disease Activity Index (SELENA-SLEDAI, a 24-item weighted lupus activity scale that ranges from 0 to 105, with higher scores indicating greater disease activity) and according to low or normal levels of complement C3, C4, or both.

Telitacicept and placebo were provided as freeze-dried powders (RemeGen), each administered as two injections once weekly on the same day. Each injection was 1 ml in volume and contained 80 mg of telitacicept or placebo.

End Points and Assessments

The primary efficacy end point at week 52 was a response on the modified SLE Responder Index 4 (SRI-4), with a response on this composite measure defined as a reduction of at least 4 points from baseline in the SELENA-SLEDAI score, no new disease activity as measured by an A (severe) score or more than one B (moderate) score on the British Isles Lupus Assessment Group (BILAG) index.

Characteristic	Telitacicept (N=167)	Placebo (N=168)
Female sex — no. (%)	152 (91.0)	157 (93.5)
Age — yr	34.8±9.8	35.1±10.4
Body-mass index	23.0±3.4	22.7±3.9
Duration of SLE disease — yr	7.5±5.5	7.2±5.3
SELENA-SLEDAI score†	11.5±3.1	11.5±3.6
BILAG, 1 A score or >1 B score — no. (%)‡	105 (62.9)	100 (59.5)
PGA score§	1.83±0.44	1.81±0.47
Renal lesions — no. (%)¶	108 (64.7)	102 (60.7)
Serum biomarkers		
Low level of C3, C4, or both — no. (%)	119 (71.3)	118 (70.2)
Positivity for antinuclear antibodies — no. (%)	160 (95.8)	165 (98.2)
Positivity for anti-dsDNA antibodies — no./total no. (%)	99/163 (60.7)	98/165 (59.4)
Urine protein level — g/24 hr	1.40±1.57	1.24±1.34
Quantitative classification of 24-hr urine protein level — no. (%)		
≤0.5 g	57 (34.1)	70 (41.7)
>0.5 g	110 (65.9)	98 (58.3)
Daily dose of glucocorticoid or prednisone equivalent — mg	15.2±11.1	13.9±10.5
Combination therapy — no. (%)		
Glucocorticoid + antimalarial agent	25 (15.0)	26 (15.5)
Glucocorticoid + immunosuppressive drug	23 (13.8)	24 (14.3)
Glucocorticoid + immunosuppressive drug + antimalarial agent	117 (70.1)	114 (67.9)

Secondary End Points at Week 52 (Full Analysis Population).

End Point	Telitacicept (N=167)	Placebo (N=168)	Difference (95% CI)
Percentage of participants with reduction of ≥4 points in SELENA-SLEDAI score	70.1	40.5	29.6 (13.1 to 46.1)
Mean change in SELENA-SLEDAI score (95% CI)†	−4.95 (−7.88 to −2.02)	−1.00 (−5.34 to 3.34)	−3.95 (−7.69 to −0.21)
Mean change in PGA score (95% CI)	−0.79 (−0.90 to −0.69)	−0.40 (−0.50 to −0.30)	−0.39 (−0.53 to −0.26)
Percentage of participants taking ≤7.5 mg/day of glucocorticoid or prednisone equivalent or with ≥25% reduction in glucocorticoid dose from baseline over wk 44 to 52	44.9	34.7	10.2 (2.0 to 22.5)
Daily dose of glucocorticoid or prednisone equivalent at wk 52 — mg‡	9.9±7.6	10.9±11.3	
Mean change in laboratory value — % (95% CI)			
IgG level	−24.05 (−29.47 to −18.63)	12.92 (7.15 to 18.69)	−36.97 (−44.30 to −29.65)
IgA level	−47.79 (−51.16 to −44.42)	3.75 (0.17 to 7.33)	−51.54 (−56.10 to −46.98)
IgM level	−55.27 (−59.51 to −51.04)	−0.06 (−4.57 to 4.45)	−55.21 (−60.93 to −49.49)
CD19+ B-cell count	−33.04 (−45.90 to −20.18)	−4.80 (−18.43 to 8.84)	−28.24 (−45.61 to −10.87)
C3 level	26.98 (16.06 to 37.90)	10.08 (−1.54 to 21.70)	16.90 (2.14 to 31.66)
C4 level	57.73 (43.96 to 71.50)	−0.01 (−14.67 to 14.65)	57.75 (39.13 to 76.36)

Adverse Events (Safety Population)

Event	Telitacicept (N=167)	Placebo (N=168)
	no. of participants (%)	
Any adverse event	153 (91.6)	142 (84.5)
Adverse event considered to be related to trial regimen†	125 (74.9)	84 (50.0)
Adverse events considered to be related to trial regimen that occurred in ≥5% of the participants in either group†		
Upper respiratory tract infection	53 (31.7)	32 (19.0)
Urinary tract infection	16 (9.6)	16 (9.5)
Lymphocyte count decreased‡	15 (9.0)	13 (7.7)
Blood IgG decreased‡	26 (15.6)	2 (1.2)
Blood IgM decreased‡	25 (15.0)	1 (0.6)
Injection-site reaction	21 (12.6)	1 (0.6)
White-cell count decreased‡	10 (6.0)	4 (2.4)
Immunoglobulins decreased‡	14 (8.4)	0
Blood IgA decreased‡	10 (6.0)	0
Adverse event leading to discontinuation from the trial	8 (4.8)	9 (5.4)
Serious adverse event	12 (7.2)	24 (14.3)
Serious adverse event considered to be related to trial regimen†§	2 (1.2)	4 (2.4)
Herpes zoster	1 (0.6)	1 (0.6)
Pneumonia	0	2 (1.2)
Upper respiratory tract infection	0	1 (0.6)
Gastroenteritis	0	1 (0.6)
Enteritis	1 (0.6)	0
Death	0	0

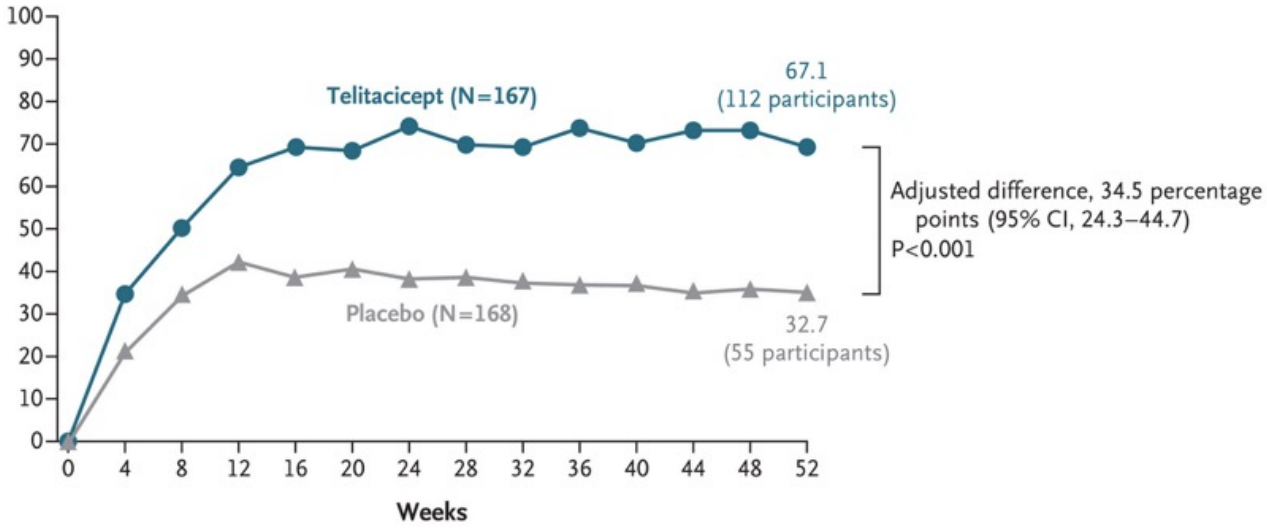

Response on the Modified SRI-4 over Time (Full Analysis Population).

A response on the modified SLE Responder Index 4 (SRI-4) was defined as a reduction of at least 4 points in the Safety of Estrogens in Lupus Erythematosus National Assessment–Systemic Lupus Erythematosus Disease Activity Index (SELENA-SLEDAI) score (ranging from 0 to 105, with higher scores indicating greater disease activity), no new disease activity as measured on the British Isles Lupus Assessment Group index, and no worsening in the Physician's Global Assessment score. Data after treatment failure and missing data were imputed as nonresponse. The between-group difference in incidence of response, 95% confidence interval (CI), and P value were obtained on the basis of a logistic-regression model, in combination with the bootstrap method, with trial group, baseline SELENA-SLEDAI score (≤9 vs. >9), and baseline complement level (low C3 or C4 [or both] vs. normal) as covariates. The full analysis population was defined as all the participants who had undergone randomization and received at least one dose of telitacicept or placebo.


Current Treatments
• Glucocorticoids
• Antimalarial agents
• Immunosuppressants
• Biologic agents


Telitacicept
Placebo
N=167
N=168
Once Weekly
52 Weeks
+
Standard therapy

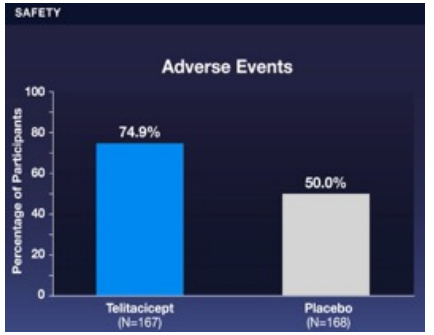
SAFETY
Adverse Events
Percentage of Participants
100
80
60
40
20
0
74.9%
50.0%
Telitacicept
(N=167)
Placebo
(N=168)

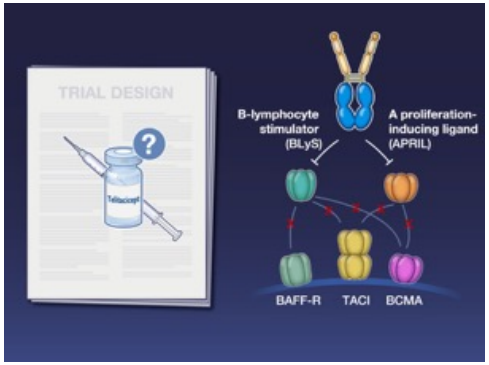
TRIAL DESIGN
B-lymphocyte stimulator (BLyS)
A proliferation-inducing ligand (APRIL)
BAFF-R
TACI
BCMA

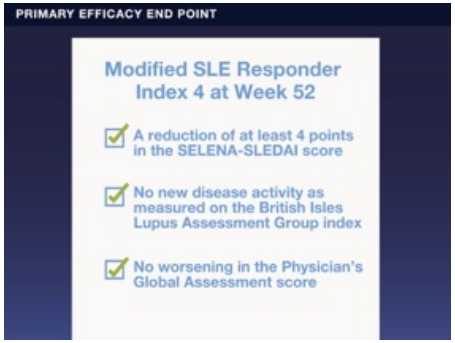
PRIMARY EFFICACY END POINT
Modified SLE Responder Index 4 at Week 52
A reduction of at least 4 points in the SELENA-SLEDAI score
No new disease activity as measured on the British Isles Lupus Assessment Group index
No worsening in the Physician's Global Assessment score

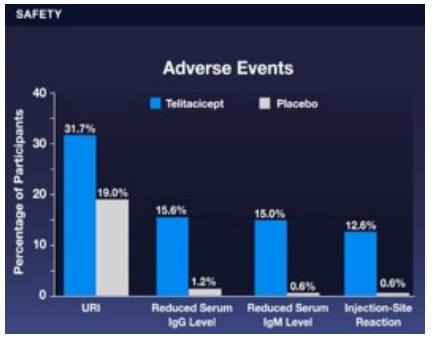
SAFETY
Adverse Events
Telitacicept
Placebo
Percentage of Participants
40
30
20
10
0
31.7%
19.0%
15.6%
1.2%
15.0%
0.6%
12.6%
0.6%
URI
Reduced Serum IgG Level
Reduced Serum IgM Level
Injection-Site Reaction


TRIAL DESIGN
• Phase 3
• Double-blind
• Randomized
• Controlled
• In China

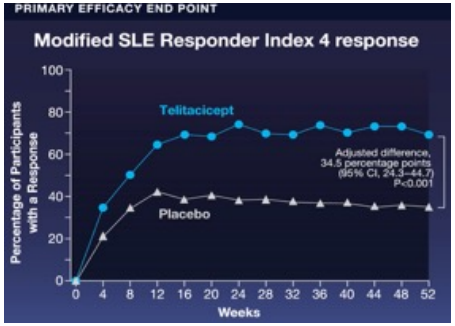
PRIMARY EFFICACY END POINT
Modified SLE Responder Index 4 response
Percentage of Participants with a Response
100
80
60
40
20
0
Telitacicept
Placebo
Adjusted difference, 34.5 percentage points (95% CI, 24.3–44.7) P<0.001
0
4
8
12
16
20
24
28
32
36
40
44
48
52
Weeks


Addition of telitacicept once weekly increased the likelihood of a clinical response at week 52

Die Adenosin-Desaminase (ADA) ist das Enzym, das die Umwandlung von Adenosin zu Inosin katalysiert.

Diese Reaktion ist Teil des Recyclings der Purinnukleotide in allen Lebewesen außer den Pflanzen. Beim Menschen kommt ADA in allen Geweben vor, besonders aber in T-Lymphozyten, wo sie, gebunden an DPP4 in den Zellkontakten zwischen Lymphozyt und Epithel lokalisiert ist und daher eine wichtige Rolle bei der Immunreaktion spielt.

Mutationen im ADA-Gen können zu ADA-Mangel und dieser zu einer angeborenen schweren Störung des Immunsystems (SCID) führen. Erhöhte Spiegel lassen sich in serösen Körperflüssigkeiten bei Infektionen mit Mycobakterien (z. B. bei Tuberkulose) als hoch sensitive Nachweismethode feststellen.

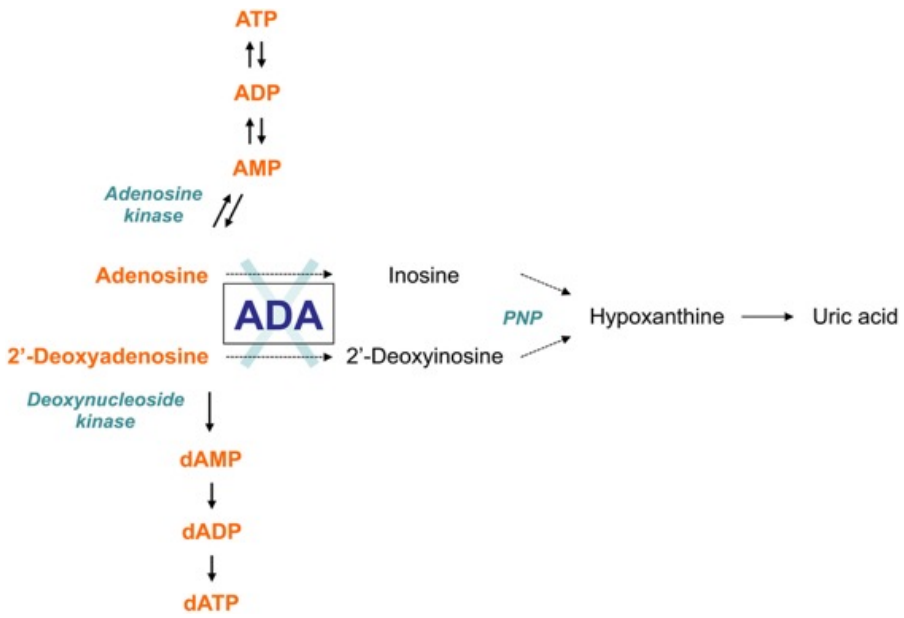

SCID steht für Schwerer kombinierter Immundefekt, eine Gruppe seltener angeborener Erkrankungen, die durch einen stark geschwächten oder fehlenden Immunschutz gekennzeichnet ist. Die Störung betrifft hauptsächlich die T-Zellen, was zu einer verminderten oder fehlenden Abwehr gegen Bakterien, Viren und Pilze führt. Ohne Behandlung verläuft SCID oft tödlich, weshalb ein frühes Screening bei Neugeborenen in Deutschland seit 2019 verfügbar ist. Eine weitere Bedeutung hat SCID in der Psychologie, wo es für das Strukturierte Klinische Interview für DSM-5®-Störungen steht.

Ein Mangel des Enzyms Adenosin-Desaminase (ADA) führt zu SCID, da die fehlende Funktion dieses Enzyms einen Purinstoffwechsel-Stau verursacht. Dies führt zur Akkumulation von schädlichen Stoffwechselprodukten, insbesondere Desoxyadenosintriphosphat (dATP). Hohe dATP-Konzentrationen hemmen die Ribonukleotid-Reduktase, was die DNA-Synthese stört. Dadurch können sich die Lymphozyten nicht teilen und entwickeln sich nicht richtig, was zu einem schweren kombinierten Immundefekt führt.

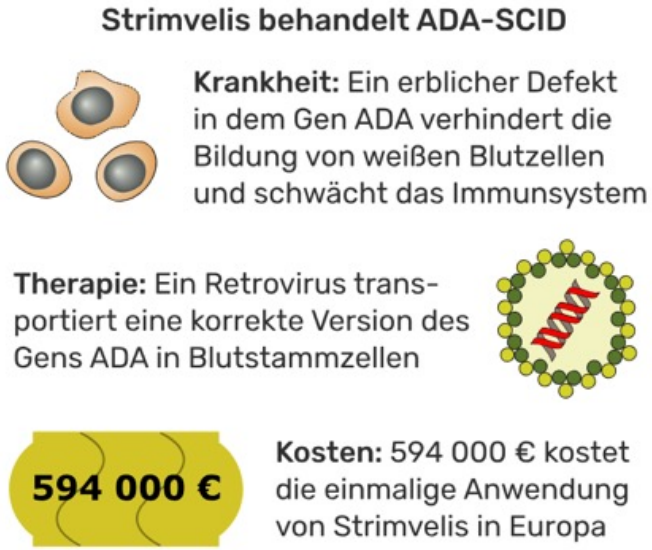

Long-Term Safety and Efficacy of Gene Therapy for Adenosine Deaminase Deficiency

Background

Severe combined immunodeficiency (SCID) due to adenosine deaminase (ADA) deficiency (ADA-SCID) is a life-threatening inborn error of immunity for which lentiviral gene therapy has been investigated in clinical trials.

Methods

Between 2012 and 2019, we treated patients who had ADA-SCID with busulfan nonmyeloablative conditioning followed by transplantation with autologous CD34+ hematopoietic stem cells transduced ex vivo with a lentiviral vector encoding human *ADA*. The primary efficacy end points were overall survival and event-free survival (defined as survival free from rescue allogeneic hematopoietic stem-cell transplantation, reinitiation of enzyme-replacement therapy, and additional gene therapy). Secondary end points included no receipt of immunoglobulin-replacement therapy, the presence of protective titers to tetanus or pneumococcal vaccines, and sustained discontinuation of fungal or viral prophylaxis. We now report the long-term results from this cohort representing 474 patient-years of follow-up, with a median follow-up of 7.5 years.

Conclusions

These long-term findings in a large patient cohort show the sustained clinical efficacy and safety of autologous CD34+ hematopoietic stem-cell lentiviral gene therapy for ADA-SCID, indicating that it is a curative treatment.

Ex vivo autologous hematopoietic stem-cell gene therapy has emerged as a safe and effective therapeutic approach for ADA-SCID and obviates the risks associated with alloreactivity and immune suppression. Long-term efficacy has been shown for γ-retroviral–mediated gene therapy for ADA-SCID, but insertional oncogenesis remains a risk, and T-cell leukemia was reported in one patient. In contrast to γ-retroviral vectors, third-generation self-inactivating lentiviral vectors have been engineered for improved safety through removal of transforming elements in the viral long terminal repeats (part of the lentivirus genome) to avoid transactivation of oncogenes. We therefore developed a self-inactivating lentiviral vector, EFS-ADA LV, and tested it in the treatment of children with ADA-SCID in nonrandomized, open-label, phase 1–2 clinical studies in the United States and the United Kingdom. We have previously reported the initial results of these studies with 24 to 36 months of follow-up of 50 pediatric patients with ADA-SCID, which showed 100% overall survival and more than 95% event-free survival. Here, we report comprehensive long-term follow-up efficacy and safety data for 62 patients with a minimum of 5 years of follow-up after gene therapy, representing 474 patient-years of follow-up.

Supplemental Table 1. Demographic characteristics of the patients

Characteristic	U.S. Study	U.K. Study
Sex – no. (%)		
Female	18 (55)	13 (45)
Male	15 (45)	16 (55)
Race – no. (%)*		
Asian	0	4 (14)
Black	2 (6)	8 (28)
Hispanic	6 (18)	1 (3)
White	19 (58)	16 (55)
Other	5 (15)	0 (0)
Unknown	2 (6)	0 (0)
Timeline		
Median age at diagnosis (range) - months	1 (0-36)	3 (0 - 25)
Median age at time of treatment (range) - months	10 (4-51)	14 (4-194)
Median follow-up (range) - years	8 (5-10)	7 (5-11)
Trigger for diagnosis¥		
Newborn screening	23 (70)	1 (3)
Positive family history	0 (0)	4 (14)
Parental consanguinity	0 (0)	6 (21)
Severe, recurrent or persistent infection	8 (24)	27 (93)
Failure to thrive	3 (9)	12 (41)
Cytopenias	2 (6)	17 (59)
Active infection during GT - no. (%)¥¥		
Bacterial†	0 (0)	7 (24)
Fungal	0 (0)	0 (0)
Viral≠	0 (0)	19 (66)
Type of cells — no. (%)		
Bone marrow	33 (100)	3 (10)
Mobilized leukapheresis	0 (0)	26 (90)
Formulation		
Fresh	19	19 (66)
Cryopreserved	12	19 (31)
Combined (fresh & cryopreserved)	2	1 (3)
No. of products infused (%)		
1	31 (94)	28 (97)
2	2 (6)	1 (3)
CD34+ cells infused per kilogram of body weight		
Median (x 10^6)	7.4	14
Range (x 10^6)	2.1 -11.4	4.5-38.9
Drug-product vector copy-number (copies/cell)		
Median	3.7	2.7
Range	1.56-6.53	0.5-13.3
Receipt of busulfan nonmyeloablative conditioning — no. (%)	33 (100)	29 (100)
Median AUC (range) - mg x h/L	Fresh 16.6 (9.6-16.3) Cryo 19.5 (16.3-21.7)	Fresh 19.2 (13.1-30.9) Cryo 22.3 (19.6-45.4)

* Race and ethnic group were reported by the patients or their guardians.
¥Note that patients could have had more than one diagnostic triggers.
¥¥Active infections per patient. Note that each patient could have had more than one active infection.
†Five patients with BCG disease/exposure on prophylaxis, and one with Clostridium difficile in stool.
≠ 2 patients with EBV viraemia, 1 with Adenoviraemia and 1 with CMV viraemia, the rest included respiratory viruses (Coronavirus, Rhino/Enterovirus, influenzae, parainfluenza or metapneumovirus on NPA or BAL) and stool viruses (Adenovirus, Norovirus, Rotavirus, Sapovirus). The US trial required treated patients to be free of active infections.

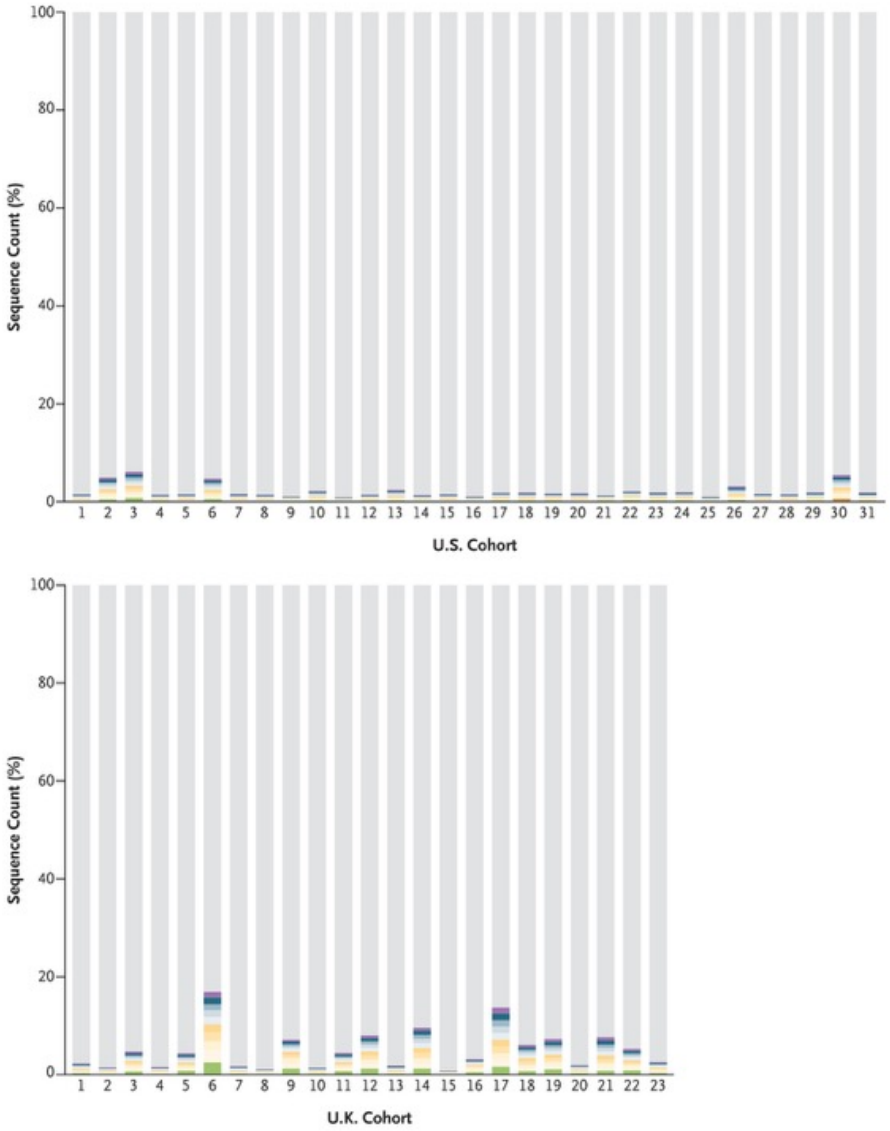

Vector Integration-Site Analysis.

The colored stacked bars represent the 10 most frequent integration sites in each sample; the gray areas represent all other detected integration sites. Vector integration-site assays were performed at a mean of 73 months (range, 24 to 120) after drug-product infusion. Additional details are provided in Figure S5 in the Supplementary Appendix.

Kaplan–Meier Curves for Event-free Survival.

Event-free survival was defined as survival free from rescue allogeneic hematopoietic stem-cell transplantation, reinitiation of enzyme-replacement therapy, or receipt of additional gene therapy. Tick marks indicate censored data.

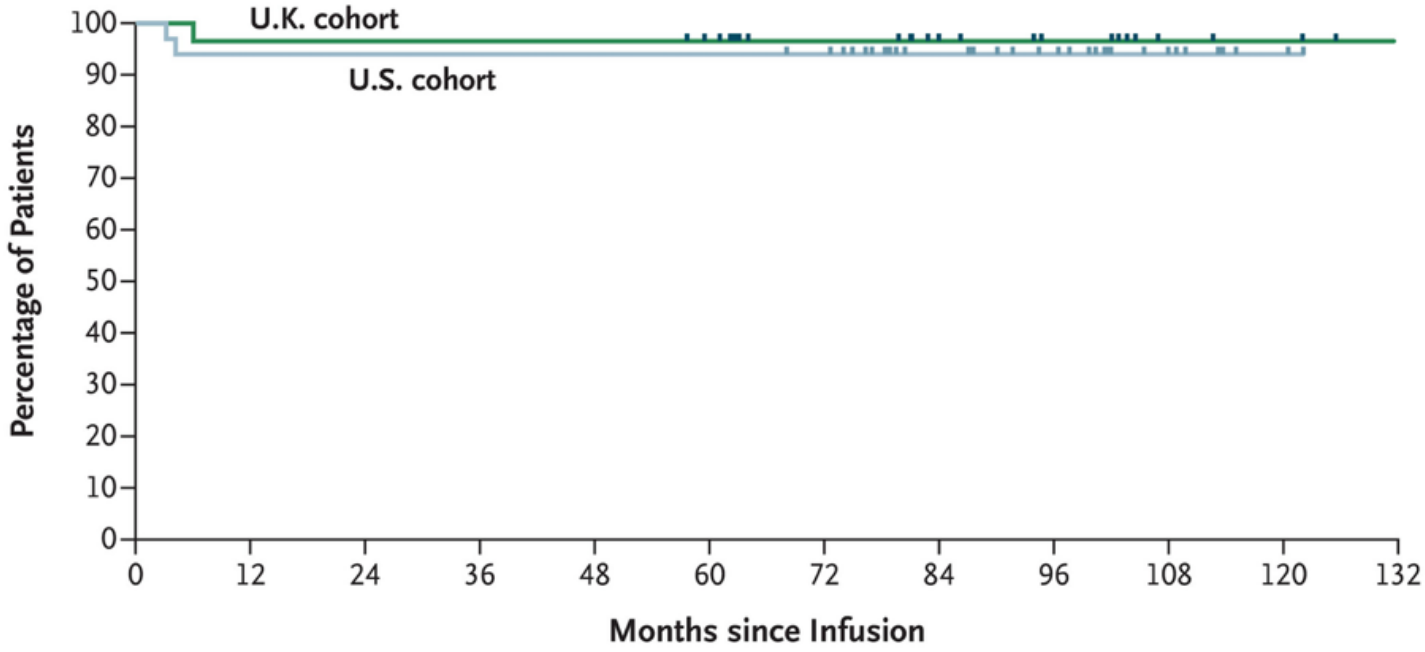

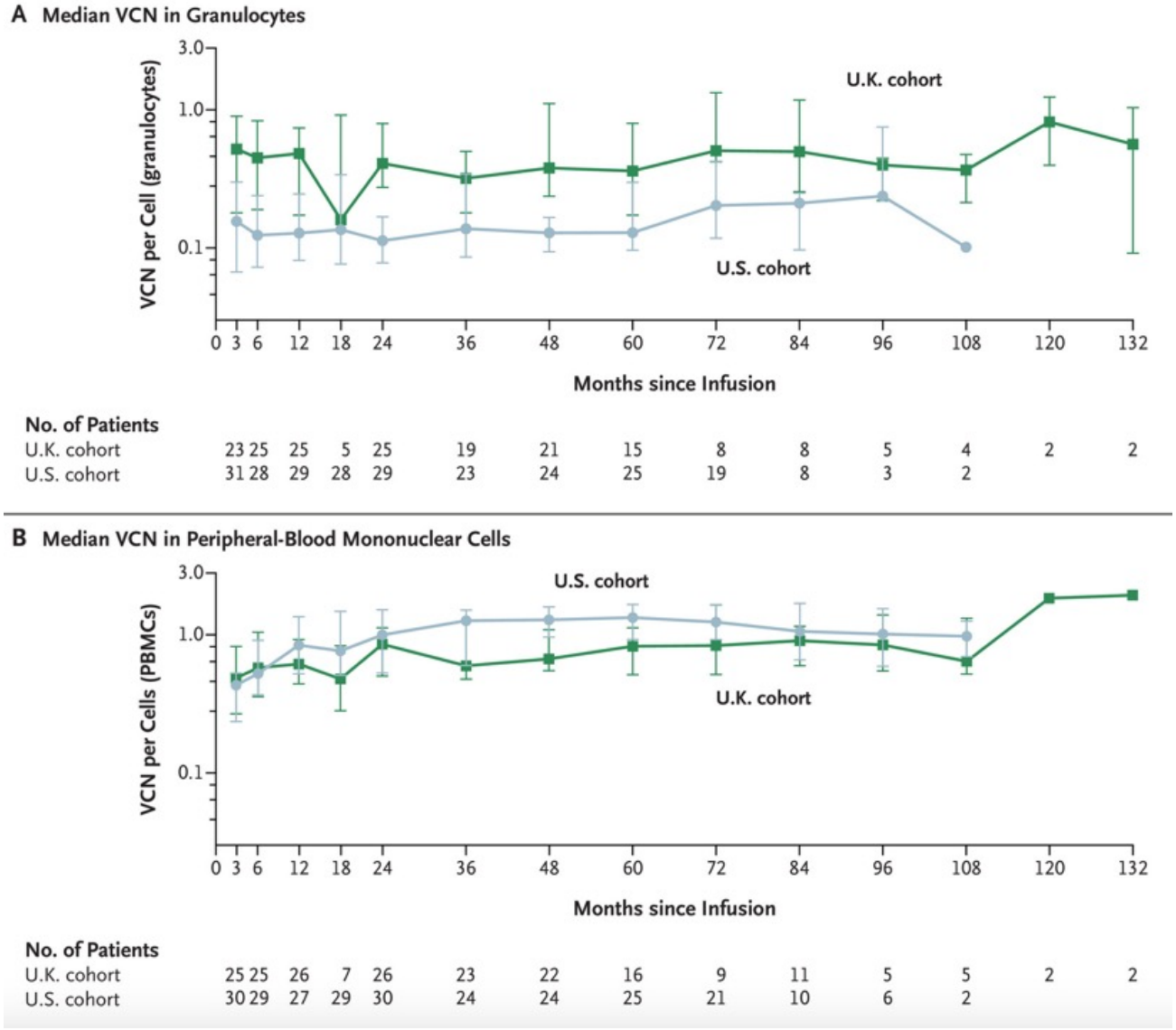

Median Vector Gene Marking in Granulocytes and Peripheral-Blood Mononuclear Cells.

Shown is the median vector copy number (VCN) in granulocytes (Panel A) and peripheral-blood mononuclear cells (Panel B) from the first follow-up after infusion of the drug product (month 3) to the latest follow-up. I bars indicate standard errors.

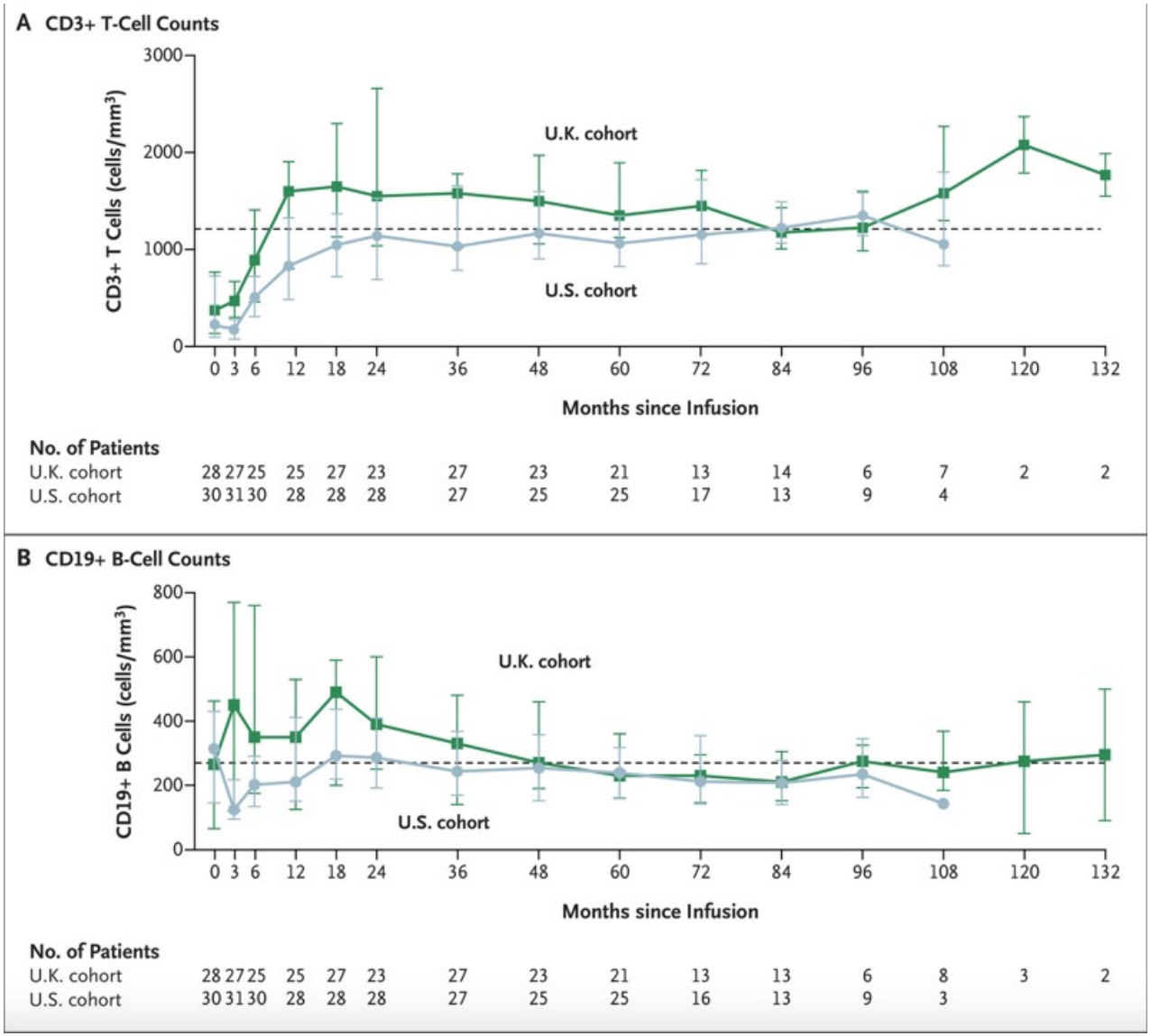

Median CD3+ T-Cell and CD19+ B-Cell Counts.

The median absolute CD3+ T-cell counts (Panel A) and CD19+ B-cell counts (Panel B) are shown as determined by flow cytometry from the first follow-up after infusion of the drug product (month 3) to the latest follow-up. Dotted lines represent the median normal lymphocyte subset count for ages of patients included in this study. I bars indicate standard errors.

Discussion

In previous studies, we reported that lentiviral gene therapy was safe and effective in 50 patients with ADA-SCID, with 100% overall survival and more than 95% event-free survival up to 36 months after infusion. The initial procedure was associated with no unacceptable side effects and complications, and most patients had full immune recovery and sustained metabolic detoxification, which led to a reduction in infections and the ability to stop enzyme-replacement therapy and immunoglobulin-replacement therapy. We can now confirm the sustained clinical benefit and excellent safety profile in a cohort expanded to 62 patients with a median follow-up of 7.5 years and a follow-up duration of more than 10 years in 5 patients. Gene marking in peripheral blood has remained stable over time, and this is reflected in durable lymphocyte counts, which have remained within normal ranges. Of note, the vector copy number in the granulocyte compartment, which is indicative of gene marking in hematopoietic stem-cell populations, has also remained stable. Alongside the robust clinical response and continued generation of naive T cells, this stability suggests that long-term repopulating hematopoietic stem-cell populations were genetically corrected. No treatment failures were recorded beyond the 1-year time point.

Säuglingssterblichkeit durch neonatale Gabe von Azithromycin verringern?

Die Säuglingssterblichkeit in Burkina Faso ist sehr hoch. Lässt sie sich eventuell durch die einmalige Gabe von Azithromycin nach der Geburt positiv beeinflussen?

Eine kalifornische Forschergruppe hat untersucht, ob durch die zweimalige Massentherapie mit Azithromycin im Bereich der Subsahara die Säuglingssterblichkeit im Alter von 1 bis 5 Monaten verringert werden kann, wenn im Alter von 8 bis 27 Tagen (Placebo-kontrolliert 1:1) eine einmalige Gabe von Azithromycin (20 mg/kg Körpergewicht) gegeben wurde.

Die Studie wurde in Burkina Faso zwischen 2019 und 2020 durchgeführt. Der primäre „Outcome" war die Sterblichkeit im Alter von 6 Monaten. Die Kinder wurden 21 Tage nach der Behandlung sowie im Alter von 3 bis 6 Monaten untersucht. Es wurden 21.832 Neugeborene in die Studie eingeschlossen. 10.898 erhielten Azithromycin und 10.934 Placebo. Im Alter von 6 Monaten waren in der Azithromycin- Gruppe 92 Säuglinge verstorben: 42 (0,44 %) und 50 (0,52 %) in der Placebo-Gruppe. Hieraus ergibt sich eine hazard ratio von 0,85 (95 %-CI, 0,56 – 1,28, p = 0,46). Schwerwiegende Nebenwirkungen traten in 0,27 % in der Behandlungsgruppe und in 0,14 % in der Placebo-Gruppe auf.

Mass Administration of Azithromycin to Infants in Mali to Reduce Mortality

Mass administration of azithromycin to children 1 to 59 months of age has been shown to reduce mortality among infants and children in this age group in some areas of sub-Saharan Africa. The largest effects have appeared to be among infants younger than 12 months of age, within 3 months after treatment; this observation motivated the design of the current trial.

In this trial, we randomly assigned villages in Mali, West Africa, in a 3:4:2 ratio to receive distributions of placebo, azithromycin two times a year, or azithromycin four times a year. Infants 1 to 11 months of age received, in doses of 20 mg per kilogram of body weight, placebo every 3 months (control group); azithromycin at two quarterly visits from January through June and placebo at two quarterly visits from July through December (twice-yearly azithromycin group); or azithromycin every 3 months (quarterly azithromycin group). The primary outcome was death within 3 months after eligibility had been confirmed, analyzed in the intention-to-treat population.

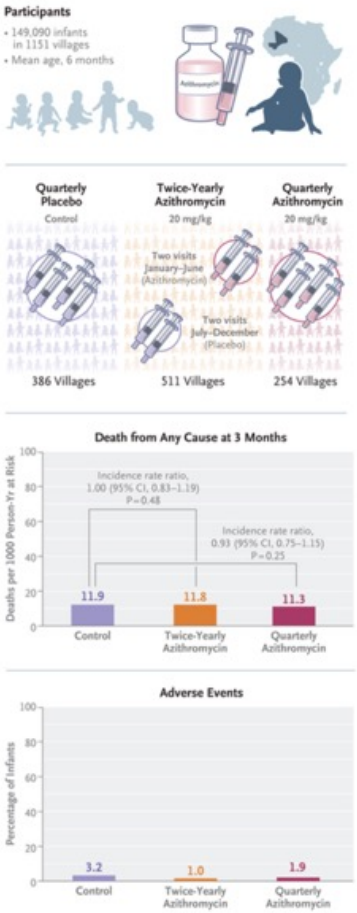

The MORDOR (Macrolides Oraux pour Réduire les Décès avec un Oeil sur la Résistance) trial, which was conducted in Niger, Malawi, and Tanzania, specifically examined the effect of twice-yearly mass administration of azithromycin on mortality in children 1 to 59 months of age.[4] Results of that trial showed a significant 13.5% lower incidence of death from any cause among children who received azithromycin than among those who received placebo, with 6.6 fewer deaths per 1000 person-years. The largest reductions were among infants 1 to 5 months of age (24.9% lower mortality with azithromycin than with placebo) and in Niger (18.1% lower mortality with azithromycin). A secondary analysis suggested that much of the protective effect was observed in the first 3 months after treatment, which has important implications for dosing frequency.

As a result of these findings, the World Health Organization (WHO) issued conditional guidelines in 2020 that recommend consideration of mass administration of azithromycin to infants 1 to 11 months of age in high-mortality settings. This age restriction was designed to maximize benefits while minimizing the risks of antimicrobial resistance.

In the LAKANA (Large-Scale Assessment of the Key Health-Promoting Activities of Two New Mass Drug Administration Regimens with Azithromycin) trial, we evaluated the effects of mass administration of azithromycin in Mali, West Africa, targeting infants 1 to 11 months of age, with administration either two times a year or four times a year. Here, we report the results of this trial regarding the effect of the intervention on infant and child mortality and safety.

Trial Setting, Participants, and Eligibility Criteria

This trial involved villages located in the Kayes, Kita, and Koulikoro regions, which are considered to be nonurban, accessible, and safe according to the local health authorities and research team. Eligibility criteria for administration of azithromycin or placebo included an age of 1 to 11 months (29 to 364 days), residence in a trial village, a body weight of at least 3 kg, and caregiver consent. Infants with a known allergy to macrolides or a severe illness requiring referral to a health facility were excluded from the trial.

Interventions

At each visit, infants were weighed on an electronic hanging scale (ADE M111600-01, ADE Germany), and the mobile application was used to calculate the dose in milliliters to be administered. Data collectors used syringes to administer an oral suspension of azithromycin or placebo, under direct observation and at a single dose of 20 mg per kilogram of body weight, in line with current WHO guidelines.

Outcomes

The prespecified primary outcome was death from any cause among infants 1 to 11 months of age. The unit of primary-outcome measurement was a 3-month time period, which was the interval between successive study visits.

Characteristic	Control	Twice-Yearly Azithromycin	Quarterly Azithromycin
Village Characteristics			
No. of villages	386	511	254
No. of large villages (%)†	70 (18)	88 (17)	44 (17)
Infant Characteristics			
Median no. of infants 1–11 mo of age per village	17	18	19
Total no. of infants 1–11 mo of age	13,187	18,040	8,201
Female sex (%)	49.3	49.0	49.4
Weight-for-age z score	−0.89±1.35	−0.89±1.38	−0.92±1.36
Age — mo	6.0±3.0	6.0±3.1	6.1±3.1
Age group (%)			
1–2 mo	18.7	19.0	18.4
3–5 mo	29.8	29.6	29.3
6–8 mo	29.8	28.8	29.5
9–11 mo	21.7	22.6	22.8

Variable	Control	Twice-Yearly Azithromycin	Quarterly Azithromycin
Deaths	335	437	196
Person-yr at risk	28,117.9	37,072.0	17,409.5
Deaths per 1000 person-yr at risk	11.9	11.8	11.3
Incidence rate ratio vs. control*	Reference	1.00 (0.83 to 1.19)	0.93 (0.75 to 1.15)
P value		0.48	0.25
Incidence rate difference vs. control	Reference	–0.05 (–2.31 to 2.21)	–0.91 (–3.55 to 1.73)
P value		0.96	0.50
Incidence rate ratio vs. twice-yearly azithromycin*			0.93 (0.76 to 1.15)
P value			0.25
Incidence rate difference vs. twice-yearly azithromycin			–0.85 (–3.34 to 1.64)
P value			0.50

Variable	Quarterly Azithromycin	Control	Incidence Rate Ratio (95% CI)
	no. of deaths (person-yr at risk)		
Age			
1–5 mo	82 (6,539.9)	128 (10,555.7)	1.00 (0.74–1.36)
6–11 mo	112 (10,321.2)	199 (16,728.4)	0.89 (0.68–1.16)
Sex			
Male	100 (8,919.3)	159 (14,411.7)	1.00 (0.75–1.32)
Female	96 (8,490.2)	176 (13,706.2)	0.87 (0.65–1.14)
Weight-for-age z score			
Less than –2	26 (1,807.4)	42 (2,979.2)	1.17 (0.83–1.66)
–2 or greater	64 (6,448.2)	88 (10,506.7)	1.01 (0.61–1.68)
Received seasonal malaria chemoprevention ≤3 mo before mass administration			
Yes	3 (295.6)	2 (412.2)	2.07 (0.34–12.50)
No	193 (17,192.7)	333 (27,825.4)	0.92 (0.74–1.14)
Household asset index			
At or below median	69 (6,452.5)	132 (9,358.8)	0.79 (0.57–1.08)
Above median	127 (10,957.1)	203 (18,759.1)	1.03 (0.80–1.33)
WASH index			
At or below median	66 (5,874.8)	100 (10,068.7)	1.10 (0.78–1.54)
Above median	130 (11,534.7)	235 (18,049.2)	0.86 (0.67–1.10)

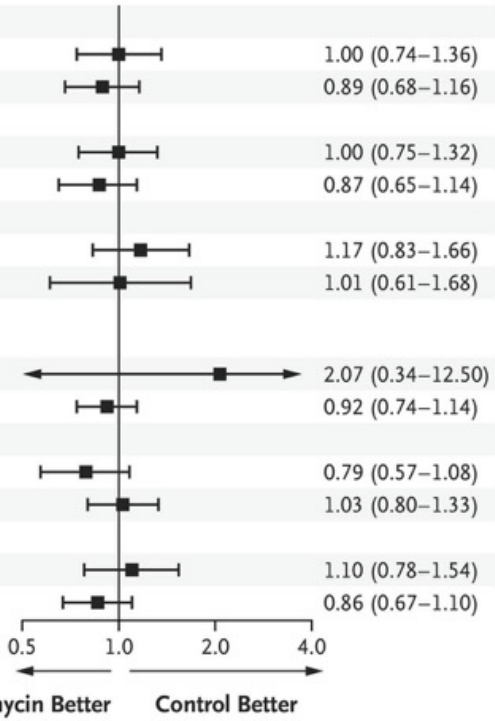

Subgroup Analysis of All-Cause Mortality among Infants 1 to 11 Months of Age at the Time of Mass Administration.

Shown is the difference between the control and quarterly azithromycin groups in all-cause mortality among infants 1 to 11 months of age at the time of mass administration. The incidence rate ratio was not modified according to infant age, sex, weight-for-age z score, recent treatment with seasonal malaria chemoprevention, household asset index, or WASH (access to clean water, sanitation, and hygiene) index. The x axis of this figure uses a logarithmic scale for visual clarity and symmetry. However, the numerical values shown in the far-right column represent incidence rate ratios, not log-transformed coefficients.


Preventable diseases claim millions of young lives
Particularly during infancy
High-mortality regions

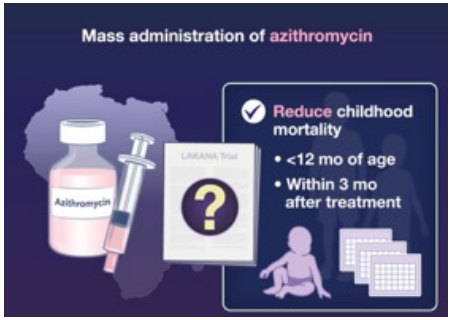
Mass administration of azithromycin
Azithromycin
LAKANA Trial
?
Reduce childhood mortality
• <12 mo of age
• Within 3 mo after treatment

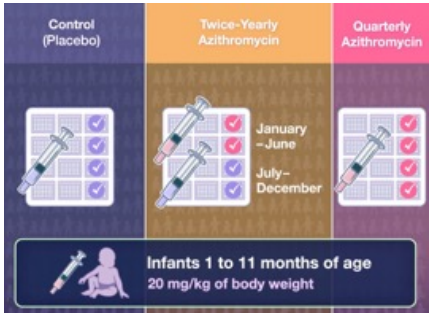
Control (Placebo)
Twice-Yearly Azithromycin
Quarterly Azithromycin
January–June
July–December
Infants 1 to 11 months of age
20 mg/kg of body weight

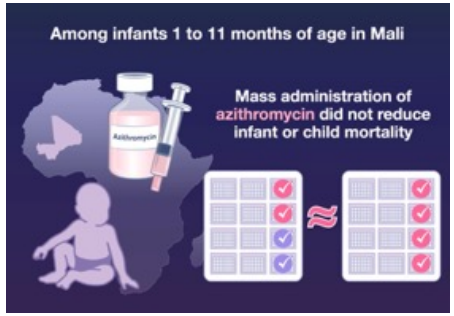
Among infants 1 to 11 months of age in Mali
Azithromycin
Mass administration of azithromycin did not reduce infant or child mortality

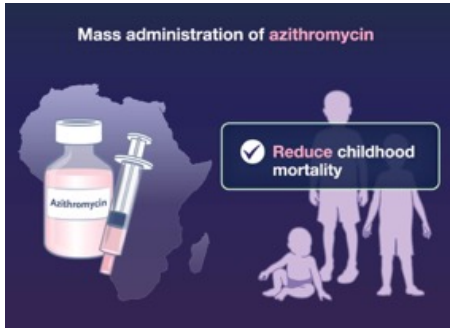
Mass administration of azithromycin
Azithromycin
Reduce childhood mortality


Control (Placebo)
Twice-Yearly Azithromycin
Quarterly Azithromycin


PRIMARY OUTCOME
Incidence of Death from Any Cause at 3 Months
Incidence rate ratio, quarterly vs. control, 0.93 (95% CI, 0.75–1.15); P=0.25
Incidence rate ratio, twice-yearly vs. control, 1.00 (95% CI, 0.83–1.19); P=0.48
Incidence rate ratio, quarterly vs. twice-yearly, 0.93 (95% CI, 0.76–1.15); P=0.25
Deaths per 1000 Person-Years at Risk
11.9
11.8
11.3
Control
Twice-Yearly Azithromycin
Quarterly Azithromycin

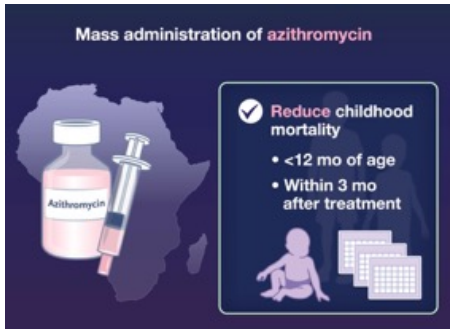
Mass administration of azithromycin
Azithromycin
Reduce childhood mortality
• <12 mo of age
• Within 3 mo after treatment


Control (Placebo)
Twice-Yearly Azithromycin
Quarterly Azithromycin
x2
x4
386 Villages
511 Villages
254 Villages


SAFETY
Adverse Events
Percentage of Infants
3.2%
1.0%
1.9%
Control
Twice-Yearly Azithromycin
Quarterly Azithromycin

Hair Loss in Women

A 46-year-old premenopausal woman presents with a 3-year history of progressive thinning and shedding of her scalp hair. She has well-controlled hypertension and relates no recent surgery, weight loss, or change in her medications or medical conditions. She has mild hirsutism treated with plucking. On examination, she has a decrease in hair density in the central scalp with frontal accentuation, retention of her anterior hairline, absence of scalp inflammation, and release of multiple hairs on a gentle hair pull. Eyebrows and eyelashes are intact. How would you treat this patient?

The Clinical Problem

Female-pattern hair loss is the most common cause of hair loss in women. The prevalence of this condition is 3 to 12% among women of European descent in their 20s and 30s, 14 to 28% among those in their 50s, and 56% among those older than 70 years of age. The prevalence is lower among Asian women — 12 to 25% among those older than 70 years of age — and is unknown among women of African descent owing to the common overlap of the clinical findings of female-pattern hair loss with those of early central centrifugal cicatricial alopecia. It is unclear whether the decrease in hair density or diameter (or both) commonly seen in older persons, known as senescent or involutional alopecia, is a distinct entity or a part of pattern hair loss (i.e., pattern hair loss that occurs in men or women).

KEY CLINICAL POINTS

Hair Loss in Women

- Female-pattern hair loss is common and increases with age. Distinguishing between early-onset and late-onset female-pattern hair loss and establishing the presence or absence of hyperandrogenism or hyperandrogenemia may identify subpopulations of patients with varied etiologic factors and response to treatment.
- The major clinical features of female-pattern hair loss are a pattern of central-scalp hair loss with or without frontal accentuation, preservation of follicular ostia, and variation of hair-shaft diameter. A scalp biopsy can confirm the disorder and determine the potential for regrowth.
- One treatment strategy for female-pattern hair loss is to start with either 5% topical minoxidil twice a day or a low dose of oral minoxidil and escalate the latter if no unacceptable side effects occur (e.g., symptomatic low blood pressure, peripheral edema, or hypertrichosis).
- Antiandrogen agents or 5α-reductase inhibitors are effective treatments in women with female-pattern hair loss and are useful in combination with minoxidil.
- For patients with female-pattern hair loss who prefer to avoid medications or wish to augment their medical therapy, microneedling, platelet-rich plasma, nonablative fractional laser treatment, and low-level light therapy may be useful.

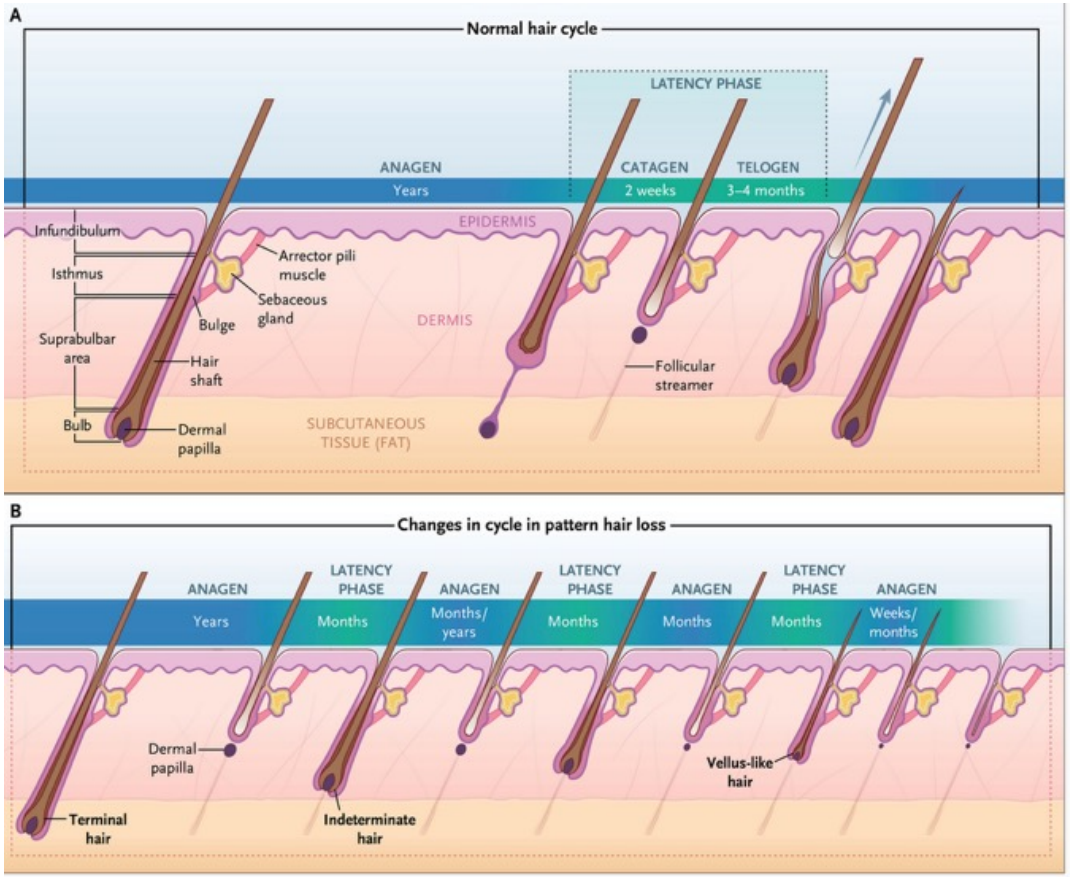

The Hair Cycle with Normal Hair Growth and with Pattern Hair Loss.

Panel A shows the hair cycle of a normal-scalp terminal hair. The cycle includes 3-to-6-year periods of active hair growth (anagen) separated by periods of inactivity. This latency phase is initiated by a brief period of apoptosis-driven regression of the inferior portion of the hair follicle and upward movement of the remaining follicle and its dermal papilla to the area immediately below the arrector pili muscle. This brief transition period (catagen) is followed by a quiescent period (telogen) that lasts several months. At the conclusion of telogen, the hair shaft is shed (exogen), anagen is reinitiated, and the anagen follicle moves downward along the collapsed follicular streamer to its former location in the subcutaneous tissue. Panel B shows the hair cycle in pattern hair loss. In male-pattern or female-pattern hair loss, the process of miniaturization of individual hairs in affected follicular units drives the degree and location of the hair loss. The dermal papilla and the bulb of affected hairs, which determine the diameter of the hair shaft, synchronously become smaller and the duration of the anagen phase, which determines the length of the hair shaft, becomes shorter over several cycles. An additional period of quiescence called kenogen follows telogen in pattern hair loss, which lengthens the latency phase between active anagen phases and increases the time that affected follicles and follicular ostia may remain empty of hair shafts. In severe pattern hair loss, this miniaturization process can evolve into actual follicular loss. The net result is a decrease in follicular density and volume.

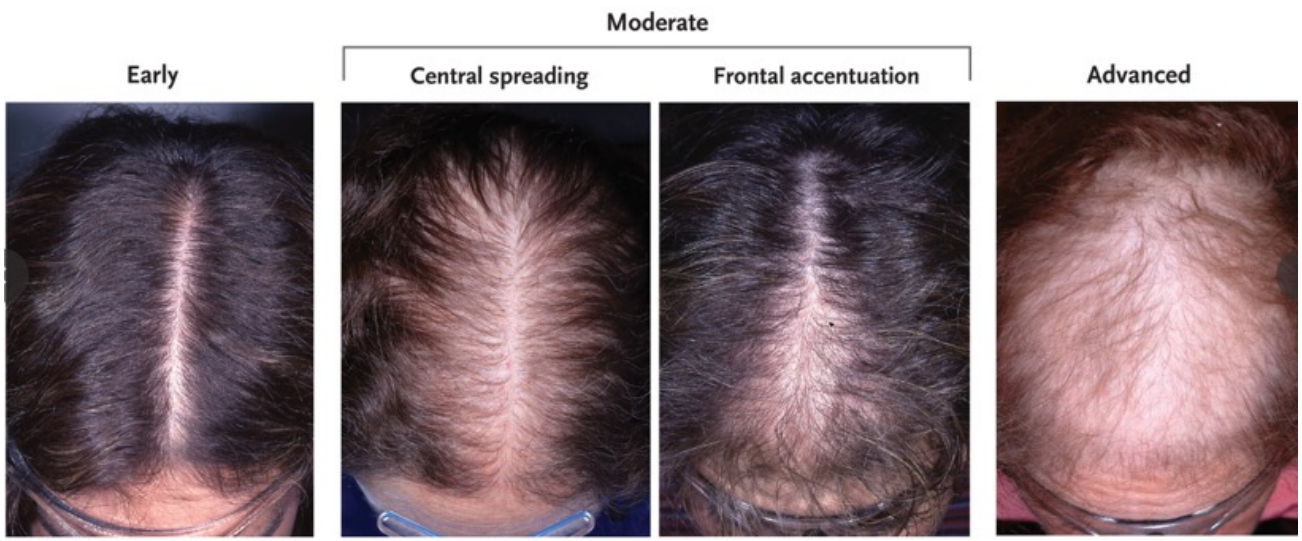

Severity Scale for Female-Pattern Hair Loss.

Patients with female-pattern hair loss may present with minimal evidence of scalp hair loss. A midline part in early female-pattern hair loss usually will show an increase in part width and a decrease in hair density (left panel) that are especially notable when compared with that in the occiput. An increasing part width from the vertex toward the anterior hairline, even if subtle, will help to differentiate the condition from telogen effluvium. As female-pattern hair loss progresses, one of the two primary patterns becomes obvious — a central spreading (Ludwig) pattern (left-middle panel) or a "Christmas tree" or frontal accentuation (Olsen) pattern (right-middle panel). The degree of hair loss may occasionally progress to a marked decrease in density across the entire top of the scalp (right panel), simulating a primary cicatricial alopecia; a scalp biopsy is recommended in these cases.

	 Female-Pattern Hair Loss (FPHL)	 Chronic Telogen Effluvium	 Frontal Fibrosing Alopecia	 Fibrosing Alopecia in a Pattern Distribution	 Central Centrifugal Cicatricial Alopecia
Patient Population	After puberty through menopause, all races	Any age or race, more commonly middle-aged women	Typically postmenopausal White women but any age or race	Typically middle-aged or older women but any age or race	Typically women of African descent, any age
Pattern of Loss	Central or frontal accentuation	Global hair loss	Anterior hairline recession with or without bitemporal and parietal hairline recession	Central hair loss	Central- or vertex-spreading hair loss, balding common
Loss of Follicular Ostia	No (unless advanced with depletion of folliculosebaceous units)	No	Yes	Yes	Yes
Perifollicular or Interfollicular Erythema	No	No	Common	Common	Variable
Perifollicular Hyperkeratosis	No	No	Common	Variable	Variable
Additional Key Points	Variation in hair-shaft diameter Spares occiput Scalp biopsy if uncertain of diagnosis or if focal atrichia	Present >6 mo Diffusely positive hair pull for telogen hairs May overlap with FPHL	Possible isolated or concomitant eyebrow loss Prominent facial veins and facial papules in some cases Scalp biopsy diagnostic if clinical diagnosis uncertain	May be present with frontal fibrosing alopecia May mimic FPHL, especially FPHL with follicular depletion Scalp biopsy recommended	Early stage may be difficult to distinguish from FPHL Scalp biopsy recommended

Differential Diagnosis of Female-Pattern Hair Loss.

The conditions listed in the four right columns may warrant a scalp biopsy to distinguish them from female-pattern hair loss. In addition, miniaturization may be present histologically in each of these conditions, which would suggest concomitant female-pattern hair loss.

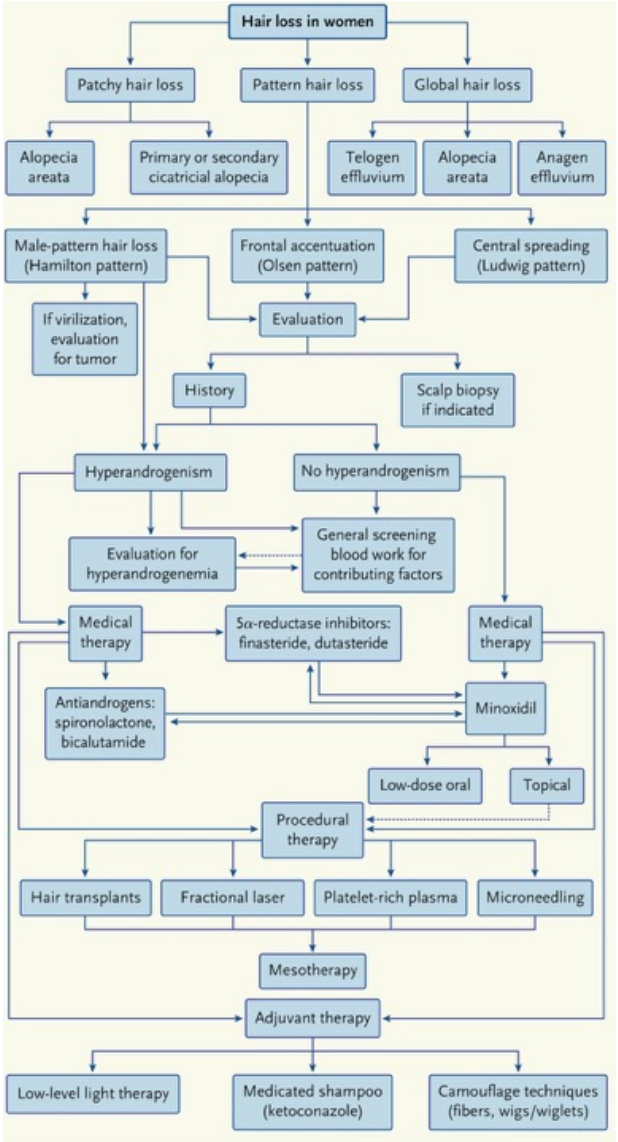

Evaluation and Treatment of Female-Pattern Hair Loss.

Treatment	Potential Mechanism of Action	Controlled Clinical Trials	Limitations of Studies	Side Effects
Microneedling[24]	Induction of percutaneous wounds purportedly leads to release of growth factors that promote angiogenesis, reversal of fibrosis, initiation of anagen, and proliferation of dermal papillae and stem cells. It may also enhance transdermal delivery of topical agents.	Trials have shown equivocal results with microneedling as monotherapy. Most trials showed significant improvement with topical minoxidil and microneedling as compared with topical minoxidil alone.	Limitations have included variation of methods used (depths of microneedling vary between 0.25 and 2.5 mm), delivery method (needling stamps, manual rollers, or automated pens with or without fractional radiofrequency), and frequency of treatments. Studies have been small, and those involving persons with FPHL or that are placebo-controlled are limited.	In general, few side effects are reported. Pain and lymphadenopathy are possible.
Low-level light therapy[25,41]	Devices include lasers (630–660 nm), light-emitting diode, or combination devices in comb, hat, or helmet form. The mechanism for hair growth is unclear, but photobiomodulation promotes anagen and a potential anti-inflammatory effect.	Double-blind, randomized, sham-controlled trials have shown an increase in hair density.[41] Use of a 650-nm low-level laser device with 5% topical minoxidil had greater efficacy than monotherapy with either treatment.[25]	Only a few devices have FDA clearance specifically for MPHL or FPHL, and all are sold online directly to patients. A comparison of results among devices is limited owing to inherent variation in light absorption of skin and hair color, variation in wavelength, and treatment specifics including frequency of use.	Side effects are few but include pruritus, pain or tenderness, paresthesia, urticaria, dermatitis, irritation, dry skin, and headaches.
Platelet-rich plasma[38-40]	Platelet-rich plasma is a blood-derived product with a concentration of platelets that is 3 to 5 times that of whole blood, ideally 1,000,000 per microliter. Therapeutic potential lies with the release from activated platelet alpha granules of various growth factors, cytokines, and cell-adhesion molecules, enhancing a transition of telogen to anagen and prolonging anagen.	Many single-site trials (including half-head-controlled trials†) have shown an increase in hair-shaft diameter from baseline.	All devices are FDA-cleared, but there is no standardization of process (anticoagulants, single or double centrifugation, spin rate, force or duration of centrifugation, activation of platelets, and number of red cells or leukocytes) or treatment specifics (platelet concentration; volume injected; number, depth of, and distance between injections; and frequency of treatments). There are few multisite, paired-comparison, randomized, placebo-controlled trials and few studies of FPHL in which there was a period of washout of other current hair-related treatments.	Local discomfort is the most commonly reported side effect.
Fractional laser treatment[42-44]	Nonablative fractional lasers stimulate hair growth through fractional photothermolysis (i.e., controlled dermal damage) while maintaining the integrity of the epidermis with minimal thermal effect. Ablative fractional lasers penetrate deeper and may have more efficacy but greater risk of side effects than nonablative fractional lasers. Lasers may assist topical drug delivery as well.	A prospective, open-label, single-blind, controlled trial involving patients with FPHL treated with a nonablative 1550-nm fractional laser (10 treatments 2 weeks apart) documented an increase in hair density.[43] In a single-center, retrospective trial, an FDA-cleared nonablative 1565-nm laser resulted in visible hair growth in participants with either FPHL or MPHL.[44]	Studies of fractional laser treatment for pattern hair loss vary with respect to use of ablative or nonablative lasers, wavelength, spot size, energy, interval of treatment, and recommended number of sessions. Because no medication or invasive treatment is involved, fractional lasers have a wide range of applicability to diverse populations with hair loss.	Side effects are related to laser type and treatment specifics and range from mild erythema and warmth to pruritus, dryness, mild ulceration, and pigmentary changes.
Mesotherapy[45,46]	Microinjection of medications (minoxidil, dutasteride, or bicalutamide), botulinum toxin, or various purported growth promoters into the mesoderm (mid-dermis) may bypass systemic reactions of medications and enhance local efficacy.	A trial involving 126 women with FPHL who received dutasteride mesotherapy or saline (12 sessions over 18 weeks) showed significant photographic improvement (62.8% vs. 17.5%) and an increase in mean hair diameter and patient self-assessment with mesotherapy as compared with placebo.[45]	Limitations include variability in agent, concentration, vehicle, solvent, frequency and number of sessions, and injection technique; few placebo-controlled trials or comparisons with an oral agent; a lack of data on blood or plasma levels of the agent used; small studies with or without washout of other hair treatments; and few studies involving participants with FPHL.	Side effects include headache, injection-site pain, local site reactions, infection, frontal edema, and hair loss.
Hair transplants	The goal is to add hair from the occipital scalp that is uninvolved with pattern hair loss to areas with low hair density.	Follicular unit extraction is the preferred method.	Success of treatment depends on the density and caliber of hair in the donor area and control of ongoing pattern hair loss.	Continued medical therapy is warranted to prevent further loss.

Conclusions and Recommendations

The patient in the vignette has a combination of late-onset female-pattern hair loss, chronic telogen effluvium, and hirsutism. Her workup revealed mildly elevated free and total testosterone levels but did not indicate the source of telogen effluvium, as is often the case. A biopsy was not essential for diagnosis.

I would start treatment with combination therapy, either spironolactone or finasteride for both the hirsutism and the female-pattern hair loss and either topical or oral minoxidil to address both the female-pattern hair loss and the chronic telogen effluvium, providing counsel on the continued need for contraception while she is still of childbearing potential. Standardized photographs of the central scalp with a midline part (as shown in Figure 2) are a simple and effective measure to help both the physician and the patient determine the efficacy of treatment, and trichoscopic evaluation of changes in hair-shaft diameter and density documents the mechanism of improvement.

Pneumococcal Sepsis in a Patient with Asplenia and Hypogammaglobulinemia

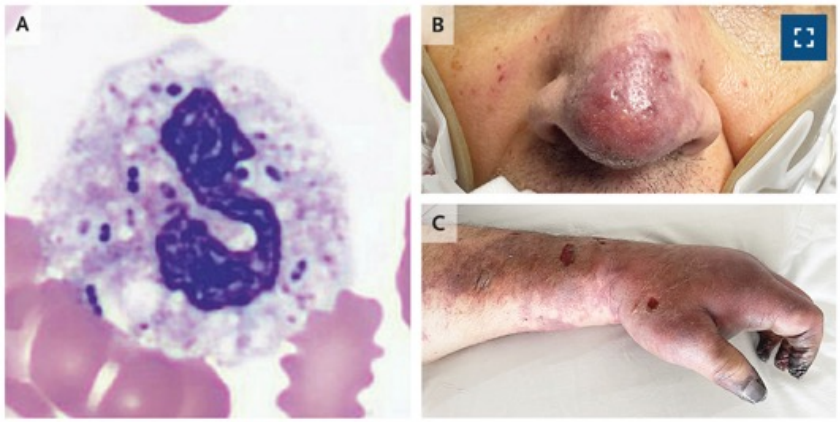

A 52-year-old man with a history of traumatic splenectomy and treated mantle-cell lymphoma presented with a 5-day history of dry cough and nasal congestion and a 2-day history of dyspnea and confusion. Three years earlier, the lymphoma had been treated with chimeric antigen receptor (CAR) T-cell therapy. The lymphoma had been complicated by persistent hypogammaglobulinemia, for which intermittent immune globulin infusions had been given. The patient had had appropriate pneumococcal vaccinations and had received penicillin prophylaxis for 12 months after CAR T-cell therapy. At the current presentation, his body temperature was 102.7°F (39.3°C), heart rate 128 beats per minute, blood pressure 78/48 mm Hg, and oxygen saturation 84% while he was breathing 6 liters of oxygen by nasal cannula. Physical examination was notable for coarse breath sounds and cyanosis of the hands and feet. A chest radiograph showed multifocal consolidations. Computed tomography of the head showed maxillary sinusitis. The patient was admitted to the intensive care unit. Serum immunoglobulin levels were undetectable. Blood cultures grew *Streptococcus pneumoniae* 7 hours after collection. Encapsulated diplococci were seen in 20% of neutrophils on a peripheral-blood smear (Panel A, Wright's stain). A diagnosis of septic shock from invasive pneumococcal infection was made. Multiorgan dysfunction and purpura fulminans of the nose (Panel B) and fingers (Panel C) developed. On hospital day 8, the patient died.

Stercoral Colitis

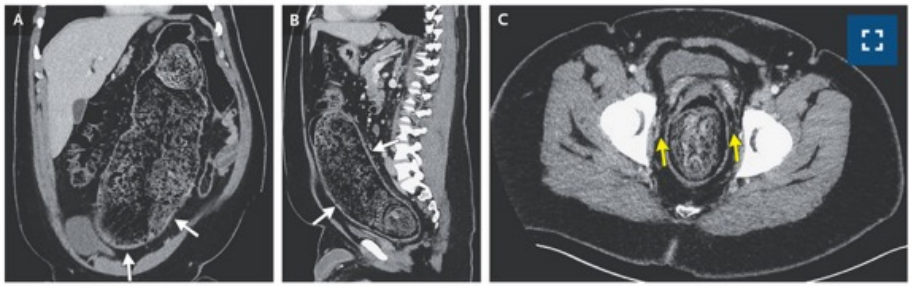

A 23-year-old man with autism spectrum disorder and recurrent hospitalizations for severe constipation presented to the emergency department with a 1-week history of abdominal pain on his left side, nausea, and vomiting. Owing to behavioral challenges, the patient had difficulty adhering to a bowel regimen for chronic constipation as an outpatient. A previous evaluation for Hirschsprung's disease had been negative. Physical examination was notable for abdominal distention and mild tenderness to palpation on the left side of the abdomen. The serum lactate level was normal. Computed tomography of the abdomen and pelvis revealed distention of the colon by a large stool burden and mural thickening (Panels A and B, white arrows) and perirectal fat stranding (Panel C, yellow arrows). (Panels A, B, and C show the coronal, sagittal, and axial views, respectively.) A diagnosis of stercoral colitis was made. In stercoral colitis, chronically impacted feces distend the colon, resulting in inflammation. In some cases, the fecaloma may lead to focal-pressure necrosis or perforation. Treatment with an aggressive bowel regimen was given, and fecal disimpaction was performed by means of flexible sigmoidoscopy. At discharge, the patient was having several bowel movements per day on a bowel regimen. At a follow-up visit at the gastroenterology clinic approximately 5 months after discharge, anorectal manometry showed nonrelaxation of the anorectal angle, which was thought to be related to puborectalis muscular dysfunction. Pelvic-floor physical therapy was initiated.

Case 29-2025: A 43-Year-Old Woman with Depression, Suicidal Ideation, and Fever

The patient began to have worsening anhedonia, anxiety, and suicidal ideation, including plans to intentionally ingest an overdose of medication. On the day of the current admission, the patient presented to the emergency department of this hospital for evaluation. She reported 2 months of nonproductive cough without night sweats or weight loss. Multiple psychosocial stressors were present, including intimate partner violence, limited financial resources, and unstable housing. The patient was admitted to the psychiatry service for management of anhedonia and suicidality.

The patient's medical history was notable for human immunodeficiency virus (HIV) infection with associated neuropathy, which she had acquired 17 years earlier; adherence to antiretroviral medications had been limited in the 2 years preceding this evaluation. The patient had a history of bipolar disorder, as well as seizure disorder that was secondary to traumatic brain injury. She did not take any medications but had previously received a prescription for combination antiretroviral therapy (ART) with bictegravir, tenofovir alafenamide, and emtricitabine. Her surgical history was notable for Roux-en-Y gastric bypass that had been performed 10 years earlier. The patient had unstable housing; She smoked cocaine as well as one pack of cigarettes per day, and she drank alcohol recreationally. She had not traveled outside New England for several years.

The CD4+ T-cell count was 25 per microliter (reference range, 295 to 1471), and the HIV RNA viral load was 144,000 copies per milliliter (assay range, 20 to 10,000,000). The lactate dehydrogenase level was 227 U per liter (reference range, 110 to 210). Urinalysis showed no evidence of pyuria, hematuria, or proteinuria. Anteroposterior chest radiograph revealed innumerable micronodules that were evenly distributed throughout both lungs.

Variable	Reference Range, Adults†	On Initial Presentation
Hemoglobin (g/dl)	13.5–17.5	10.7
Hematocrit (%)	41.0–53.0	34.0
White-cell count (per μl)	4500–11,000	8630
Differential count (per μl)		
Neutrophils	1800–7700	7580
Lymphocytes	1000–4800	350
Monocytes	200–1200	560
Eosinophils	0–900	20
Basophils	0–300	30
Immature granulocytes	0–100	90
Platelet count (per μl)	150,000–400,000	426,000
Sodium (mmol/liter)	135–145	136
Potassium (mmol/liter)	3.4–5.0	2.9
Chloride (mmol/liter)	98–108	97
Carbon dioxide (mmol/liter)	23–32	25
Urea nitrogen (mg/dl)	8–25	14
Creatinine (mg/dl)	0.60–1.50	0.6
Calcium (mg/dl)	8.5–10.5	8.6
Aspartate aminotransferase (U/liter)	10–40	22
Alanine aminotransferase (U/liter)	10–55	11
Alkaline phosphatase (U/liter)	15–115	221
Total bilirubin (mg/dl)	<1.2	0.2
Albumin (g/dl)	3.3–5.0	2.4
Globulin (g/dl)	1.9–4.1	3.9
Lactate dehydrogenase (U/liter)	110–210	227
Creatine kinase (U/liter)	40–150	56

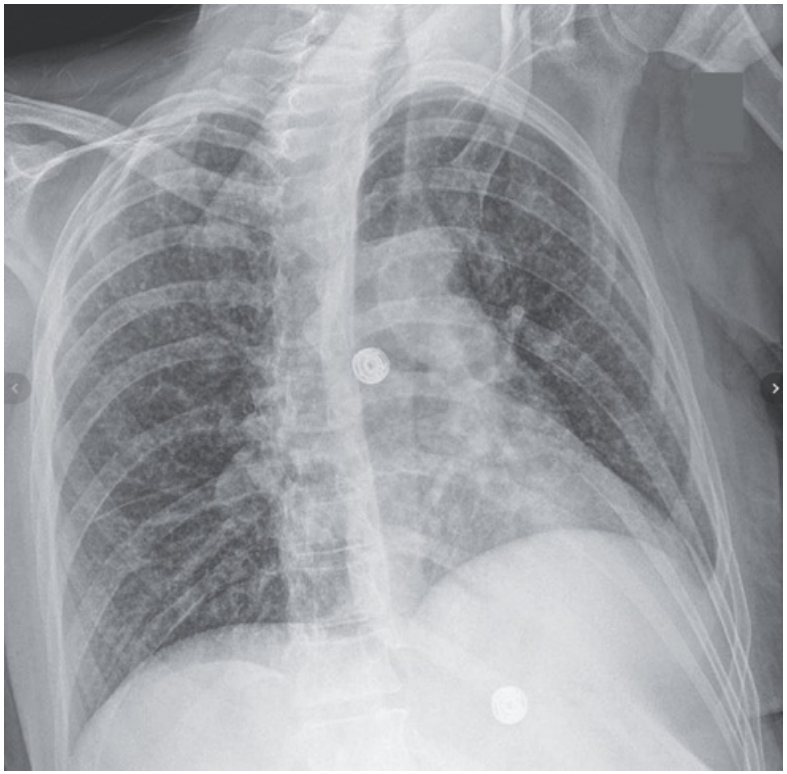

Differential Diagnosis

Underlying Immunologic Defect

What is the nature and severity of this patient's underlying immunologic defect? HIV infection causes various host defense impairments. In addition to the defects in cellular immunity caused by CD4+ T-cell lymphopenia, HIV infection leads to dysregulation of humoral immunity and innate immunity.

Salient Clinical Features

First, the patient reported a 2-month history of cough, a feature consistent with a subacute or chronic tempo of illness. Second, chest imaging showed diffuse micronodular opacities that were evenly distributed throughout both lungs, which is consistent with a miliary pattern. Third, routine blood testing revealed an elevated alkaline phosphatase level in the presence of normal levels of aspartate aminotransferase, alanine aminotransferase, and bilirubin, findings that suggest the possibility of an infiltrative liver disorder and thereby invoke a multisystem process. Fourth, the lactate dehydrogenase level was only mildly elevated, below the level typically seen in patients with pneumocystis pneumonia, disseminated histoplasmosis, or non-Hodgkin's lymphoma. Fifth, hematologic studies revealed thrombocytosis. It is notable that most opportunistic infections either have no effect on the platelet count or result in thrombocytopenia. In contrast, tuberculosis and certain cancers can be associated with thrombocytosis.

Additional Imaging Studies

On the second hospital day, CT of the chest was performed. One day later, CT of the abdomen and pelvis was performed with the administration of oral and intravenous contrast material in the portal venous phase. Magnetic resonance imaging (MRI) of the head was performed after the administration of gadolinium-based contrast material.

Additional Imaging Studies of the Chest, Abdomen, and Head.

CT of the chest was performed after the administration of intravenous contrast material, and the lung kernel was used as the image-reconstruction algorithm. An axial image (Panel A) shows nodules measuring 1 to 3 mm in diameter that are evenly distributed throughout both lungs (arrows), which is consistent with a miliary distribution. A coronal reformatted image in a soft-tissue window (Panel B) shows an enlarged right upper paratracheal lymph node with central low attenuation and a thickened rim (arrow). CT of the abdomen and pelvis was performed with the administration of oral and intravenous contrast material in the portal venous phase. A coronal reformatted image (Panel C) shows a lesion in the liver with central low attenuation and a thickened rim (top arrow), a similar lesion in the pancreatic head (middle arrow), and a necrotic upper mesenteric lymph node (bottom arrow). Multiple enlarged retroperitoneal lymph nodes with central low attenuation are also present. MRI of the head was performed after the administration of gadolinium-based contrast material. A T1-weighted image (Panel D) shows a single subtle 3-mm focus of enhancement (arrow) in the right temporo-occipital subcortical white matter.

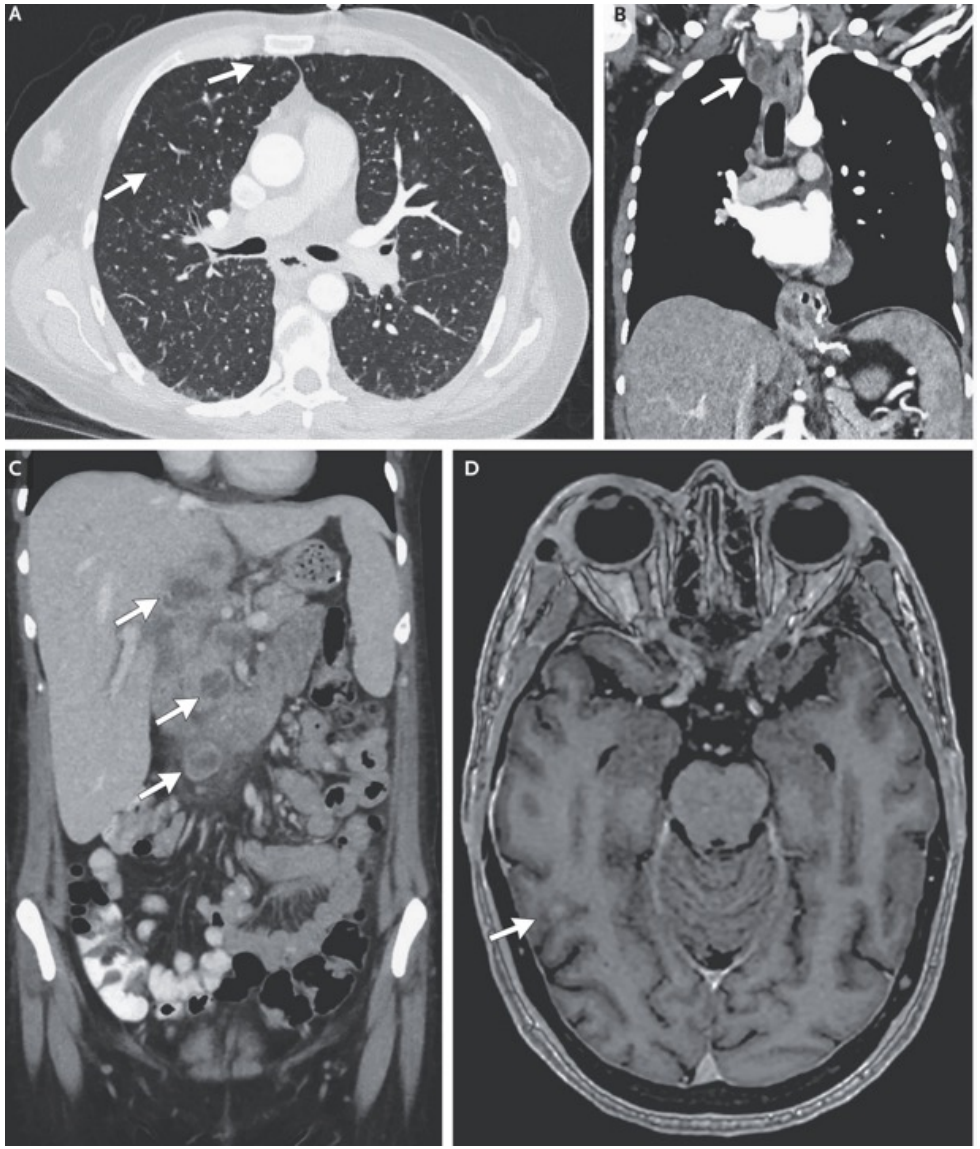

A transbronchial-biopsy specimen from a paratracheal lymph node that was obtained during bronchoscopy showed fragments of histiocytic aggregates with palisading and associated acute inflammation, findings suggestive of necrotizing granulomas. Special staining for acid-fast bacteria showed abundant slender bacilli that had morphologic features consistent with *M. tuberculosis* complex. After 9 weeks, cultures were positive for *M. tuberculosis*. In addition, nucleic acid amplification testing performed by the Massachusetts State Public Health Laboratory confirmed the diagnosis of *M. tuberculosis*. Antimicrobial susceptibility testing did not detect any antimicrobial resistance.

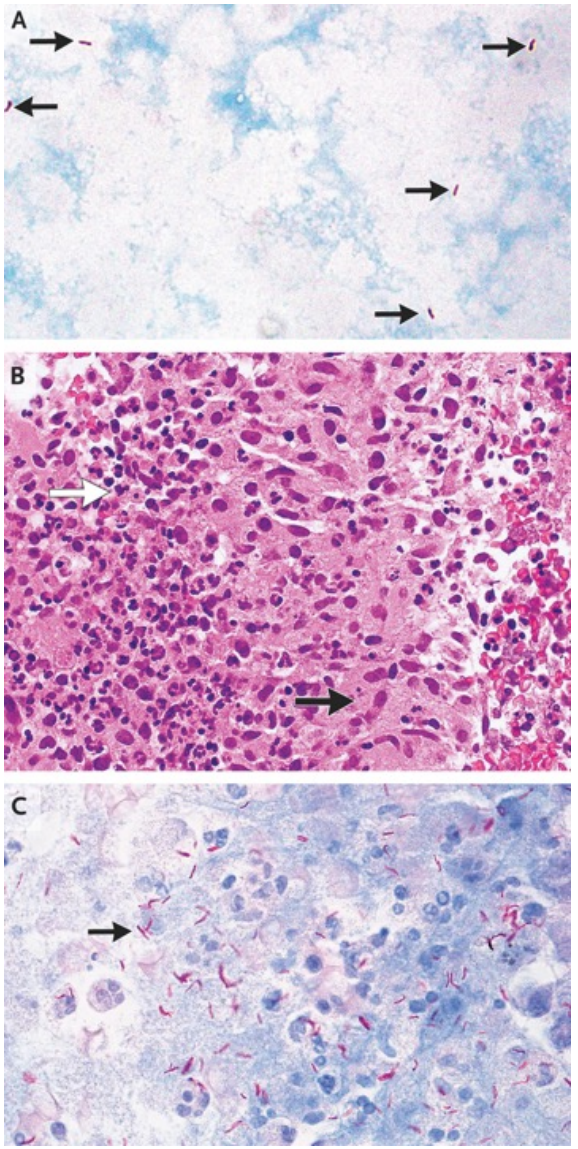

Sputum and Lymph Node–Biopsy Specimens.

Acid-fast staining of a sputum specimen (Panel A) highlights slender bacilli (arrows), a finding that is consistent with mycobacterium species but is nonspecific. Hematoxylin and eosin staining of a transbronchial-biopsy specimen from a paratracheal lymph node (Panel B) shows histiocytic aggregates with palisading (black arrow, indicating a representative histiocyte) admixed with acute inflammation and nuclear debris (white arrow), findings consistent with necrotizing granulomas. Acid-fast staining of the transbronchial-biopsy specimen (Panel C) shows numerous slender forms (arrow) located in the areas suggestive of necrotizing granulomas that had morphologic features consistent with *Mycobacterium tuberculosis* complex.

This patient had a favorable response to antituberculous therapy, without clinically important side effects or laboratory complications, and the fever promptly resolved. Nine days after the initiation of antituberculous therapy, ART with emtricitabine, tenofovir disoproxil fumarate, and dolutegravir was started.

One week later, while the course of dexamethasone was being tapered, fever with a high temperature recurred, prompting concerns for resistant tuberculosis, an additional undiagnosed opportunistic infection, an adverse drug reaction, or IRIS. No additional infectious source of fever or evidence of drug hypersensitivity was identified on extensive evaluation, which made IRIS the presumptive explanation for the fever. The HIV RNA viral load obtained 12 days after the initiation of ART was 113 copies per milliliter, indicating a robust virologic response, which is a known risk factor for IRIS. Glucocorticoid therapy was reinitiated and resulted in prompt resolution of the fever.

Follow-up

The patient was discharged to a medical respite facility after 33 days of treatment with antituberculous therapy, ART, and a tapering course of glucocorticoids. At a follow-up visit with her infectious disease physician 3 months after discharge, antituberculous therapy and ART were continued; the CD4+ T-cell count was 94 per microliter, and the HIV RNA viral load was undetectable. Three months after discharge from the hospital, the patient was again hospitalized for depression and suicidality in the context of housing concerns.

Final Diagnosis

Disseminated *Mycobacterium tuberculosis* infection.

Global Burden of Disease (GBD)

The GBD study is the largest and most comprehensive effort to quantify health loss across places and over time, so health systems can be improved and disparities eliminated.

607 billion+
highly standardized and comprehensive estimates measure health outcomes and systems.

463
health outcomes and risk factors provide a powerful basis for insights on global health trends and challenges.

204
countries and territories, plus dozens of subnational locations show trends at regional, national, and local levels.

17,000+
individuals from 167 countries and territories collaborate in vetting GBD data sources and estimates.

On this page: Overview | Key findings | Data | Publications | About GBD

Featured

REPORT

Global Burden of Disease 2023: Findings from the GBD 2023 Study

The latest global burden of diseases, injuries, and risk factors study (gbd) – an update through the year 2023 – provides a comprehensive picture of the world's health following the COVID-19 pandemic.

READ THE REPORT

Global age-sex-specific all-cause mortality and life expectancy estimates for 204 countries and territories and 660 subnational locations, 1950–2023: a demographic analysis for the Global Burden of Disease Study 2023

Summary

Background Comprehensive, comparable, and timely estimates of demographic metrics—including life expectancy and age-specific mortality—are essential for evaluating, understanding, and addressing trends in population health. The COVID-19 pandemic highlighted the importance of timely and all-cause mortality estimates for being able to respond to changing trends in health outcomes, showing a strong need for demographic analysis tools that can produce all-cause mortality estimates more rapidly with more readily available all-age vital registration (VR) data. The Global Burden of Diseases, Injuries, and Risk Factors Study (GBD) is an ongoing research effort that quantifies human health by estimating a range of epidemiological quantities of interest across time, age, sex, location, cause, and risk. This study—part of the latest GBD release, GBD 2023—aims to provide new and updated estimates of all-cause mortality and life expectancy for 1950 to 2023 using a novel statistical model that accounts for complex correlation structures in demographic data across age and time.

Methods We used 24 025 data sources from VR, sample registration, surveys, censuses, and other sources to estimate all-cause mortality for males, females, and all sexes combined across 25 age groups in 204 countries and territories as well as 660 subnational units in 20 countries and territories, for the years 1950–2023. For the first time, we used complete birth history data for ages 5–14 years, age-specific sibling history data for ages 15–49 years, and age-specific mortality data from Health and Demographic Surveillance Systems. We developed a single statistical model that incorporates both parametric and non-parametric methods, referred to as OneMod, to produce estimates of all-cause mortality for each age-sex-location group. OneMod includes two main steps: a detailed regression analysis with a generalised linear modelling tool that accounts for age-specific covariate effects such as the Socio-demographic Index (SDI) and a population attributable fraction (PAF) for all risk factors combined; and a non-parametric analysis of residuals using a multivariate kernel regression model that smooths across age and time to adaptably follow trends in the data without overfitting. We calibrated asymptotic uncertainty estimates using Pearson residuals to produce 95% uncertainty intervals (UIs) and corresponding 1000 draws. Life expectancy was calculated from age-specific mortality rates with standard demographic methods. For each measure, 95% UIs were calculated with the 25th and 975th ordered values from a 1000-draw posterior distribution.

Findings In 2023, 60·1 million (95% UI 59·0–61·1) deaths occurred globally, of which 4·67 million (4·59–4·75) were in children younger than 5 years. Due to considerable population growth and ageing since 1950, the number of annual deaths globally increased by 35·2% (32·2–38·4) over the 1950–2023 study period, during which the global age-standardised all-cause mortality rate declined by 66·6% (65·8–67·3). Trends in age-specific mortality rates between 2011 and 2023 varied by age group and location, with the largest decline in under-5 mortality occurring in east Asia (67·7% decrease); the largest increases in mortality for those aged 5–14 years, 25–29 years, and 30–39 years occurring in high-income North America (11·5%, 31·7%, and 49·9%, respectively); and the largest increases in mortality for those aged 15–19 years and 20–24 years occurring in Eastern Europe (53·9% and 40·1%, respectively). We also identified higher than previously estimated mortality rates in sub-Saharan Africa for all sexes combined aged 5–14 years (87·3% higher in GBD 2023 than GBD 2021 on average across countries and territories over the 1950–2021 period) and for females aged 15–29 years (61·2% higher), as well as lower than previously estimated mortality rates in sub-Saharan Africa for all sexes combined aged 50 years and older (13·2% lower), reflecting advances in our modelling approach. Global life expectancy followed three distinct trends over the study period. First, between 1950 and 2019, there were considerable improvements, from 51·2 (50·6–51·7) years for females and 47·9 (47·4–48·4) years for males in 1950 to 76·3 (76·2–76·4) years for females and 71·4 (71·3–71·5) years for males in 2019. Second, this period was followed by a decrease in life expectancy during the COVID-19 pandemic, to 74·7 (74·6–74·8) years for females and 69·3 (69·2–69·4) years for males in 2021. Finally, the world experienced a period of post-pandemic recovery in 2022 and 2023, wherein life expectancy generally returned to pre-pandemic (2019) levels in 2023 (76·3 [76·0–76·6] years for females and 71·5 [71·2–71·8] years for males). 194 (95·1%) of 204 countries and territories experienced at least partial post-pandemic recovery in age-standardised mortality rates by 2023, with 61·8% (126 of 204) recovering to or falling below pre-pandemic levels. There were several mortality trajectories during and following the pandemic across countries and territories. Long-term mortality trends also varied considerably between age groups and locations, demonstrating the diverse landscape of health outcomes globally.

Interpretation This analysis identified several key differences in mortality trends from previous estimates, including higher rates of adolescent mortality, higher rates of young adult mortality in females, and lower rates of mortality in older age groups in much of sub-Saharan Africa. The findings also highlight stark differences across countries and territories in the timing and scale of changes in all-cause mortality trends during and following the COVID-19 pandemic (2020–23). Our estimates of evolving trends in mortality and life expectancy across locations, ages, sexes, and SDI levels in recent years as well as over the entire 1950–2023 study period provide crucial information for governments, policy makers, and the public to ensure that health-care systems, economies, and societies are prepared to address the world's health needs, particularly in populations with higher rates of mortality than previously known. The estimates from this study provide a robust framework for GBD and a valuable foundation for policy development, implementation, and evaluation around the world.

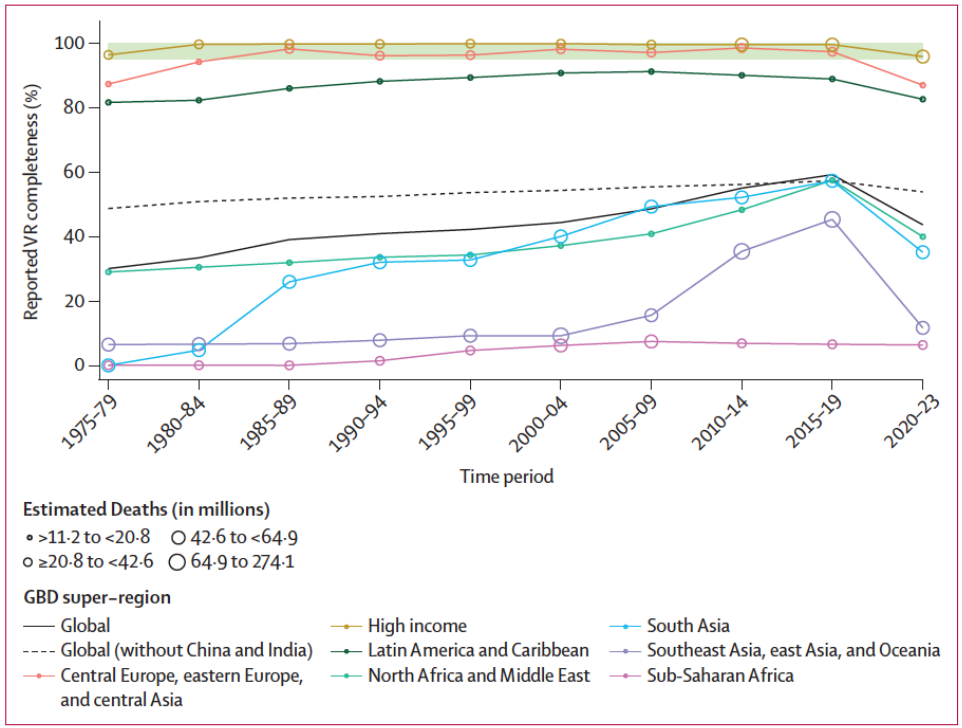

Figure 1: **Completeness of reported VR system data by GBD super-region, 1975–2023**
Completeness is defined as the total number of deaths registered in all VR systems within a super-region during a 5-year period divided by the total number of estimated deaths within that super-region and period, with 100% completeness indicating that all deaths were registered. The size of the datapoints represents the number of estimated deaths. The solid black line shows global completeness, the dashed black line indicates global completeness excluding China and India, and the other coloured lines indicate GBD super-regions. The green shaded box indicates complete registration (defined as >95%). GBD=Global Burden of Diseases, Injuries, and Risk Factors Study. VR=vital registration.

Figure 2: **Annual change in number of deaths, for broad age groups and all ages combined, 1970–2023**
Annual change is defined as the difference between the number of deaths in the current year and the preceding year. The y-axis scales differ by age group. The large change in the age groups 5–14 years and 15–39 years between 1994 and 1995 was due to deaths during the Rwandan genocide. The large change in the age groups 15–39 years, 40–59 years, and ≥60 years between 2020 and 2022 was due to deaths during the COVID-19 pandemic. GBD=Global Burden of Diseases, Injuries, and Risk Factors Study.

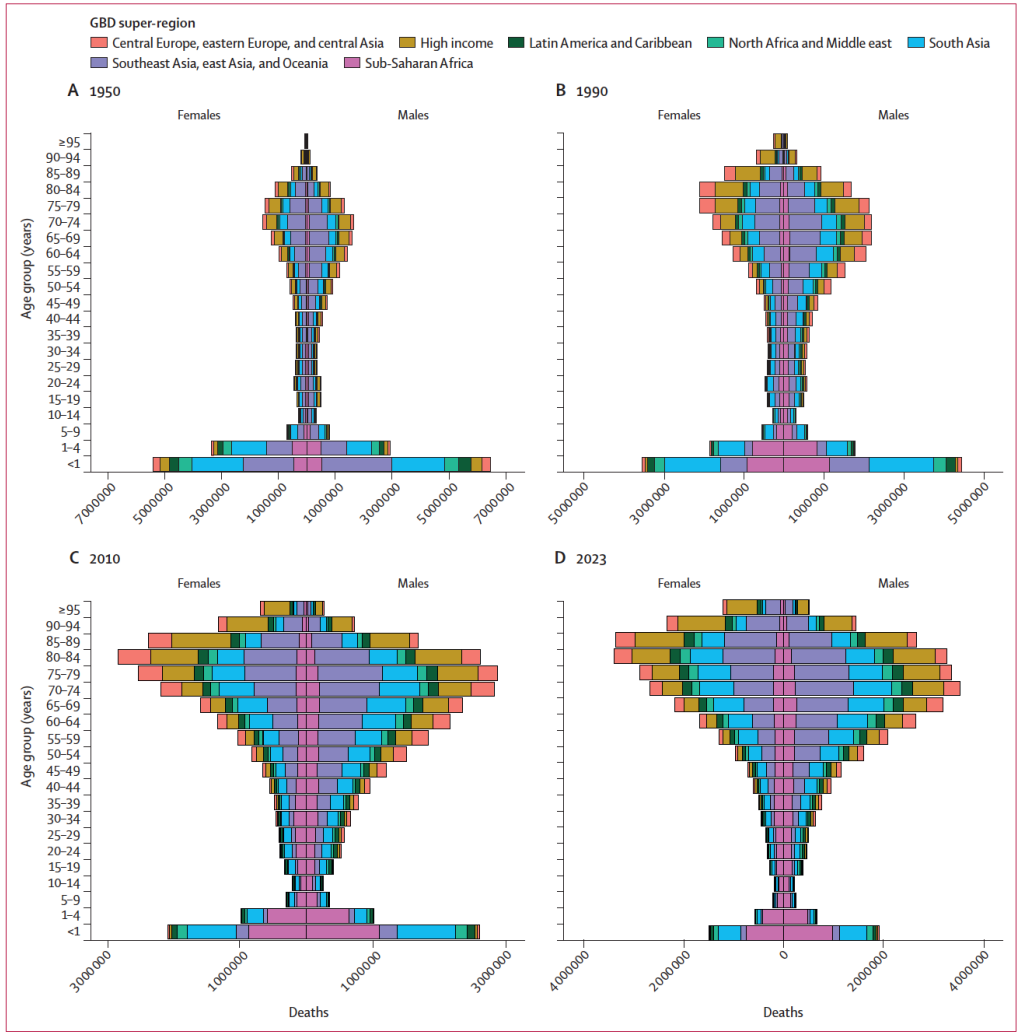

Figure 3: **Age-specific deaths by sex and GBD super-region, in 1950 (A), 1990 (B), 2010 (C), and 2023 (D)**
The number of female deaths (left side) can be compared to male deaths (right side) by age group for four distinct years. The x-axis scales differ by year. Different colours show GBD super-regions. GBD=Global Burden of Diseases, Injuries, and Risk Factors Study.

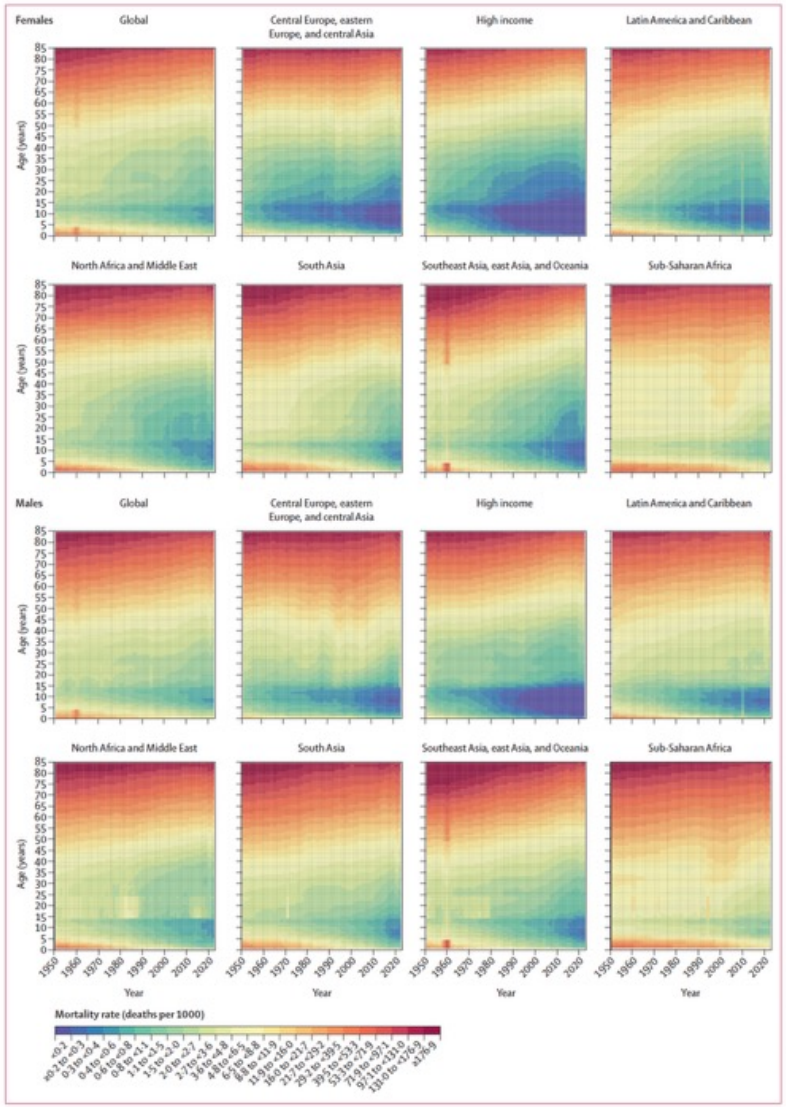

Figure 4: **All-cause mortality rates globally and by GBD super-region across the lifespan in females and males, 1950–2023**
Mortality rates are expressed as the number of deaths per 1000 population. GBD=Global Burden of Diseases, Injuries, and Risk Factors Study.

A

	Neonatal	<1 year	<5 years	5–14 years	15–19 years	20–24 years	25–29 years	30–39 years	40–49 years	50–59 years	60–79 years	≥80 years
Andean Latin America	−64·3%	−71·9%	−80·4%	−83·4%	−69·9%	−73·9%	−73·9%	−70·7%	−64·5%	−54·2%	−46·3%	−47·4%
East Asia	−68·1%	−74·8%	−80·2%	−81·1%	−74·3%	−67·9%	−57·4%	−50·3%	−50·7%	−48·6%	−52·6%	−52·4%
South Asia	−46·9%	−59·3%	−67·4%	−61·5%	−41·4%	−45·2%	−45·4%	−43·4%	−41·8%	−39·8%	−41·8%	−37·7%
North Africa and Middle East	−64·7%	−76·4%	−81·9%	−69·7%	−51·1%	−55·9%	−55·7%	−56·5%	−48·5%	−37·9%	−39·5%	−34·3%
High-income Asia Pacific	−91·2%	−91·3%	−92·9%	−91·0%	−94·0%	−92·4%	−87·7%	−80·7%	−71·7%	−65·5%	−60·8%	−44·3%
Southeast Asia	−61·9%	−68·7%	−76·1%	−73·2%	−61·0%	−61·0%	−57·0%	−54·7%	−52·3%	−51·5%	−54·5%	−42·6%
Central Latin America	−70·0%	−74·2%	−79·6%	−82·6%	−65·2%	−63·9%	−64·7%	−64·6%	−61·3%	−48·5%	−39·1%	−19·1%
Tropical Latin America	−65·8%	−71·8%	−78·7%	−80·0%	−46·9%	−43·6%	−45·7%	−51·5%	−48·2%	−38·2%	−41·4%	−33·0%
Western sub-Saharan Africa	−17·9%	−23·9%	−40·8%	−40·7%	−26·0%	−34·7%	−33·1%	−23·2%	−20·8%	−23·8%	−22·5%	−24·2%
Eastern sub-Saharan Africa	−22·6%	−17·7%	−30·5%	−28·8%	3·2%	−9·5%	−9·4%	2·3%	−2·8%	−16·6%	−19·8%	−27·3%
Central sub-Saharan Africa	−28·7%	−26·3%	−38·6%	−40·2%	−23·2%	−31·0%	−28·1%	−18·2%	−24·3%	−34·8%	−31·0%	−23·5%
Southern Latin America	−74·8%	−75·6%	−79·1%	−75·5%	−68·5%	−68·1%	−64·6%	−60·2%	−51·1%	−42·3%	−22·8%	−21·7%
Central Asia	−55·2%	−65·2%	−71·3%	−69·9%	−52·3%	−50·8%	−42·6%	−35·9%	−27·7%	−25·3%	−26·6%	−25·3%
Oceania	−56·1%	−65·3%	−71·7%	−65·8%	−47·7%	−50·6%	−48·8%	−44·6%	−42·9%	−42·3%	−45·9%	−36·0%
Central Europe	−82·0%	−83·3%	−85·6%	−74·9%	−67·6%	−68·3%	−63·3%	−42·3%	−19·1%	−8·1%	−16·0%	−20·0%
Western Europe	−85·6%	−84·8%	−85·9%	−73·9%	−51·5%	−52·6%	−54·6%	−48·8%	−44·1%	−36·8%	−34·1%	−30·5%
Southern sub-Saharan Africa	−51·1%	−51·3%	−62·3%	−69·5%	−52·3%	−58·5%	−56·6%	−46·5%	−43·7%	−45·8%	−47·8%	−39·9%
Caribbean	−43·8%	−46·1%	−54·6%	−59·2%	−43·9%	−49·2%	−46·9%	−42·0%	−41·2%	−36·8%	−21·7%	−35·3%
Australasia	−70·7%	−67·9%	−69·7%	−68·5%	−33·9%	−31·3%	−28·8%	−41·9%	−49·7%	−45·2%	−33·7%	−31·1%
High-income North America	−71·0%	−67·7%	−68·2%	−61·1%	−31·8%	−34·0%	−28·2%	−30·5%	−45·5%	−42·2%	−31·7%	−26·2%
Eastern Europe	−67·1%	−71·1%	−77·9%	−53·9%	−21·8%	−19·1%	−3·3%	−1·1%	12·2%	2·9%	−10·8%	−16·2%

Percentage change, 1950–1990

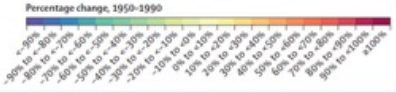

B

	Neonatal	<1 year	<5 years	5–14 years	15–19 years	20–24 years	25–29 years	30–39 years	40–49 years	50–59 years	60–79 years	≥80 years
Andean Latin America	−57·1%	−63·5%	−66·7%	−47·2%	−31·4%	−30·4%	−25·2%	−26·7%	−25·9%	−19·5%	−13·7%	−11·5%
East Asia	−75·9%	−77·1%	−75·9%	−57·8%	−65·1%	−68·3%	−55·9%	−49·6%	−44·4%	−50·0%	−43·9%	−26·9%
South Asia	−47·8%	−54·1%	−59·8%	−62·0%	−46·2%	−40·0%	−33·4%	−27·7%	−27·9%	−28·4%	−21·5%	−12·2%
North Africa and Middle East	−51·2%	−56·9%	−59·4%	−56·0%	−30·5%	−27·4%	−27·9%	−31·8%	−31·0%	−27·0%	−26·1%	−21·2%
High-income Asia Pacific	−59·0%	−57·6%	−56·1%	−54·9%	−50·8%	−38·6%	−36·9%	−37·5%	−35·0%	−35·7%	−32·8%	−24·0%
Southeast Asia	−45·9%	−55·0%	−57·9%	−52·2%	−33·5%	−25·6%	−16·1%	−14·1%	−13·6%	−12·2%	−17·1%	−14·6%
Central Latin America	−41·8%	−51·7%	−55·7%	−47·5%	−13·3%	−14·4%	−16·9%	−22·4%	−26·6%	−25·2%	−23·6%	−16·9%
Tropical Latin America	−41·8%	−61·2%	−58·6%	−26·9%	8·8%	−2·8%	−14·7%	−24·0%	−23·5%	−23·3%	−20·3%	−15·6%
Western sub-Saharan Africa	−29·3%	−38·8%	−48·1%	−46·3%	−32·3%	−29·0%	−17·6%	−2·4%	−2·9%	−13·4%	−12·0%	−10·7%
Eastern sub-Saharan Africa	−32·2%	−49·1%	−55·8%	−56·6%	−55·9%	−54·7%	−42·9%	−24·5%	−13·1%	−7·1%	−8·7%	−6·2%
Central sub-Saharan Africa	−25·9%	−39·4%	−45·9%	−37·3%	−25·2%	−32·1%	−25·5%	−7·0%	−1·1%	−8·0%	−3·0%	−7·1%
Southern Latin America	−50·0%	−53·7%	−52·3%	−33·0%	−1·0%	−7·4%	−14·0%	−23·8%	−31·6%	−29·7%	−22·9%	−10·8%
Central Asia	−38·2%	−47·4%	−47·0%	−31·7%	−25·2%	−26·2%	−17·7%	−7·7%	−15·9%	−13·9%	10·2%	−6·0%
Oceania	−11·1%	−19·9%	−22·7%	−29·1%	−23·0%	−8·5%	7·1%	9·9%	−3·5%	−5·7%	−9·6%	−5·0%
Central Europe	−60·3%	−67·8%	−68·4%	−53·7%	−38·3%	−38·1%	−40·7%	−44·8%	−33·1%	−23·3%	−24·9%	−21·0%
Western Europe	−48·8%	−55·0%	−55·8%	−54·1%	−52·6%	−51·0%	−48·7%	−43·6%	−33·8%	−31·7%	−37·8%	−20·4%
Southern sub-Saharan Africa	−7·0%	−7·2%	−6·0%	20·8%	12·5%	30·8%	100·7%	180·2%	124·1%	57·5%	29·5%	3·6%
Caribbean	−25·8%	−30·8%	−34·7%	−33·9%	−20·3%	−16·3%	−12·1%	−16·9%	−20·1%	−14·6%	−18·3%	−6·0%
Australasia	−38·5%	−48·5%	−49·5%	−45·7%	−46·5%	−48·0%	−40·9%	−27·2%	−26·1%	−41·5%	−46·3%	−18·4%
High-income North America	−30·6%	−34·9%	−39·7%	−45·7%	−43·2%	−21·2%	−21·3%	−26·9%	−14·0%	−21·2%	−31·8%	−8·9%
Eastern Europe	−50·1%	−51·6%	−45·1%	−44·4%	−26·0%	−8·9%	21·9%	39·1%	14·7%	3·3%	1·0%	−12·0%

Percentage change, 1990–2011

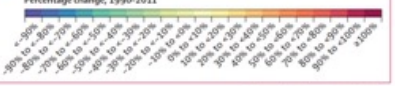

(Figure 5 continues on next page)

Figure 5: **Percentage change in age-specific mortality rates by GBD region, 1950–1990 (A), 1990–2011 (B), and 2011–2023 (C)**
Percentage change for a year range is calculated as the difference in the estimates between the second year and the first year, divided by the estimate in the first year. The boxes range from blue (indicating a decrease in mortality rate between the 2 years), to yellow (indicating no or minimal change between the 2 years), to red (indicating an increase in mortality rate between the 2 years). Darker colours represent a more substantial change. GBD regions are listed in descending order by greatest increase in life expectancy from 1950 to 2023. GBD=Global Burden of Diseases, Injuries, and Risk Factors Study.

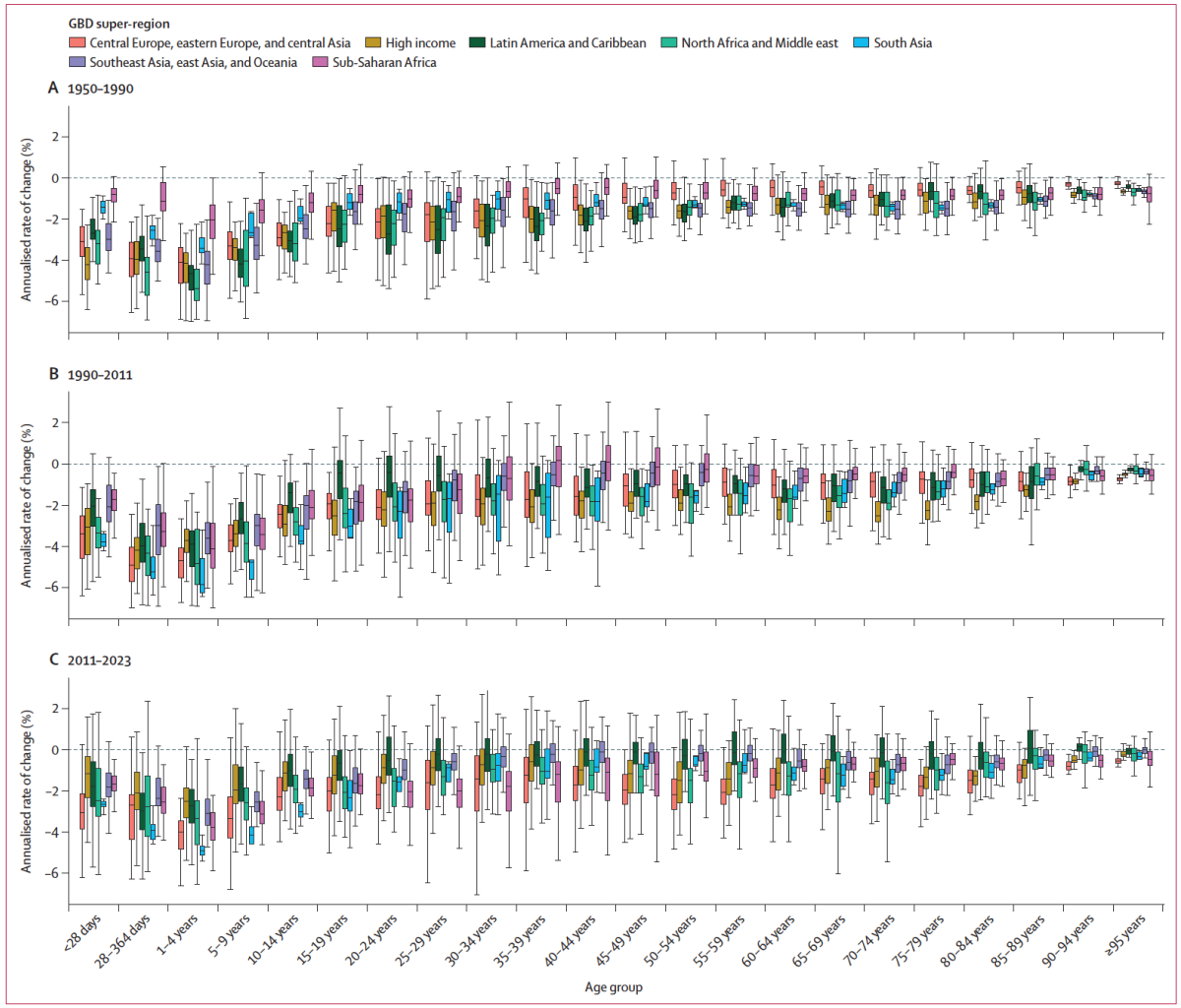

Figure 6: **Distribution of ARC in age-specific mortality rates across countries and territories by GBD super-region, 1950–1990 (A), 1990–2011 (B), and 2011–2023 (C)**
Percentage change for a year range is calculated as the difference in the estimates between the second year and the first year, divided by the estimate in the first year. The boxes represent the middle 50% of the distribution (25th and 75th percentiles), the horizontal line in the boxes indicates the median, and the whiskers show the middle 95% of the distribution (2·5th and 97·5th percentiles). GBD=Global Burden of Diseases, Injuries, and Risk Factors Study.

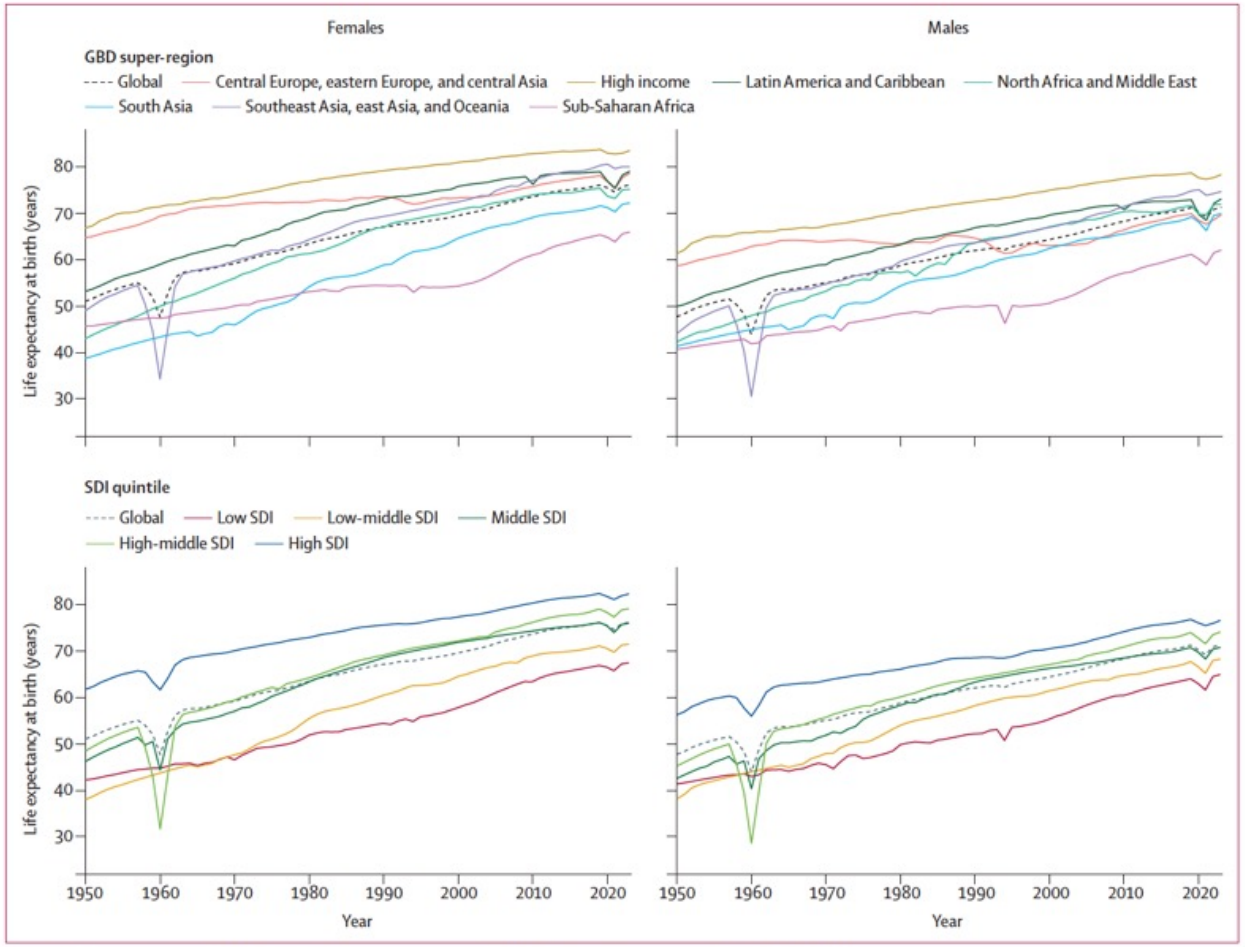

Figure 7: **Life expectancy at birth across GBD super-regions and SDI quintiles in females and males, 1950–2023**
The different colours represent GBD super-regions in the top row and SDI quintiles in the bottom row. The decline in life expectancy in 1960 for the southeast Asia, east Asia, and Oceania super-region (purple line) was due to famine. GBD=Global Burden of Diseases, Injuries, and Risk Factors Study. SDI=Socio-demographic Index.

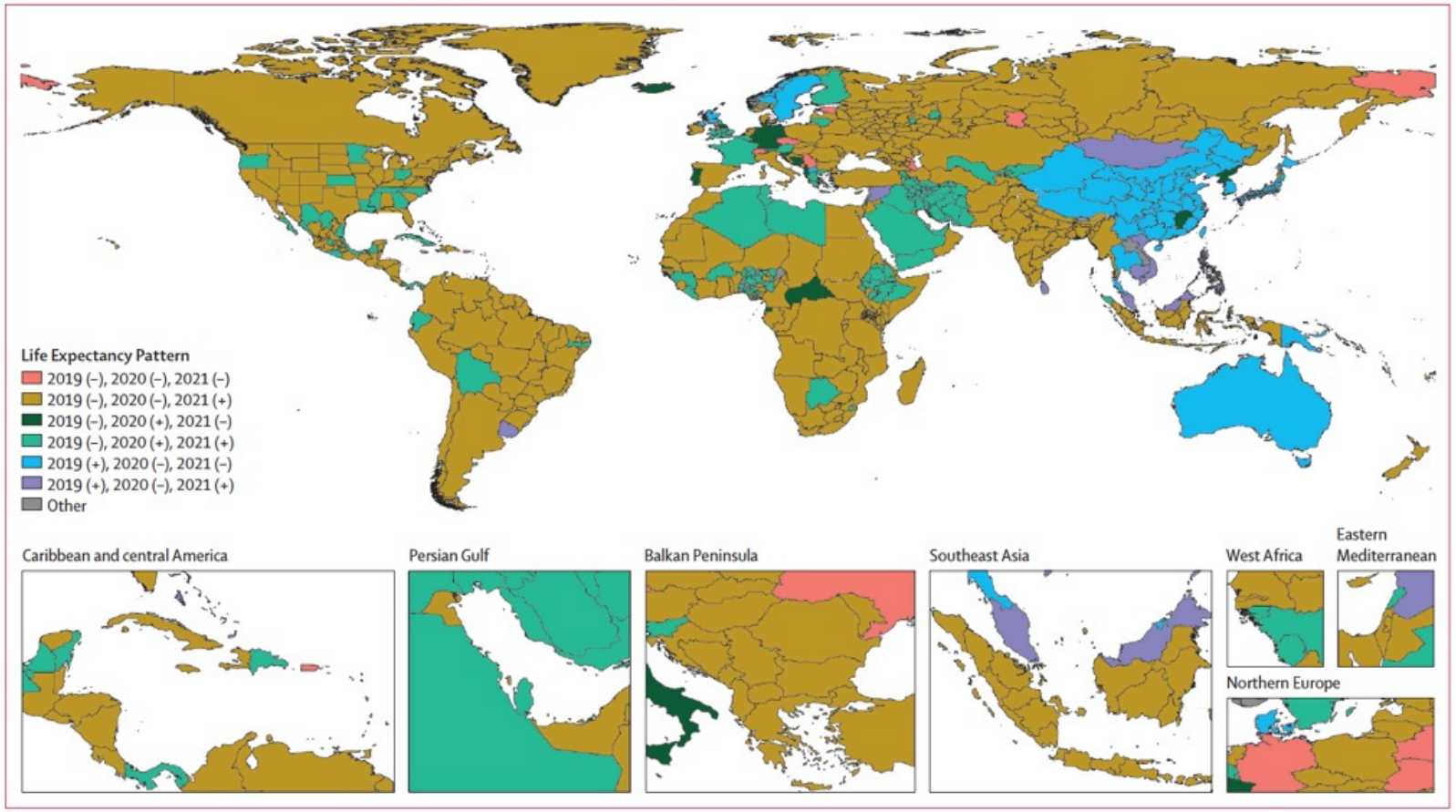

Figure 8: **Patterns of location-specific changes in life expectancy during and following the COVID-19 pandemic (2019–22)**
The life expectancy pattern is based on whether life expectancy increased (+) or decreased (–) between two adjacent years. The + or – after 2019 compares 2019 to 2020, the + or – after 2020 compares 2020 to 2021, and the + or – after 2021 compares 2021 to 2022. For example, the – after 2019 indicates that life expectancy was lower in 2020 compared to 2019. The Other category corresponds to the remaining 2 life expectancy patterns not otherwise listed.

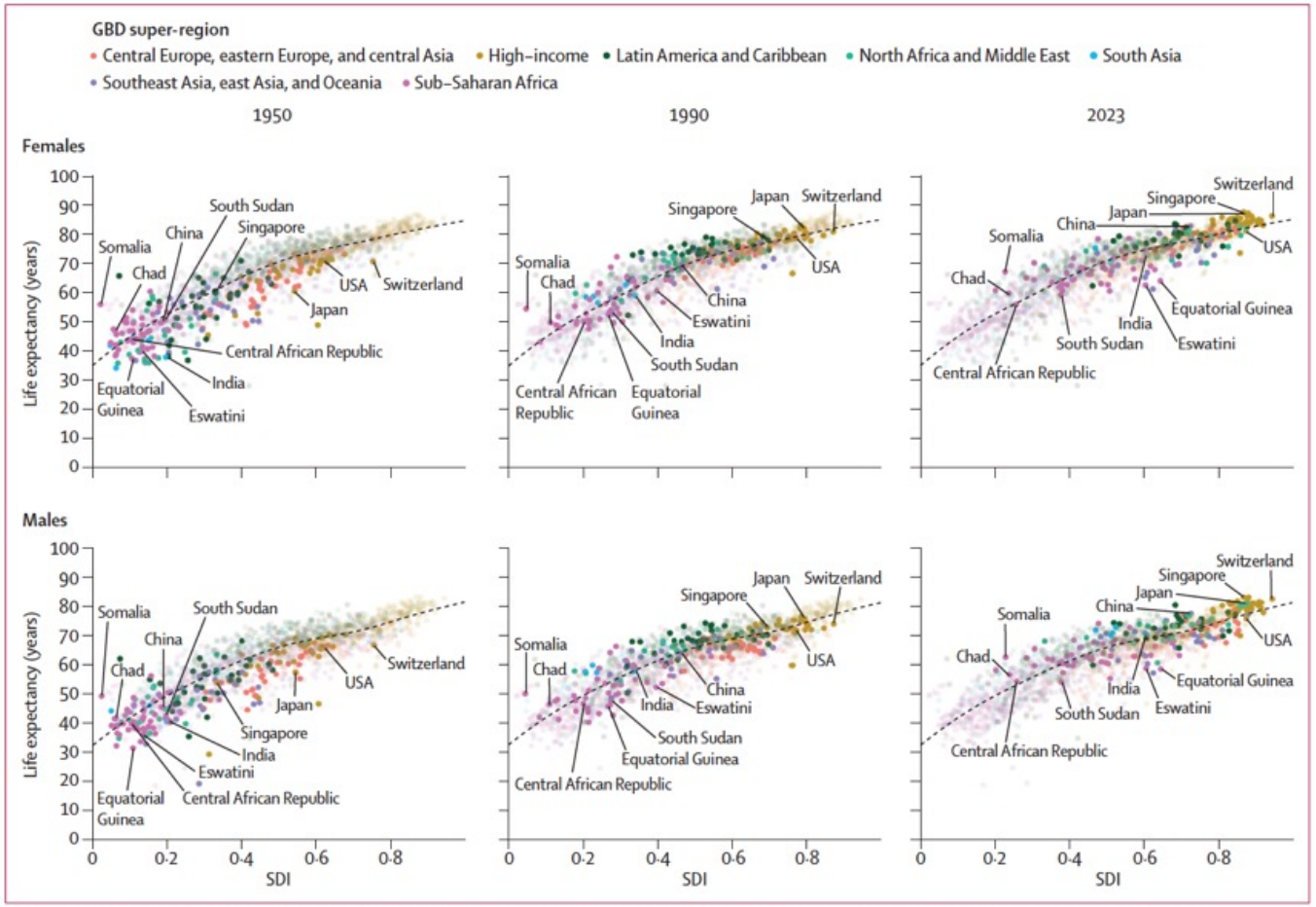

Figure 9: **National life expectancy at birth versus SDI, and expected life expectancy based on SDI, in females and males, in 1950, 1990, and 2023**
Life expectancy at birth is shown for 204 countries and territories coloured by GBD super-region. Transparent points in all plots show every fifth year between 1950, 2015, and 2023 in the first two columns. The black line represents the expected life expectancy at birth based on SDI, and the shaded area corresponds to 95% uncertainty intervals. The labelled countries are those mentioned in the Results section for having the highest or lowest value of a mortality indicator. GBD=Global Burden of Diseases, Injuries, and Risk Factors Study. SDI=Socio-demographic Index.

Research in context

Evidence before this study

The UN Population Division of the Department of Economic and Social Affairs (UNPD) produces estimates and projections of global, regional, and national demographic metrics that are updated biannually. Its latest findings, published in the World Population Prospects 2024 revision, incorporated estimates of excess mortality due to the COVID-19 pandemic from WHO and the World Mortality Database from 2021 as well as weekly or monthly death registration data for 2022 and 2023 from selected countries. WHO releases all-cause mortality estimates that differ from those of UNPD, most recently with the World Health Statistics 2024 report and associated Global Health Estimates. Some national statistics offices also produce their own demographic indicators. The Organisation for Economic Co-operation and Development and the EU, among others, release mortality estimates less regularly and typically only for selected metrics or locations. The Global Burden of Diseases, Injuries, and Risk Factors Study (GBD) generates regularly updated and globally comparable health metrics, including all-cause mortality and life expectancy, for past years, and, for certain metrics, forecasts up to the year 2100. The current GBD 2023 cycle is directly preceded by GBD 2021, which reported demographic estimates for 204 countries and territories and 811 subnational locations for each year from 1950 to 2021. Although each of these studies represents important efforts to provide insights into all-cause mortality estimates, only GBD demographic estimates are informed by and comparable to estimates of disease, injury, and risk factor burden; they are also the only estimates to comply with the GATHER statement, which identify best practices for reporting global health estimates.

Added value of this study

GBD 2023 developed a novel methodology to directly use age-specific demographic data in a single statistical model that accounts for complex correlation structures in demographic data across age and time. This model, OneMod, includes two primary components: a complex functional generalised linear model specification, and residual smoothing with a multivariate kernel regression model. This is a notable methodological improvement from GBD 2021 and UNPD approaches, which use multiple separate models for mortality indicators that are then input to model life table systems to estimate age patterns of mortality. The new model is simpler, more transparent, and facilitates the use of standard techniques for statistical inference and model assessment. Furthermore, our model uses covariates to capture mortality effects due to HIV/AIDS and the COVID-19 pandemic in locations with little to no data, rather than post-hoc incorporation of estimates from separate models. GBD 2023 used a suite of customised and validated data processing and modelling tools, systematically analysing thousands of data sources to produce global, regional, national, and subnational demographic estimates by age and sex for each year from 1950 to 2023. For the first time, GBD 2023 included data from complete birth histories for children and adolescents aged 5–14 years, used age-specific mortality data from sibling histories rather than a summary of the probability of death from those aged 15–60 years, and incorporated age-specific mortality data from 38 Health and Demographic Surveillance System sites. Compared to GBD 2021, GBD 2023 incorporated 3127 additional data sources, which includes 1211 location-years of provisional all-age vital registration data, which had not previously been used and which provide more timely information. All estimates are packaged within freely accessible data-sharing and visualisation tools.

Implications of all the available evidence

Our study shows higher than previously estimated adolescent mortality and young adult female mortality in much of sub-Saharan Africa, as well as lower old-age mortality in the same region. It also highlights a diversity of trends in all-cause mortality during the COVID-19 pandemic and recovery periods of 2020–23, with stark differences in the timing and extent of mortality fluctuations across countries. Globally comparable estimates show substantial variation between and within countries and territories, which allows analysis of key patterns that can be compared across regions. Additionally, our analyses of evolving long-term trends in mortality and life expectancy across age groups, sexes, and Socio-demographic Index levels reveal changing dynamics and patterns with implications for the future of health-care systems, economies, and societies. Collectively, the estimates reported here provide a robust framework for GBD and a valuable foundation for policy evaluation, development, and implementation around the world.

Global burden of 292 causes of death in 204 countries and territories and 660 subnational locations, 1990–2023: a systematic analysis for the Global Burden of Disease Study 2023

Summary

Background Timely and comprehensive analyses of causes of death stratified by age, sex, and location are essential for shaping effective health policies aimed at reducing global mortality. The Global Burden of Diseases, Injuries, and Risk Factors Study (GBD) 2023 provides cause-specific mortality estimates measured in counts, rates, and years of life lost (YLLs). GBD 2023 aimed to enhance our understanding of the relationship between age and cause of death by quantifying the probability of dying before age 70 years (70q0) and the mean age at death by cause and sex. This study enables comparisons of the impact of causes of death over time, offering a deeper understanding of how these causes affect global populations.

Methods GBD 2023 produced estimates for 292 causes of death disaggregated by age-sex-location-year in 204 countries and territories and 660 subnational locations for each year from 1990 until 2023. We used a modelling tool developed for GBD, the Cause of Death Ensemble model (CODEm), to estimate cause-specific death rates for most causes. We computed YLLs as the product of the number of deaths for each cause-age-sex-location-year and the standard life expectancy at each age. Probability of death was calculated as the chance of dying from a given cause in a specific age period, for a specific population. Mean age at death was calculated by first assigning the midpoint age of each age group for every death, followed by computing the mean of all midpoint ages across all deaths attributed to a given cause. We used GBD death estimates to calculate the observed mean age at death and to model the expected mean age across causes, sexes, years, and locations. The expected mean age reflects the expected mean age at death for individuals within a population, based on global mortality rates and the population's age structure. Comparatively, the observed mean age represents the actual mean age at death, influenced by all factors unique to a location-specific population, including its age structure. As part of the modelling process, uncertainty intervals (UIs) were generated using the 2·5th and 97·5th percentiles from a 250-draw distribution for each metric. Findings are reported as counts and age-standardised rates. Methodological improvements for cause-of-death estimates in GBD 2023 include a correction for the misclassification of deaths due to COVID-19, updates to the method used to estimate COVID-19, and updates to the CODEm modelling framework. This analysis used 55 761 data sources, including vital registration and verbal autopsy data as well as data from surveys, censuses, surveillance systems, and cancer registries, among others. For GBD 2023, there were 312 new country-years of vital registration cause-of-death data, 3 country-years of surveillance data, 51 country-years of verbal autopsy data, and 144 country-years of other data types that were added to those used in previous GBD rounds.

Findings The initial years of the COVID-19 pandemic caused shifts in long-standing rankings of the leading causes of global deaths: it ranked as the number one age-standardised cause of death at Level 3 of the GBD cause classification hierarchy in 2021. By 2023, COVID-19 dropped to the 20th place among the leading global causes, returning the rankings of the leading two causes to those typical across the time series (ie, ischaemic heart disease and stroke). While ischaemic heart disease and stroke persist as leading causes of death, there has been progress in reducing their age-standardised mortality rates globally. Four other leading causes have also shown large declines in global age-standardised mortality rates across the study period: diarrhoeal diseases, tuberculosis, stomach cancer, and measles. Other causes of death showed disparate patterns between sexes, notably for deaths from conflict and terrorism in some locations. A large reduction in age-standardised rates of YLLs occurred for neonatal disorders. Despite this, neonatal disorders remained the leading cause of global YLLs over the period studied, except in 2021, when COVID-19 was temporarily the leading cause. Compared to 1990, there has been a considerable reduction in total YLLs in many vaccine-preventable diseases, most notably diphtheria, pertussis, tetanus, and measles. In addition, this study quantified the mean age at death for all-cause mortality and cause-specific mortality and found noticeable variation by sex and location. The global all-cause mean age at death increased from 46·8 years (95% UI 46·6–47·0) in 1990 to 63·4 years (63·1–63·7) in 2023. For males, mean age increased from 45·4 years (45·1–45·7) to 61·2 years (60·7–61·6), and for females it increased from 48·5 years (48·1–48·8) to 65·9 years (65·5–66·3), from 1990 to 2023. The highest all-cause mean age at death in 2023 was found in the high-income super-region, where the mean age for females reached 80·9 years (80·9–81·0) and for males 74·8 years (74·8–74·9). By comparison, the lowest all-cause mean age at death occurred in sub-Saharan Africa, where it was 38·0 years (37·5–38·4) for females and 35·6 years (35·2–35·9) for males in 2023. Lastly, our study found that all-cause 70q0 decreased across each GBD super-region and region from 2000 to 2023, although with large variability between them. For females, we found that 70q0 notably increased from drug use disorders and conflict and terrorism. Leading causes that increased 70q0 for males also included drug use disorders, as well as diabetes. In sub-Saharan Africa, there was an increase in 70q0 for many non-communicable diseases (NCDs). Additionally, the mean age at death from NCDs was lower than the expected mean age at death for this super-region. By comparison, there was an increase in 70q0 for drug use disorders in the high-income super-region, which also had an observed mean age at death lower than the expected value.

Interpretation We examined global mortality patterns over the past three decades, highlighting—with enhanced estimation methods—the impacts of major events such as the COVID-19 pandemic, in addition to broader trends such as increasing NCDs in low-income regions that reflect ongoing shifts in the global epidemiological transition. This study also delves into premature mortality patterns, exploring the interplay between age and causes of death and deepening our understanding of where targeted resources could be applied to further reduce preventable sources of mortality. We provide essential insights into global and regional health disparities, identifying locations in need of targeted interventions to address both communicable and non-communicable diseases. There is an ever-present need for strengthened health-care systems that are resilient to future pandemics and the shifting burden of disease, particularly among ageing populations in regions with high mortality rates. Robust estimates of causes of death are increasingly essential to inform health priorities and guide efforts toward achieving global health equity. The need for global collaboration to reduce preventable mortality is more important than ever, as shifting burdens of disease are affecting all nations, albeit at different paces and scales.

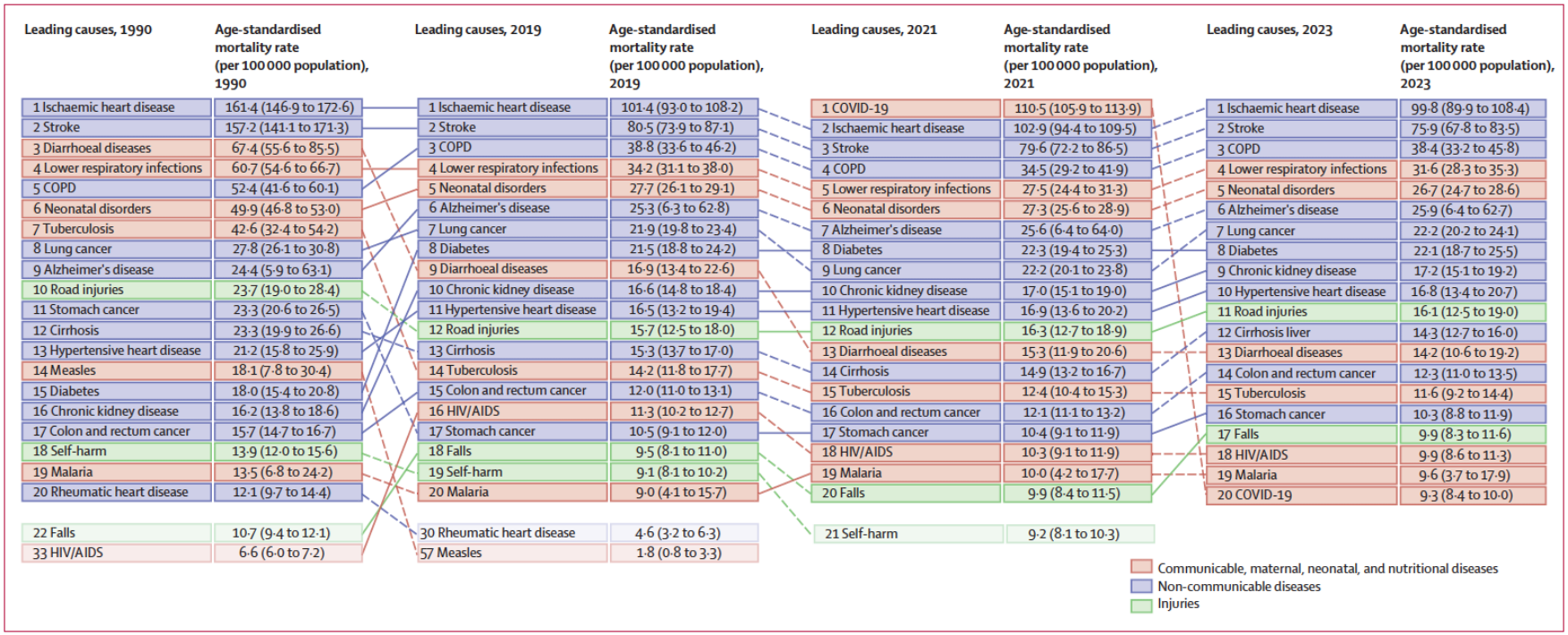

Figure 1: **Leading Level 3 causes of global deaths and age-standardised mortality rate per 100 000 population for all sexes combined, 1990, 2019, 2021, and 2023**

The 20 leading causes of death are shown in descending order. Causes are connected by lines between time periods; solid lines represent an increase or lateral shift in rank and dashed lines represent decreases in rank. Alzheimer's disease=Alzheimer's disease and other dementias. Cirrhosis=cirrhosis and other chronic liver diseases. COPD=chronic obstructive pulmonary disease. Lung cancer=tracheal, bronchus, and lung cancer.

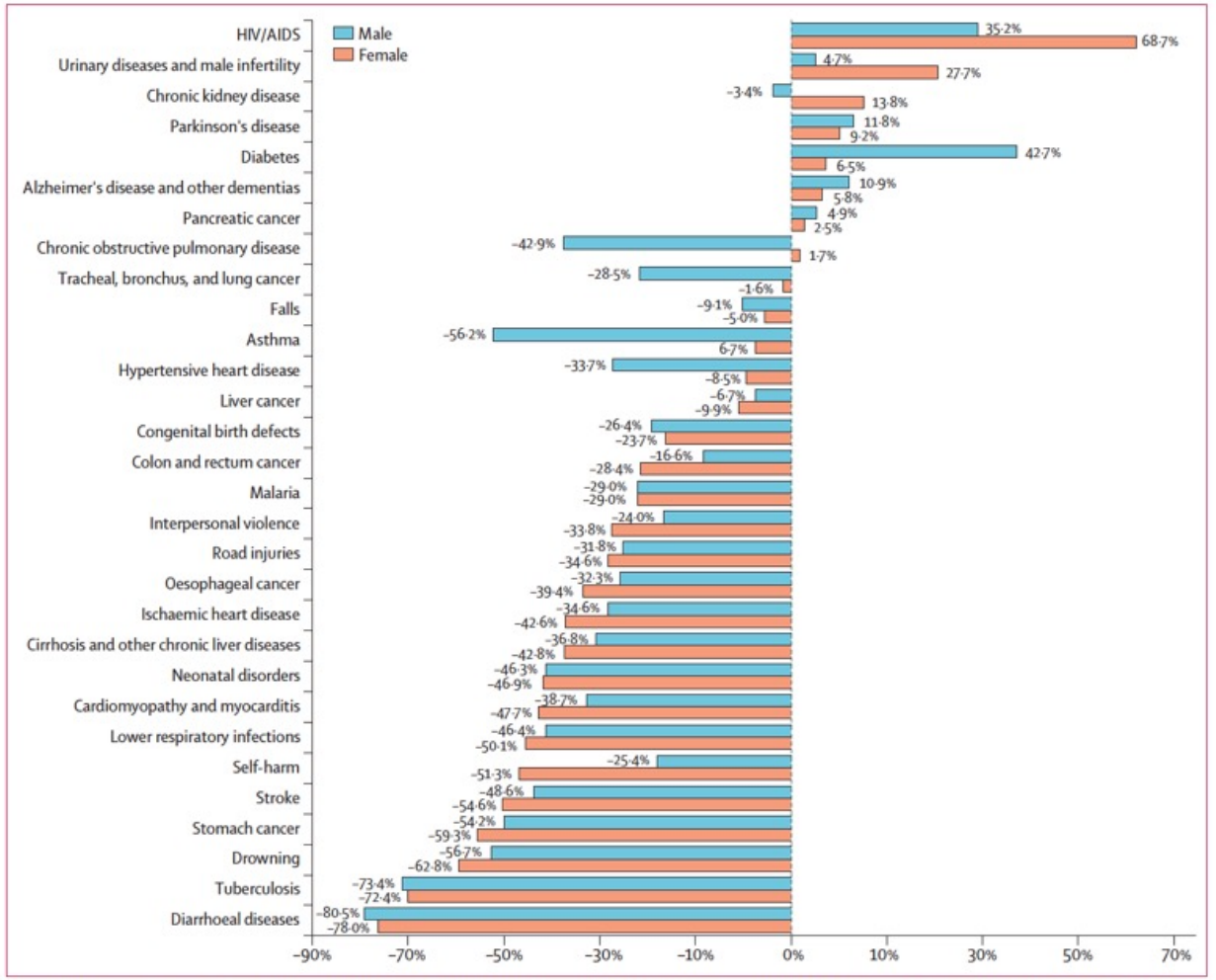

Figure 2: **Percentage change in global age-standardised mortality rate from 1990 to 2023 among the leading 30 Level 3 causes of death, for males and females**

Figure shows the top 30 causes according to their global age-standardised mortality rate, sorted by percentage change from 1990 to 2023 in females, in descending order. COVID-19 and causes affecting only one sex (ie, cervical cancer) were omitted.

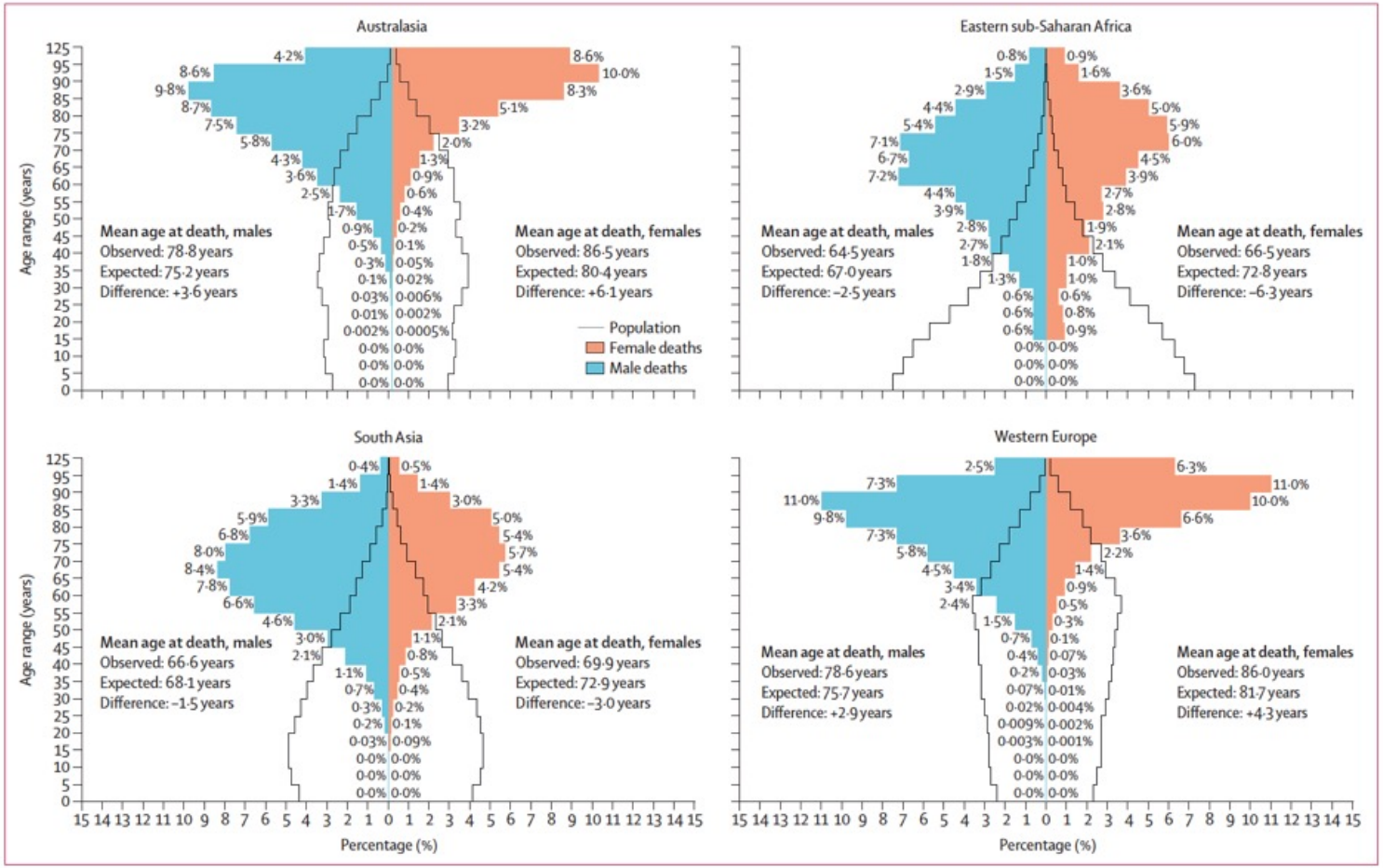

Figure 3: **Comparison of age at death for ischaemic heart disease between four regions for males and females**

Graphs show the distribution of ischaemic heart disease deaths by age and sex within each region. Percentages represent the number of ischaemic heart disease deaths for a given age-sex group out of the total ischaemic heart disease deaths within a region (all ages and sexes combined), or the total number of individuals in a given age-sex group out of the total population in the region. The expected mean age at death is the result of calculating the mean age at death after applying the global mortality rate to a country's population by age and sex for a given cause; a positive difference indicates that the observed mean age at death is higher than expected.

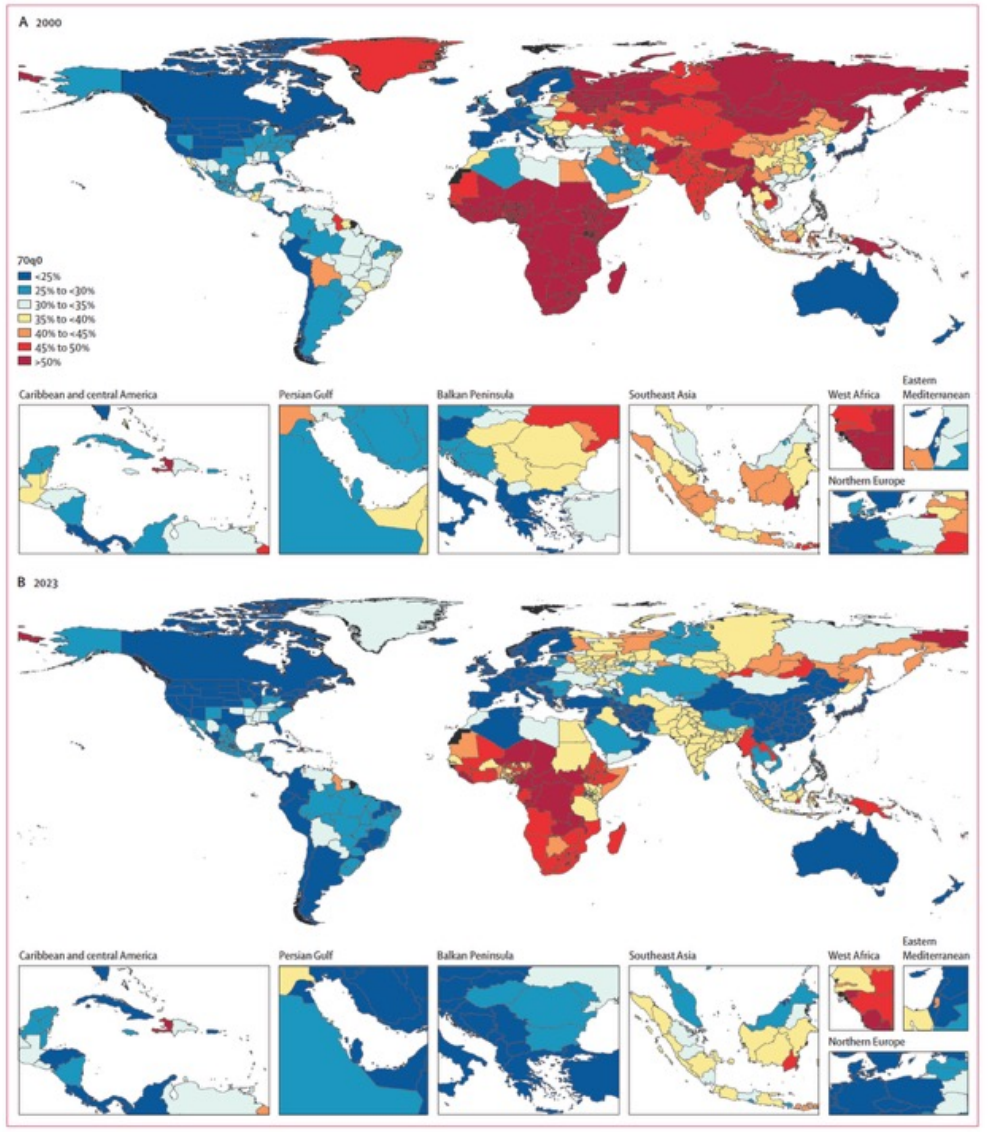
A 2000
70q0
<25%
25% to <30%
30% to <35%
35% to <40%
40% to <45%
45% to 50%
>50%
Caribbean and central America
Persian Gulf
Balkan Peninsula
Southeast Asia
West Africa
Eastern Mediterranean
Northern Europe
B 2023
Caribbean and central America
Persian Gulf
Balkan Peninsula
Southeast Asia
West Africa
Eastern Mediterranean
Northern Europe

	Global	Central Europe, eastern Europe, and central Asia	High income	Latin America and Caribbean	North Africa and Middle East	South Asia	Southeast Asia, east Asia, and Oceania	Sub-Saharan Africa
All causes	−29·1% (33·8% to 23·9%); 65·9 vs 65·9	−33·4% (29·3% to 19·5%); 75·4 vs 73·3	−17·1% (15·6% to 12·9%); 80·9 vs 76·4	−19·1% (25·5% to 20·6%); 68·7 vs 65·4	−23·4% (31·6% to 24·3%); 62·8 vs 54·3	−26·9% (44·0% to 32·2%); 60·7 vs 56·6	−43·1% (29·7% to 16·9%); 72·8 vs 68·4	−27·8% (59·2% to 42·7%); 38·0 vs 42·5
Ischaemic heart disease	−0·5% (2·1% to 2·1%); 77·4 vs 77·4	−42·7% (5·9% to 3·4%); 80·9 vs 78·0	−40·9% (1·5% to 0·9%); 84·5 vs 81·5	−1·8% (1·8% to 1·8%); 77·8 vs 76·9	−0·8% (3·9% to 3·8%); 73·5 vs 72·3	38·9% (2·4% to 3·4%); 69·9 vs 72·9	−8·2% (2·1% to 1·9%); 78·7 vs 76·6	81·1% (0·6% to 1·0%); 69·2 vs 72·6
Stroke	−20·7% (2·4% to 1·9%); 75·8 vs 75·8	−60·7% (4·7% to 1·8%); 80·5 vs 76·7	−45·8% (1·0% to 0·5%); 85·1 vs 80·0	−27·7% (1·8% to 1·3%); 74·8 vs 75·2	−26·4% (3·0% to 2·2%); 72·6 vs 70·7	48·2% (1·9% to 2·9%); 71·0 vs 71·4	−46·0% (4·5% to 2·5%); 76·1 vs 75·1	51·7% (1·1% to 1·7%); 67·4 vs 70·3
Neonatal disorders	−51·5% (2·8% to 1·4%); 0·1 vs 0·1	−32·0% (0·5% to 0·3%); 0·1 vs 0·1	−55·8% (0·3% to 0·1%); 0·1 vs 0·1	−68·1% (2·4% to 0·8%); 0·1 vs 0·1	−66·8% (3·8% to 1·3%); 0·1 vs 0·1	−57·1% (5·6% to 2·4%); 0·0 vs 0·1	−79·8% (1·5% to 0·3%); 0·1 vs 0·1	−22·0% (5·2% to 4·1%); 0·1 vs 0·1
Lower respiratory infections	−51·2% (2·3% to 1·1%); 55·7 vs 55·7	−38·8% (1·0% to 0·6%); 61·3 vs 66·5	−11·7% (0·3% to 0·2%); 85·2 vs 74·5	−38·8% (1·6% to 1·0%); 71·2 vs 55·7	−62·3% (2·5% to 0·9%); 52·7 vs 37·7	−60·4% (3·8% to 1·5%); 45·2 vs 41·6	−71·6% (1·5% to 0·4%); 70·1 vs 62·7	−32·9% (4·6% to 3·1%); 31·8 vs 23·0
Breast cancer	33·6% (0·7% to 1·0%); 63·0 vs 63·0	−26·2% (1·5% to 1·1%); 68·0 vs 65·5	−28·9% (1·5% to 1·1%); 73·2 vs 69·1	35·6% (0·8% to 1·1%); 63·2 vs 62·0	99·0% (0·5% to 1·1%); 58·1 vs 57·7	139·3% (0·4% to 1·1%); 58·6 vs 58·6	6·3% (0·8% to 0·9%); 60·1 vs 63·0	227·9% (0·4% to 1·2%); 57·4 vs 56·2
HIV/AIDS	−58·2% (1·9% to 0·8%); 40·8 vs 40·8	132·3% (0·1% to 0·3%); 40·9 vs 44·2	−66·7% (0·1% to 0·0%); 48·8 vs 45·0	−48·6% (0·8% to 0·4%); 40·8 vs 40·9	−0·9% (0·2% to 0·2%); 38·8 vs 38·5	−73·6% (0·4% to 0·3%); 41·8 vs 38·5	−29·8% (0·2% to 0·2%); 43·8 vs 43·4	−61·7% (10·6% to 4·1%); 40·5 vs 33·7
Diabetes	42·7% (0·6% to 0·8%); 72·0 vs 72·0	33·1% (0·4% to 0·6%); 75·3 vs 73·3	−34·6% (0·4% to 0·3%); 81·0 vs 76·3	18·9% (1·2% to 1·4%); 72·0 vs 71·4	27·8% (0·7% to 0·9%); 71·6 vs 67·6	119·4% (0·7% to 1·5%); 70·2 vs 68·3	2·4% (0·6% to 0·7%); 71·4 vs 71·5	52·6% (0·4% to 0·5%); 66·9 vs 66·4
Chronic obstructive pulmonary disease	12·3% (0·6% to 0·7%); 78·5 vs 78·5	−31·0% (0·3% to 0·2%); 78·6 vs 78·8	18·5% (0·4% to 0·5%); 81·3 vs 81·6	−10·9% (0·4% to 0·4%); 79·6 vs 78·1	22·1% (0·3% to 0·3%); 76·6 vs 74·9	56·8% (1·1% to 1·8%); 75·3 vs 75·2	−38·3% (0·9% to 0·5%); 81·2 vs 77·7	85·5% (0·1% to 0·2%); 73·1 vs 75·4
Diarrhoeal diseases	−72·0% (2·2% to 0·6%); 52·6 vs 52·6	−74·7% (0·1% to 0·0%); 62·9 vs 63·8	33·8% (0·0% to 0·0%); 84·2 vs 70·6	−79·2% (0·8% to 0·2%); 57·3 vs 52·5	−84·6% (1·1% to 0·2%); 24·0 vs 37·0	−75·4% (4·8% to 1·2%); 65·6 vs 40·6	−77·4% (0·6% to 0·1%); 63·2 vs 59·7	−64·4% (5·8% to 2·1%); 26·8 vs 22·6
Road injuries	−20·3% (0·8% to 0·6%); 42·3 vs 42·3	−64·4% (0·6% to 0·2%); 47·0 vs 49·4	−56·2% (0·5% to 0·2%); 53·5 vs 52·1	−32·3% (0·8% to 0·5%); 42·2 vs 42·3	−28·5% (1·0% to 0·7%); 38·8 vs 36·6	11·4% (0·5% to 0·6%); 47·6 vs 37·2	−58·0% (1·2% to 0·5%); 50·3 vs 46·2	57·6% (0·9% to 1·5%); 32·0 vs 29·5
Cervical cancer	23·6% (0·5% to 0·6%); 56·8 vs 56·8	−28·7% (0·6% to 0·4%); 61·7 vs 59·6	−20·6% (0·3% to 0·2%); 66·9 vs 62·0	−14·1% (0·8% to 0·7%); 59·6 vs 56·0	29·7% (0·2% to 0·2%); 57·8 vs 52·7	41·3% (0·6% to 0·8%); 56·4 vs 53·2	−13·1% (0·5% to 0·4%); 60·6 vs 57·5	103·5% (0·6% to 1·2%); 49·1 vs 50·3
Tracheal, bronchus, and lung cancer	15·2% (0·5% to 0·6%); 71·6 vs 71·6	5·8% (0·6% to 0·6%); 70·5 vs 72·8	−9·5% (1·2% to 1·0%); 75·1 vs 75·4	33·7% (0·4% to 0·5%); 69·9 vs 71·1	94·0% (0·2% to 0·4%); 66·1 vs 68·0	192·6% (0·1% to 0·3%); 64·4 vs 68·7	−4·5% (1·0% to 0·9%); 71·0 vs 71·0	143·9% (0·0% to 0·1%); 62·4 vs 67·7
Chronic kidney disease	27·7% (0·5% to 0·6%); 72·1 vs 72·1	−15·3% (0·3% to 0·3%); 74·5 vs 74·3	33·9% (0·2% to 0·3%); 84·6 vs 78·9	12·8% (1·0% to 1·1%); 71·2 vs 71·4	49·4% (0·8% to 1·1%); 70·4 vs 64·4	38·1% (0·4% to 0·5%); 63·0 vs 65·3	−15·3% (0·6% to 0·5%); 69·3 vs 72·0	90·1% (0·4% to 0·7%); 58·7 vs 61·2
Congenital birth defects	−31·3% (0·8% to 0·5%); 5·4 vs 5·4	−32·1% (0·4% to 0·2%); 9·6 vs 7·8	−38·8% (0·3% to 0·2%); 18·7 vs 8·5	−45·1% (1·0% to 0·6%); 7·2 vs 5·8	−49·4% (2·4% to 1·2%); 3·7 vs 4·5	−18·0% (0·8% to 0·7%); 4·0 vs 5·1	−70·4% (0·8% to 0·2%); 8·0 vs 8·3	16·8% (1·0% to 1·2%); 3·8 vs 2·8
Tuberculosis	−60·0% (1·3% to 0·5%); 53·8 vs 53·8	−71·8% (0·3% to 0·1%); 53·6 vs 60·4	−66·9% (0·0% to 0·0%); 81·9 vs 64·0	−51·8% (0·4% to 0·2%); 51·2 vs 53·2	−57·7% (0·4% to 0·2%); 53·5 vs 45·9	−64·8% (2·9% to 1·0%); 58·9 vs 47·1	−72·5% (1·1% to 0·3%); 58·4 vs 57·0	−42·3% (2·5% to 1·4%); 45·5 vs 36·7
Cirrhosis and other chronic liver diseases	−19·3% (0·7% to 0·5%); 62·3 vs 62·3	4·4% (1·1% to 1·2%); 60·5 vs 65·8	−6·1% (0·5% to 0·5%); 69·6 vs 68·9	−13·7% (0·6% to 0·5%); 65·7 vs 61·5	−21·6% (0·8% to 0·6%); 68·5 vs 56·5	−31·3% (0·8% to 0·5%); 57·2 vs 57·3	−44·3% (0·7% to 0·4%); 63·9 vs 63·1	17·5% (0·5% to 0·6%); 53·3 vs 52·0
Maternal disorders	−52·8% (1·0% to 0·5%); 29·5 vs 29·5	−60·7% (0·1% to 0·0%); 31·8 vs 31·2	−7·1% (0·0% to 0·0%); 33·3 vs 30·5	−36·6% (0·5% to 0·3%); 30·6 vs 29·8	−54·7% (0·7% to 0·3%); 31·6 vs 29·4	−74·9% (1·7% to 0·4%); 28·8 vs 28·9	−71·6% (0·5% to 0·1%); 30·9 vs 30·7	−30·8% (2·9% to 2·0%); 29·3 vs 27·6
Colon and rectum cancer	9·4% (0·4% to 0·4%); 72·5 vs 72·5	−19·9% (0·8% to 0·7%); 73·2 vs 73·9	−21·1% (0·7% to 0·5%); 79·0 vs 77·4	57·6% (0·3% to 0·5%); 70·3 vs 71·8	69·9% (0·2% to 0·4%); 66·6 vs 67·3	89·9% (0·1% to 0·3%); 63·6 vs 68·1	−12·1% (0·5% to 0·5%); 70·3 vs 71·9	155·6% (0·1% to 0·2%); 60·3 vs 66·8
Self-harm	−41·6% (0·7% to 0·4%); 45·8 vs 45·8	−51·2% (0·7% to 0·3%); 54·0 vs 52·4	−12·6% (0·5% to 0·4%); 53·0 vs 55·2	15·5% (0·2% to 0·3%); 39·6 vs 45·1	−22·1% (0·2% to 0·2%); 35·5 vs 40·2	−21·4% (1·1% to 0·8%); 36·9 vs 40·2	−77·2% (1·0% to 0·2%); 58·1 vs 48·9	33·2% (0·2% to 0·2%); 40·7 vs 34·8
Hypertensive heart disease	40·9% (0·3% to 0·4%); 79·1 vs 79·1	−32·1% (0·4% to 0·3%); 82·0 vs 79·5	32·4% (0·1% to 0·2%); 86·9 vs 83·0	−13·7% (0·3% to 0·2%); 79·9 vs 78·7	54·0% (0·5% to 0·8%); 75·6 vs 74·1	126·5% (0·2% to 0·5%); 76·2 vs 74·7	−15·2% (0·4% to 0·3%); 79·8 vs 78·2	127·1% (0·2% to 0·5%); 72·1 vs 75·0

Increasing 70q0, mean age at death lower than expected
Increasing 70q0, mean age at death higher than expected
Decreasing 70q0, mean age at death lower than expected
Decreasing 70q0, mean age at death higher than expected

Figure 5: **Change in 70q0 between 2000 and 2023 and the observed versus expected mean age at death in 2023 for females**
The contents of each cell are as follows: percentage change in 70q0 from 2000 to 2023 (70q0 in 2000 to 70q0 in 2023); observed *vs* expected mean age at death in years. 70q0=probability of death before age 70 years.

	Global	Central Europe, eastern Europe, and central Asia	High income	Latin America and Caribbean	North Africa and Middle East	South Asia	Southeast Asia, east Asia, and Oceania	Sub-Saharan Africa
All causes	−26·4% (46·4% to 34·2%); 61·2 vs 61·2	−27·6% (57·4% to 41·5%); 65·5 vs 63·9	−21·3% (27·8% to 21·9%); 74·8 vs 70·7	−14·7% (38·3% to 32·6%); 62·0 vs 61·3	−22·9% (41·4% to 31·9%); 58·6 vs 52·8	−25·8% (51·7% to 38·4%); 58·2 vs 55·0	−33·2% (42·9% to 28·6%); 67·7 vs 64·3	−23·6% (68·3% to 52·2%); 35·6 vs 40·4
Ischaemic heart disease	4·7% (4·1% to 4·3%); 71·1 vs 73·1	−31·4% (12·9% to 8·8%); 72·2 vs 70·7	−36·1% (4·4% to 2·8%); 77·1 vs 75·3	15·6% (3·1% to 3·6%); 71·4 vs 71·2	10·4% (6·2% to 6·8%); 68·3 vs 66·6	40·3% (4·4% to 6·1%); 66·6 vs 68·1	22·7% (3·2% to 3·9%); 72·3 vs 70·8	73·6% (0·8% to 1·5%); 66·2 vs 66·6
Stroke	−15·6% (3·3% to 2·8%); 71·5 vs 71·5	−40·4% (5·9% to 3·5%); 72·6 vs 71·3	−39·7% (1·5% to 0·9%); 79·3 vs 75·5	−15·1% (1·9% to 1·6%); 71·3 vs 71·6	−30·0% (3·1% to 2·2%); 70·0 vs 67·3	30·9% (2·3% to 3·0%); 68·1 vs 68·7	−28·0% (6·1% to 4·4%); 72·0 vs 71·4	36·3% (1·3% to 1·8%); 65·6 vs 66·2
Neonatal disorders	−53·5% (3·8% to 1·9%); 0·1 vs 0·1	−24·1% (0·6% to 0·5%); 0·1 vs 0·1	−55·6% (0·4% to 0·2%); 0·1 vs 0·1	−67·0% (3·0% to 1·0%); 0·1 vs 0·1	−67·0% (4·9% to 1·6%); 0·1 vs 0·1	−60·6% (7·3% to 2·9%); 0·0 vs 0·1	−78·8% (1·9% to 0·4%); 0·1 vs 0·1	−16·5% (7·5% to 6·3%); 0·1 vs 0·1
Road injuries	−21·1% (2·2% to 1·8%); 40·9 vs 40·9	−56·5% (1·9% to 0·8%); 43·6 vs 44·4	−51·2% (1·4% to 0·7%); 49·0 vs 48·3	−19·2% (2·7% to 2·1%); 41·5 vs 40·6	−28·9% (3·0% to 2·1%); 37·6 vs 37·5	27·8% (1·6% to 2·0%); 42·1 vs 37·3	−60·3% (3·2% to 1·3%); 47·3 vs 44·1	66·6% (2·1% to 3·5%); 33·3 vs 31·3
Lower respiratory infections	−47·4% (2·6% to 1·4%); 53·0 vs 53·0	−37·8% (2·0% to 1·2%); 55·6 vs 58·9	−19·5% (0·5% to 0·4%); 81·5 vs 70·0	−28·9% (1·9% to 1·4%); 65·9 vs 53·9	−57·9% (2·6% to 1·1%); 51·1 vs 39·8	−59·0% (3·4% to 1·4%); 44·3 vs 43·3	−64·9% (1·9% to 0·7%); 66·1 vs 60·5	−29·1% (5·7% to 4·0%); 30·0 vs 23·1
Tracheal, bronchus, and lung cancer	−1·1% (1·3% to 1·3%); 69·8 vs 69·8	−31·3% (3·3% to 2·2%); 67·7 vs 69·5	−40·4% (2·8% to 1·7%); 74·1 vs 72·6	−8·5% (0·7% to 0·6%); 69·7 vs 69·7	51·6% (0·8% to 1·2%); 66·4 vs 67·0	105·5% (0·3% to 0·6%); 63·6 vs 68·1	17·0% (1·9% to 2·2%); 69·1 vs 69·4	73·6% (0·2% to 0·3%); 63·5 vs 66·9
Cirrhosis and other chronic liver diseases	−15·7% (1·5% to 1·3%); 58·0 vs 58·0	13·6% (2·0% to 2·3%); 57·2 vs 59·1	−20·4% (1·4% to 1·1%); 65·1 vs 63·1	−10·5% (1·9% to 1·7%); 59·4 vs 57·7	−20·4% (1·3% to 1·0%); 64·9 vs 54·0	−25·3% (1·6% to 1·2%); 55·0 vs 55·1	−30·9% (1·7% to 1·2%); 58·1 vs 59·0	23·8% (1·1% to 1·3%); 50·5 vs 50·9
Diabetes	75·6% (0·6% to 1·0%); 69·0 vs 69·0	83·3% (0·4% to 0·6%); 69·7 vs 69·0	−9·0% (0·6% to 0·5%); 74·8 vs 72·9	72·3% (1·0% to 1·7%); 68·2 vs 68·9	75·6% (0·5% to 0·9%); 68·7 vs 65·1	180·7% (0·6% to 1·7%); 69·2 vs 66·4	35·1% (0·6% to 0·8%); 68·3 vs 68·9	63·3% (0·5% to 0·8%); 63·7 vs 63·8
Chronic obstructive pulmonary disease	−24·9% (1·3% to 0·9%); 76·3 vs 76·3	−43·7% (1·3% to 0·7%); 73·5 vs 75·6	−8·8% (0·7% to 0·6%); 79·7 vs 78·9	−21·4% (0·6% to 0·5%); 77·3 vs 76·5	−13·6% (0·6% to 0·5%); 74·0 vs 73·3	1·7% (2·0% to 2·0%); 74·1 vs 74·1	−51·0% (1·9% to 1·0%); 77·8 vs 75·8	20·1% (0·3% to 0·3%); 71·3 vs 73·9
Self-harm	−24·3% (1·2% to 0·9%); 46·6 vs 46·6	−51·0% (3·3% to 1·6%); 48·7 vs 49·4	−18·5% (1·5% to 1·3%); 52·4 vs 54·0	19·6% (0·8% to 0·9%); 42·8 vs 46·1	6·5% (0·4% to 0·4%); 38·2 vs 42·5	3·5% (1·2% to 1·2%); 40·2 vs 42·5	−56·3% (1·0% to 0·4%); 53·8 vs 49·1	39·4% (0·6% to 0·9%); 42·2 vs 37·7
Tuberculosis	−58·0% (2·1% to 0·9%); 55·2 vs 55·2	−78·5% (1·3% to 0·3%); 53·4 vs 57·6	−69·4% (0·1% to 0·0%); 76·3 vs 62·9	−39·8% (0·6% to 0·4%); 53·9 vs 54·9	−62·8% (0·4% to 0·2%); 55·8 vs 49·6	−62·0% (4·5% to 1·7%); 59·2 vs 50·8	−64·6% (1·5% to 0·5%); 59·4 vs 57·6	−39·4% (3·6% to 2·2%); 47·2 vs 41·8
HIV/AIDS	−55·6% (1·8% to 0·8%); 42·5 vs 42·5	27·1% (0·4% to 0·5%); 41·6 vs 44·7	−71·5% (0·3% to 0·1%); 51·7 vs 46·6	−42·3% (1·2% to 0·7%); 42·5 vs 42·4	−11·1% (0·2% to 0·1%); 40·3 vs 40·5	−53·6% (0·6% to 0·3%); 42·9 vs 40·4	−24·6% (0·4% to 0·3%); 46·0 vs 44·9	−58·8% (9·1% to 3·7%); 41·6 vs 34·9
Chronic kidney disease	18·6% (0·6% to 0·7%); 69·0 vs 69·0	−10·4% (0·4% to 0·3%); 69·5 vs 69·3	44·1% (0·3% to 0·5%); 80·3 vs 74·9	34·1% (1·0% to 1·3%); 69·2 vs 69·1	23·9% (0·9% to 1·1%); 69·3 vs 62·8	4·0% (0·5% to 0·5%); 62·7 vs 64·4	−8·4% (0·7% to 0·6%); 66·7 vs 69·5	51·6% (0·6% to 0·9%); 57·6 vs 59·4
Interpersonal violence	−26·7% (0·9% to 0·7%); 35·1 vs 35·1	−68·7% (1·8% to 0·6%); 46·3 vs 38·0	−10·5% (0·4% to 0·3%); 36·0 vs 39·4	−22·3% (4·6% to 3·5%); 34·8 vs 35·0	14·5% (0·4% to 0·4%); 32·5 vs 33·7	−22·5% (0·5% to 0·4%); 39·9 vs 33·0	−66·5% (0·4% to 0·1%); 38·5 vs 37·6	5·1% (1·2% to 1·3%); 30·7 vs 29·3
Diarrhoeal diseases	−72·4% (2·3% to 0·6%); 42·7 vs 42·7	−76·7% (0·2% to 0·0%); 50·5 vs 50·1	10·4% (0·0% to 0·0%); 79·9 vs 62·7	−79·6% (0·9% to 0·2%); 47·6 vs 43·5	−83·4% (1·1% to 0·2%); 20·6 vs 30·6	−78·7% (4·0% to 0·8%); 62·9 vs 33·7	−78·5% (0·7% to 0·1%); 53·3 vs 51·8	−63·7% (7·3% to 2·6%); 20·0 vs 16·3
Stomach cancer	−31·9% (0·9% to 0·6%); 68·6 vs 68·6	−41·0% (1·3% to 0·8%); 67·6 vs 68·5	−51·1% (0·8% to 0·4%); 75·7 vs 72·1	−8·1% (0·7% to 0·6%); 68·1 vs 68·5	0·9% (0·4% to 0·4%); 67·0 vs 65·2	23·8% (0·3% to 0·4%); 64·1 vs 66·5	−44·4% (2·0% to 1·1%); 68·2 vs 68·4	56·6% (0·1% to 0·2%); 61·6 vs 64·9
Colon and rectum cancer	18·0% (0·5% to 0·6%); 69·7 vs 69·7	7·6% (0·9% to 1·0%); 70·2 vs 69·5	−19·2% (1·0% to 0·8%); 74·9 vs 73·5	84·8% (0·3% to 0·5%); 68·0 vs 69·6	76·8% (0·2% to 0·4%); 66·1 vs 65·8	80·3% (0·1% to 0·3%); 64·6 vs 67·1	35·4% (0·7% to 0·8%); 67·4 vs 69·5	127·2% (0·1% to 0·2%); 63·3 vs 65·4
Congenital birth defects	−35·5% (0·9% to 0·6%); 5·2 vs 5·2	−32·2% (0·4% to 0·3%); 8·4 vs 7·1	−41·8% (0·3% to 0·2%); 20·9 vs 8·3	−46·3% (1·1% to 0·6%); 6·8 vs 5·5	−48·5% (2·2% to 1·1%); 3·3 vs 4·6	−26·8% (1·0% to 0·8%); 3·8 vs 4·9	−70·5% (0·9% to 0·3%); 7·3 vs 8·1	26·4% (1·0% to 1·2%); 3·4 vs 2·5
Falls	−5·2% (0·5% to 0·5%); 64·6 vs 64·6	−34·7% (0·8% to 0·5%); 60·4 vs 66·0	−5·6% (0·3% to 0·3%); 79·1 vs 73·3	−6·0% (0·4% to 0·4%); 64·9 vs 64·8	−5·5% (0·4% to 0·4%); 50·8 vs 56·3	5·2% (0·6% to 0·6%); 62·2 vs 58·1	−35·5% (0·6% to 0·5%); 63·1 vs 66·2	32·6% (0·3% to 0·4%); 48·7 vs 49·4
Hypertensive heart disease	13·1% (0·4% to 0·5%); 73·5 vs 73·5	−2·7% (0·5% to 0·4%); 74·6 vs 72·9	70·5% (0·2% to 0·3%); 77·8 vs 77·4	10·5% (0·3% to 0·3%); 75·2 vs 73·7	−0·4% (0·7% to 0·7%); 72·6 vs 69·1	34·7% (0·4% to 0·5%); 71·8 vs 70·5	−19·4% (0·6% to 0·5%); 74·4 vs 73·2	58·7% (0·3% to 0·4%); 67·5 vs 69·6

Increasing 70q0, mean age at death lower than expected
Increasing 70q0, mean age at death higher than expected
Decreasing 70q0, mean age at death lower than expected
Decreasing 70q0, mean age at death higher than expected

Figure 6: **Change in 70q0 between 2000 and 2023 and the observed versus expected mean age at death in 2023 for males**
The contents of each cell are as follows: percentage change in 70q0 from 2000 to 2023 (70q0 in 2000 to 70q0 in 2023); observed *vs* expected mean age at death in years. 70q0=probability of death before age 70 years.

Research in context

Evidence before this study

The Global Burden of Diseases, Injuries, and Risk Factors Study (GBD) is a worldwide research initiative that provides comprehensive and timely assessments of mortality, morbidity, and risk factors disaggregated to granular levels that are meaningful for policy development. In the last iteration, the GBD 2021 causes-of-death publication marked a major advancement in the evidence base; the study delineated cause-specific mortality to provide insights on the primary causes of death influencing life expectancy across locations. It also identified several causes with shifting mortality trends that had important implications for targeted policy initiatives—causes that were once widespread across the globe but became increasingly localised and in need of tailored reduction strategies. The GBD 2021 causes-of-death analysis was also the first of its kind to publish worldwide estimates of deaths from the initial years of the COVID-19 pandemic, quantifying its effect on life expectancy and offering comparisons to deaths from other causes. While estimates from other studies are published periodically that assess specific causes of death among a subset of populations or across a narrower timeframe, GBD remains the only research effort to offer cause-specific estimates of mortality to this degree of time and location detail and to produce these assessments in peer-reviewed and GATHER-compliant publications.

Added value of this study

This study provides new and more robust evidence of mortality patterns across the globe, updating and extending the analysis from GBD 2021, and reanalysing the entire time series to supersede all previous GBD publications. We provide estimates of cause-specific mortality for 292 causes of death within 204 countries and territories and 660 subnational locations, disaggregated by age and sex, from 1990 to 2023. These estimates include 11 474 new sources compared with GBD 2021. This update advances mortality measurements in several ways. First, we present the probability of death before age 70 years (70q0) by sex and year to enable measurements of premature mortality by individual causes. We describe causes of death that are not following global improvements in 70q0 to highlight locations where disparities are occurring in the likelihood of dying before age 70 years. Second, we calculate the mean age at death by assigning the midpoint age of each age group for every death, followed by computing the overall mean across all deaths attributed to a given cause. Our analysis of mean age of death offers insights into a country's ability to manage different disease burdens relative to global benchmarks, independent of local population structure. Additionally, our study examines the correlation between mean age at death and the Socio-demographic Index (SDI) to evaluate whether countries at the higher end of the SDI exhibit older mean ages at death for a given cause compared with countries with a lower SDI value, while controlling for SDI's effect on population structure. This approach adds a novel dimension to understanding how sociodemographic factors influence both the risk and timing of mortality. This study also builds upon our estimates from GBD 2021 to include 2 additional years of COVID-19 analysis, providing a more comprehensive picture of COVID-19 mortality worldwide. Lastly, we report estimates for several newly disaggregated causes of death, including ulcerative colitis; Crohn's disease; thyroid disease; other endocrine, metabolic, and blood and immune disease; and electrocution.

Implications of all the available evidence

Our study offers a thorough analysis of causes of death over the past 34 years, including new findings into the full duration of the COVID-19 pandemic. We highlight causes of death that have declined in certain locations, which could lend insight for policy change and implementation. We also identify causes that persist as major sources of mortality across populations, signifying priority areas for future intervention. Additionally, our study investigated important age patterns in mortality by estimating the probability of dying from any given cause before age 70 years, thereby advancing our understanding of the relationship between age and cause of death. The Global Health 2050 report set a target to reduce the probability of premature deaths by 50% by 2050. We aim to complement and support this goal by offering an in-depth analysis of 70q0 across time, sex, and geographical locations. Lastly, our mean age of death analysis is a valuable metric for comparing observed mortality levels with expected patterns to help identify locations that are keeping pace with development trends and those that might be falling behind. Evidence from this study can be used to examine epidemiological patterns and trends across time and locations, and to gauge progress in global development goals. These findings can also guide future policy initiatives aimed at furthering reductions in cause-specific mortality and, in particular, achieving better pandemic preparedness within the context of specific locations. In aggregate, cyclical updates to GBD reflect improvements in data availability and enhanced methodology that reduce bias and improve transparency, supporting the development and implementation of new evidence-based health policies worldwide.

Burden of 375 diseases and injuries, risk-attributable burden of 88 risk factors, and healthy life expectancy in 204 countries and territories, including 660 subnational locations, 1990–2023: a systematic analysis for the Global Burden of Disease Study 2023

Summary

Background For more than three decades, the Global Burden of Diseases, Injuries, and Risk Factors Study (GBD) has provided a framework to quantify health loss due to diseases, injuries, and associated risk factors. This paper presents GBD 2023 findings on disease and injury burden and risk-attributable health loss, offering a global audit of the state of world health to inform public health priorities. This work captures the evolving landscape of health metrics across age groups, sexes, and locations, while reflecting on the remaining post-COVID-19 challenges to achieving our collective global health ambitions.

Methods The GBD 2023 combined analysis estimated years lived with disability (YLDs), years of life lost (YLLs), and disability-adjusted life-years (DALYs) for 375 diseases and injuries, and risk-attributable burden associated with 88 modifiable risk factors. Of the more than 310 000 total data sources used for all GBD 2023 (about 30% of which were new to this estimation round), more than 120 000 sources were used for estimation of disease and injury burden and 59 000 for risk factor estimation, and included vital registration systems, surveys, disease registries, and published scientific literature. Data were analysed using previously established modelling approaches, such as disease modelling meta-regression version 2.1 (DisMod-MR 2.1) and comparative risk assessment methods. Diseases and injuries were categorised into four levels on the basis of the established GBD cause hierarchy, as were risk factors using the GBD risk hierarchy. Estimates stratified by age, sex, location, and year from 1990 to 2023 were focused on disease-specific time trends over the 2010–23 period and presented as counts (to three significant figures) and age-standardised rates per 100 000 person-years (to one decimal place). For each measure, 95% uncertainty intervals [UIs] were calculated with the 2·5th and 97·5th percentile ordered values from a 250-draw distribution.

Findings Total numbers of global DALYs grew 6·1% (95% UI 4·0–8·1), from 2·64 billion (2·46–2·86) in 2010 to 2·80 billion (2·57–3·08) in 2023, but age-standardised DALY rates, which account for population growth and ageing, decreased by 12·6% (11·0–14·1), revealing large long-term health improvements. Non-communicable diseases (NCDs) contributed 1·45 billion (1·31–1·61) global DALYs in 2010, increasing to 1·80 billion (1·63–2·03) in 2023, alongside a concurrent 4·1% (1·9–6·3) reduction in age-standardised rates. Based on DALY counts, the leading level 3 NCDs in 2023 were ischaemic heart disease (193 million [176–209] DALYs), stroke (157 million [141–172]), and diabetes (90·2 million [75·2–107]), with the largest increases in age-standardised rates since 2010 occurring for anxiety disorders (62·8% [34·0–107·5]), depressive disorders (26·3% [11·6–42·9]), and diabetes (14·9% [7·5–25·6]). Remarkable health gains were made for communicable, maternal, neonatal, and nutritional (CMNN) diseases, with DALYs falling from 874 million (837–917) in 2010 to 681 million (642–736) in 2023, and a 25·8% (22·6–28·7) reduction in age-standardised DALY rates. During the COVID-19 pandemic, DALYs due to CMNN diseases rose but returned to pre-pandemic levels by 2023. From 2010 to 2023, decreases in age-standardised rates for CMNN diseases were led by rate decreases of 49·1% (32·7–61·0) for diarrhoeal diseases, 42·9% (38·0–48·0) for HIV/AIDS, and 42·2% (23·6–56·6) for tuberculosis. Neonatal disorders and lower respiratory infections remained the leading level 3 CMNN causes globally in 2023, although both showed notable rate decreases from 2010, declining by 16·5% (10·6–22·0) and 24·8% (7·4–36·7), respectively. Injury-related age-standardised DALY rates decreased by 15·6% (10·7–19·8) over the same period. Differences in burden due to NCDs, CMNN diseases, and injuries persisted across age, sex, time, and location. Based on our risk analysis, nearly 50% (1·27 billion [1·18–1·38]) of the roughly 2·80 billion total global DALYs in 2023 were attributable to the 88 risk factors analysed in GBD. Globally, the five level 3 risk factors contributing the highest proportion of risk-attributable DALYs were high systolic blood pressure (SBP), particulate matter pollution, high fasting plasma glucose (FPG), smoking, and low birthweight and short gestation—with high SBP accounting for 8·4% (6·9–10·0) of total DALYs. Of the three overarching level 1 GBD risk factor categories—behavioural, metabolic, and environmental and occupational—risk-attributable DALYs rose between 2010 and 2023 only for metabolic risks, increasing by 30·7% (24·8–37·3); however, age-standardised DALY

rates attributable to metabolic risks decreased by 6·7% (2·0–11·0) over the same period. For all but three of the 25 leading level 3 risk factors, age-standardised rates dropped between 2010 and 2023—eg, declining by 54·4% (38·7–65·3) for unsafe sanitation, 50·5% (33·3–63·1) for unsafe water source, and 45·2% (25·6–72·0) for no access to handwashing facility, and by 44·9% (37·3–53·5) for child growth failure. The three leading level 3 risk factors for which age-standardised attributable DALY rates rose were high BMI (10·5% [0·1 to 20·9]), drug use (8·4% [2·6 to 15·3]), and high FPG (6·2% [–2·7 to 15·6]; non-significant).

Interpretation Our findings underscore the complex and dynamic nature of global health challenges. Since 2010, there have been large decreases in burden due to CMNN diseases and many environmental and behavioural risk factors, juxtaposed with sizeable increases in DALYs attributable to metabolic risk factors and NCDs in growing and ageing populations. This long-observed consequence of the global epidemiological transition was only temporarily interrupted by the COVID-19 pandemic. The substantially decreasing CMNN disease burden, despite the 2008 global financial crisis and pandemic-related disruptions, is one of the greatest collective public health successes known. However, these achievements are at risk of being reversed due to major cuts to development assistance for health globally, the effects of which will hit low-income countries with high burden the hardest. Without sustained investment in evidence-based interventions and policies, progress could stall or reverse, leading to widespread human costs and geopolitical instability. Moreover, the rising NCD burden necessitates intensified efforts to mitigate exposure to leading risk factors—eg, air pollution, smoking, and metabolic risks, such as high SBP, BMI, and FPG—including policies that promote food security, healthier diets, physical activity, and equitable and expanded access to potential treatments, such as GLP-1 receptor agonists. Decisive, coordinated action is needed to address long-standing yet growing health challenges, including depressive and anxiety disorders. Yet this can be only part of the solution. Our response to the NCD syndemic—the complex interaction of multiple health risks, social determinants, and systemic challenges—will define the future landscape of global health. To ensure human wellbeing, economic stability, and social equity, global action to sustain and advance health gains must prioritise reducing disparities by addressing socioeconomic and demographic determinants, ensuring equitable health-care access, tackling malnutrition, strengthening health systems, and improving vaccination coverage. We live in times of great opportunity.

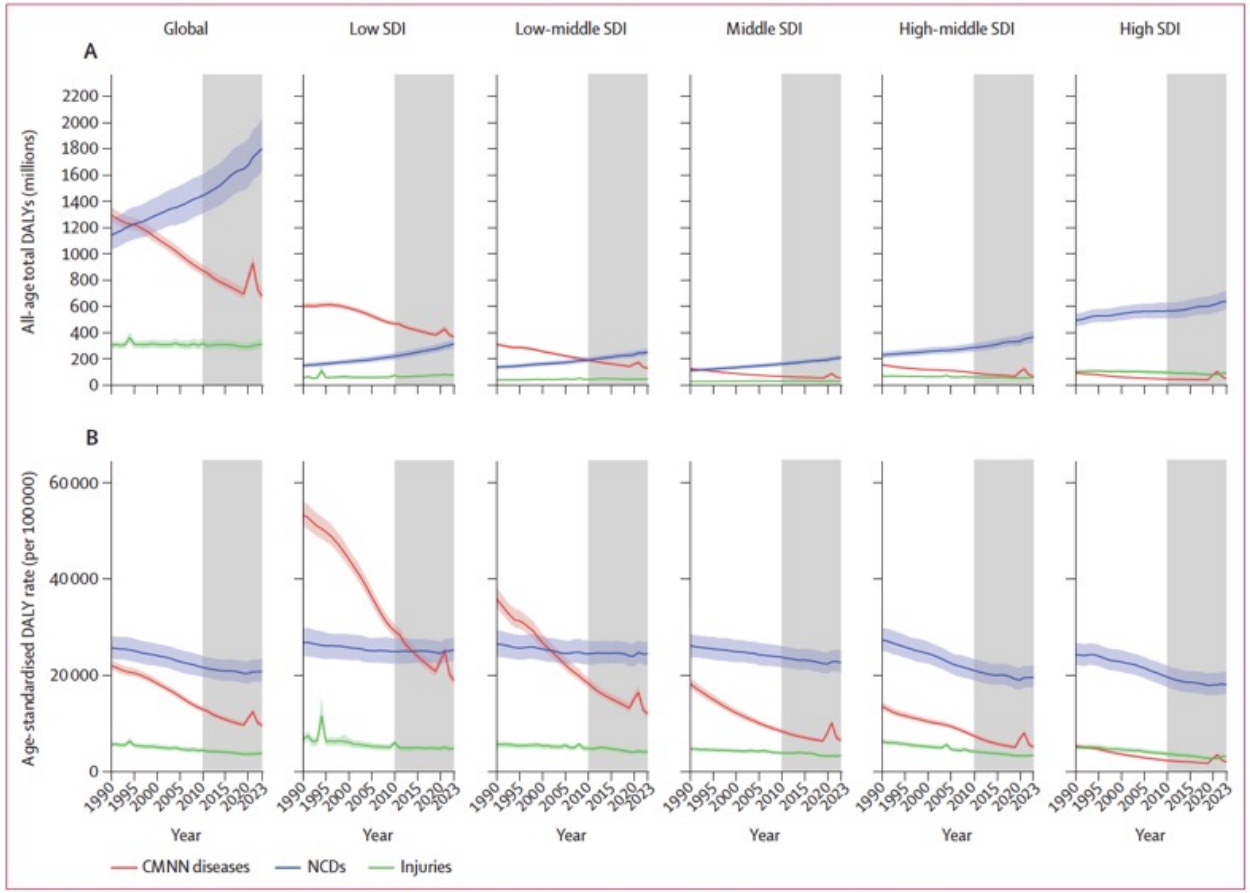

Figure 1: **Trends of total DALYs (A) and age-standardised DALY rates (B) by GBD level 1 cause and by SDI quintile, 1990–2023**
The grey shading indicates the 2010–23 period. The bump in injury-related DALYs that can be seen in the low SDI and global panels in 1994 is largely the result of the Rwanda genocide. The larger bump in CMNN diseases in almost all plots in 2021 and 2022 is the larger DALY effect of the COVID-19 pandemic. Shading around mean trend lines represents 95% uncertainty intervals. CMNN=communicable, maternal, neonatal, and nutritional. DALY=disability-adjusted life-year. GBD=Global Burden of Diseases, Injuries, and Risk Factors Study. NCDs=non-communicable diseases. SDI=Socio-demographic Index.

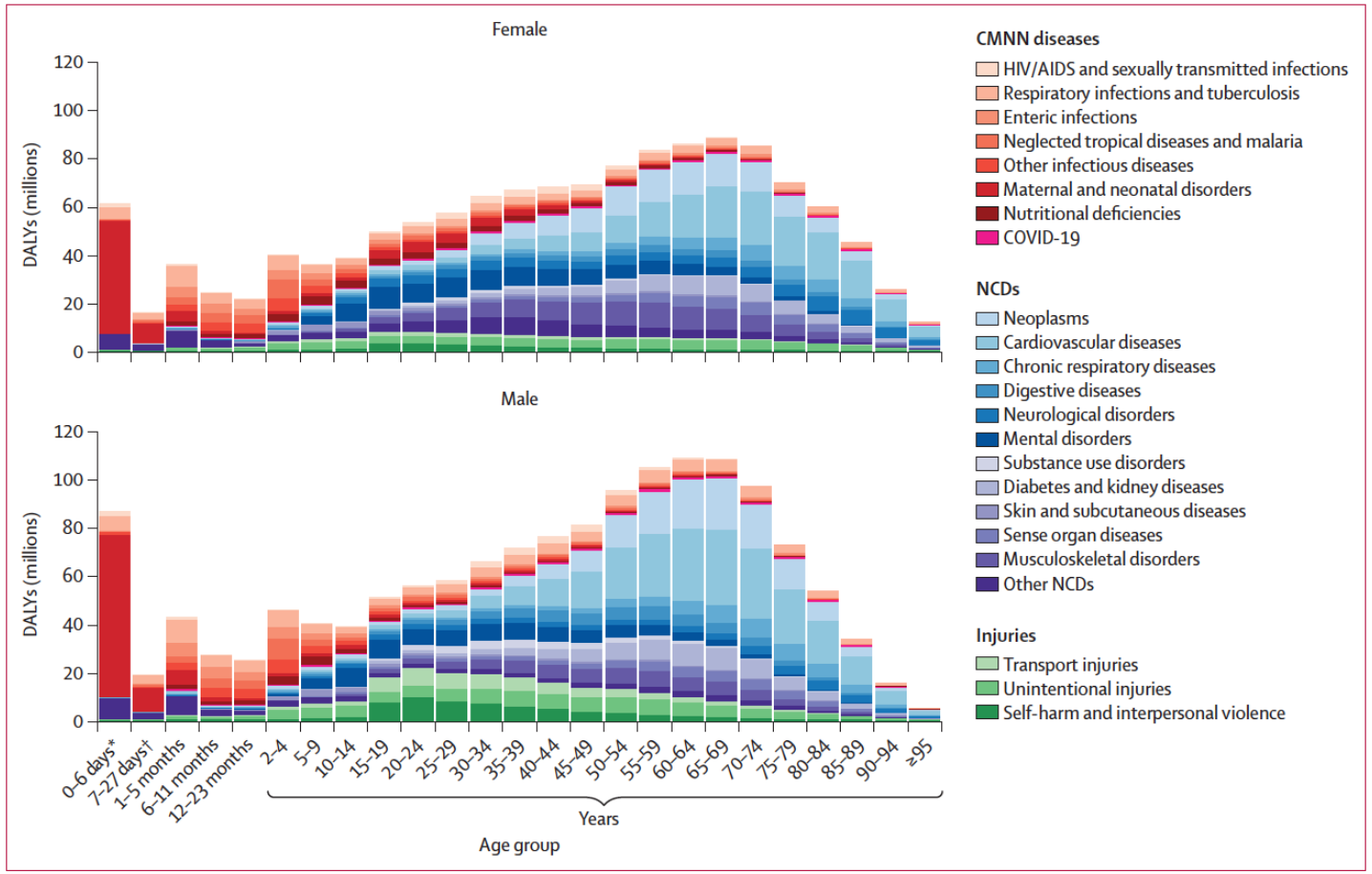

Figure 2: **The distribution of global DALYs across age and sex for GBD level 2 causes in 2023**

CMNN=communicable, maternal, neonatal, and nutritional. DALYs=disability-adjusted life-years. GBD=Global Burden of Diseases, Injuries, and Risk Factors Study. NCDs=non-communicable diseases. *Early neonatal. †Late neonatal.

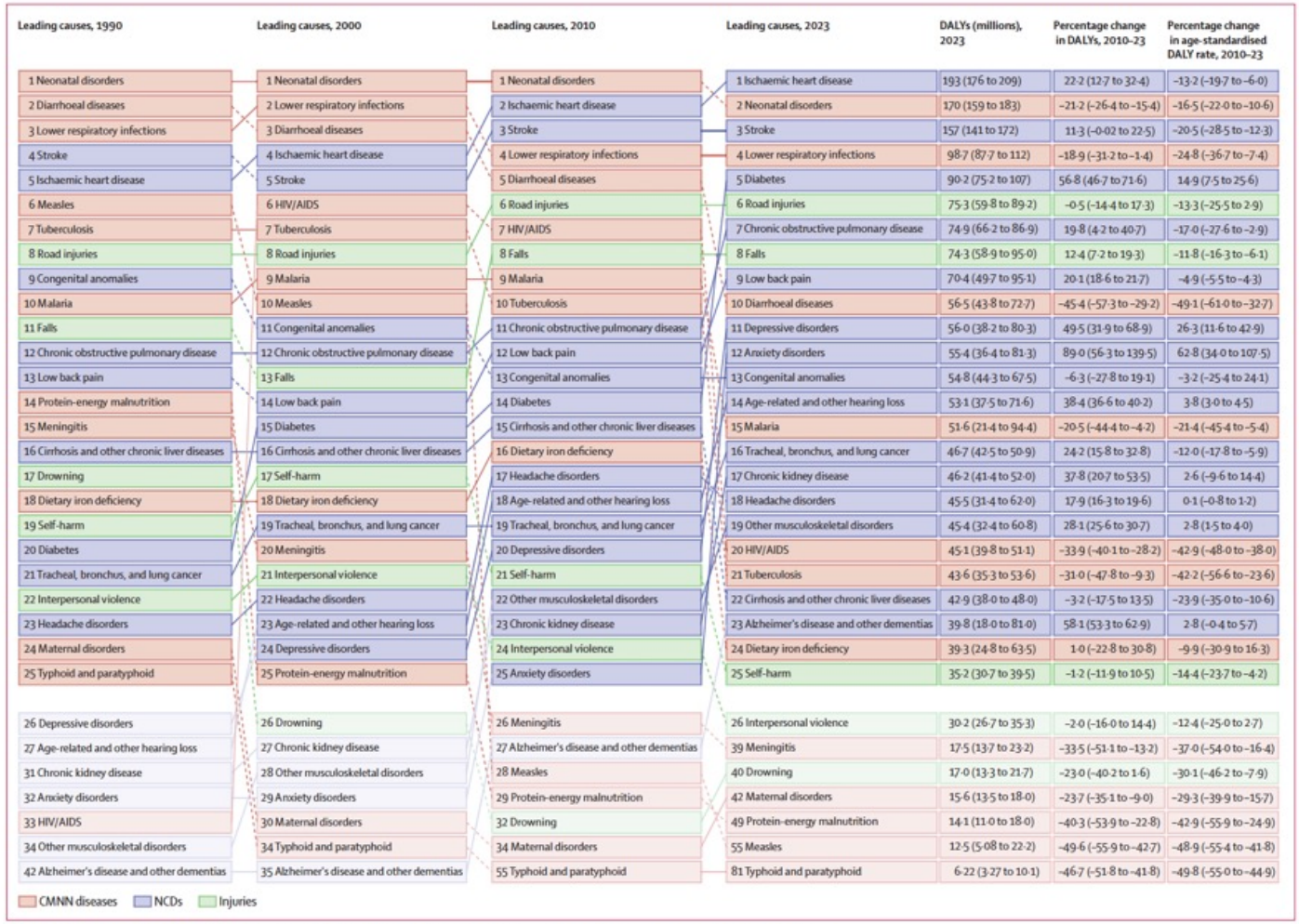

Figure 3: **Leading 25 GBD level 3 causes of global DALYs in 1990, 2000, 2010, and 2023, for both sexes combined, and all ages**

Causes are connected by lines between time periods: solid lines represent an increase or no change in rank, and dashed lines represent a decrease in rank. Faded colours indicate that the cause is not within the top 25 causes of DALYs for that year. Data in parentheses are 95% uncertainty intervals. DALY=disability-adjusted life-year. GBD=Global Burden of Diseases, Injuries, and Risk Factors Study.

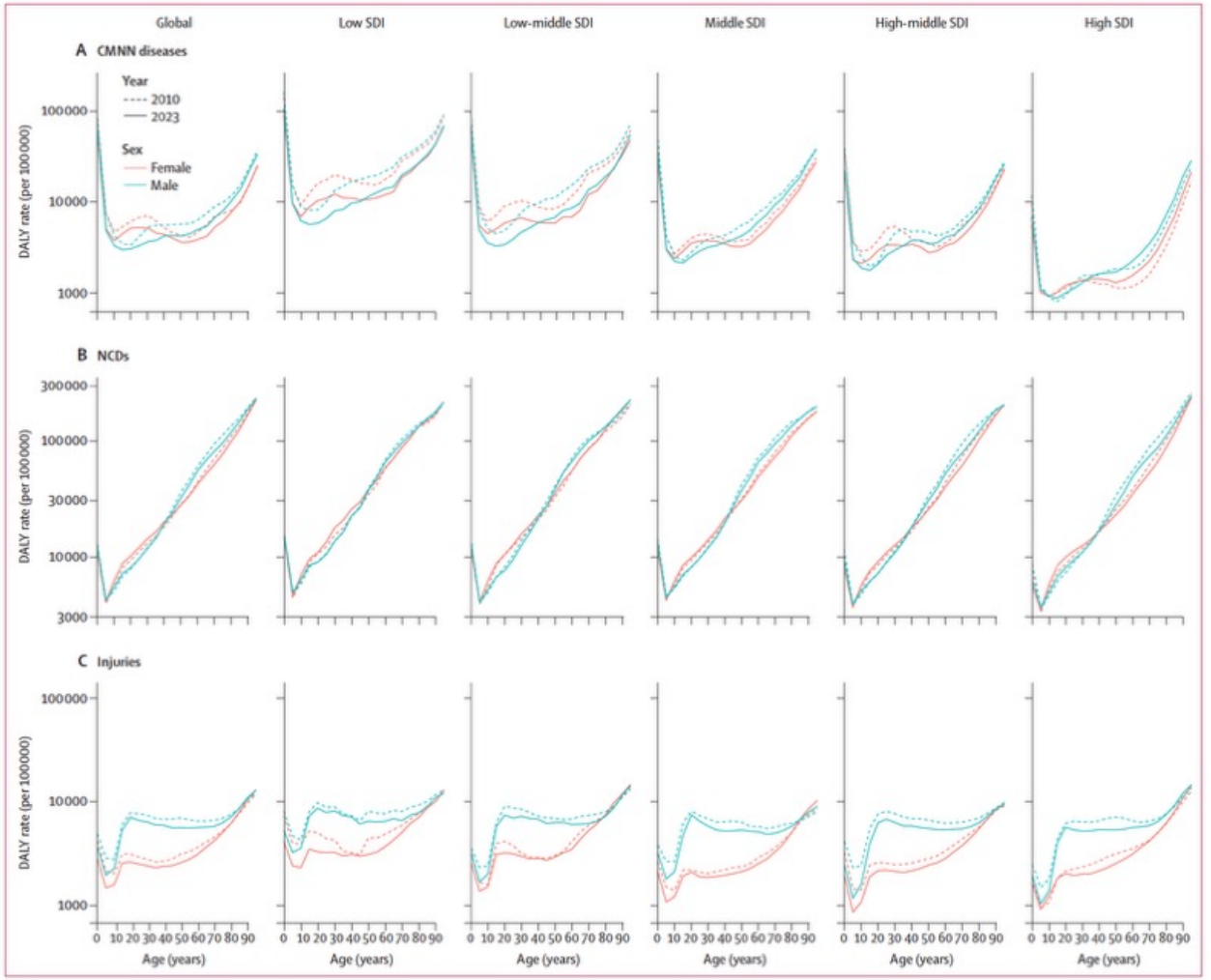

Figure 4: **Age-specific DALY rates for CMNN diseases (A), NCDs (B), and injuries (C), by age, sex, year, and SDI quintile**
The y axis shows DALYs per 100 000 person-years on a logarithmic scale. CMNN=communicable, maternal, neonatal, and nutritional. DALY=disability-adjusted life-year. GBD=Global Burden of Diseases, Injuries, and Risk Factors Study. NCDs=non-communicable diseases. SDI=Socio-demographic Index.

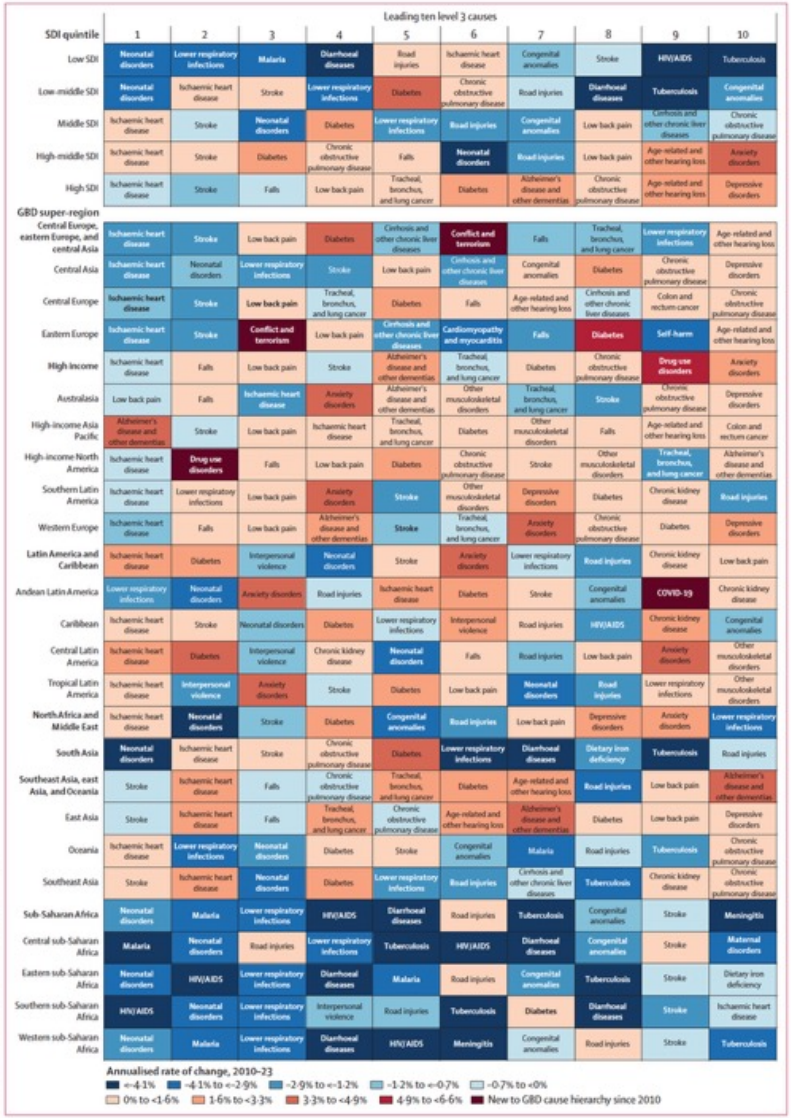

Figure 5: Leading ten GBD level 3 causes of 2023 DALYs by SDI quintile, GBD region and super-region, and annualised rate of change between 2010 and 2023
Level 3 causes are ranked by 2023 DALY counts from left (first) to right (tenth) for each GBD region and SDI quintile, with GBD super-regions in bold. DALY=disability-adjusted life-year. GBD=Global Burden of Diseases, Injuries, and Risk Factors Study. SDI=Socio-demographic Index.

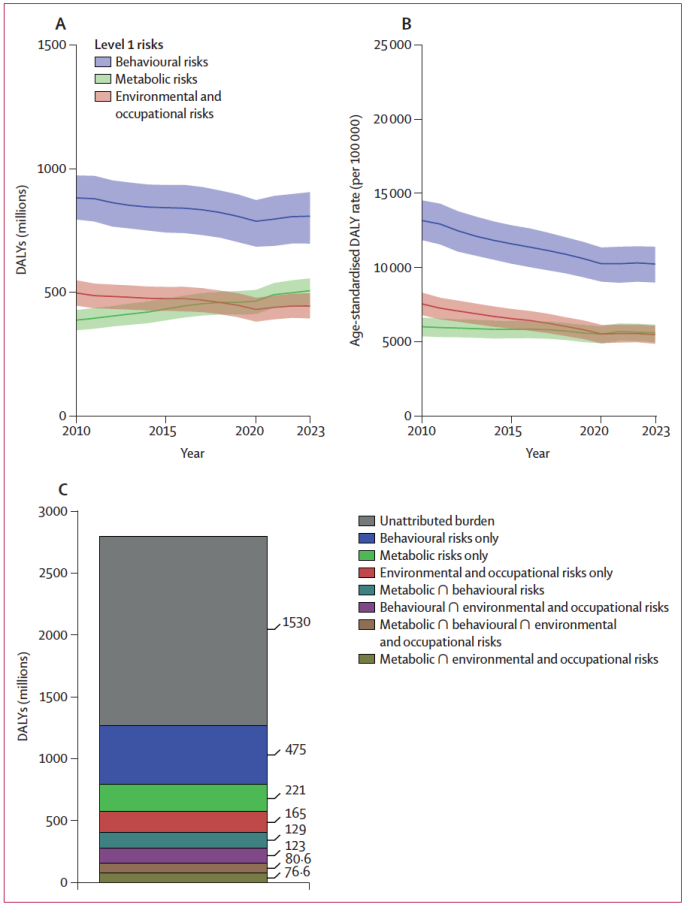

Figure 6: Global DALYs attributable to GBD level 1 risk factors
(A) Global DALY counts attributable to level 1 risks, 2010–23. (B) Age-standardised DALY rates attributable to level 1 risks, 2010–23. (C) Global total DALY counts unattributed or attributable to level 1 risk factors, 2023. Mean estimates by level 1 risk factor in panels A and B are represented by coloured lines; the shading indicates 95% uncertainty intervals. For panel C, ∩ refers to a burden that is attributed to two or all three level 1 risk factors (ie, the intersecting set of DALYs that belong to both or all three risk factors). Mean estimates in panels A and B are aggregated to include all DALYs attributable exclusively to the specific level 1 risk factor plus those attributable to the intersection of that risk and one or both of the other level 1 risk factors (ie, for a single year, the DALY counts combined across the three lines sum to more than the total number of attributable DALYs for that year). In GBD 2023, 45·6% of total global DALYs were attributable to risk factors (appendix 3 table S13). DALY=disability-adjusted life-year. GBD=Global Burden of Diseases, Injuries, and Risk Factors Study.

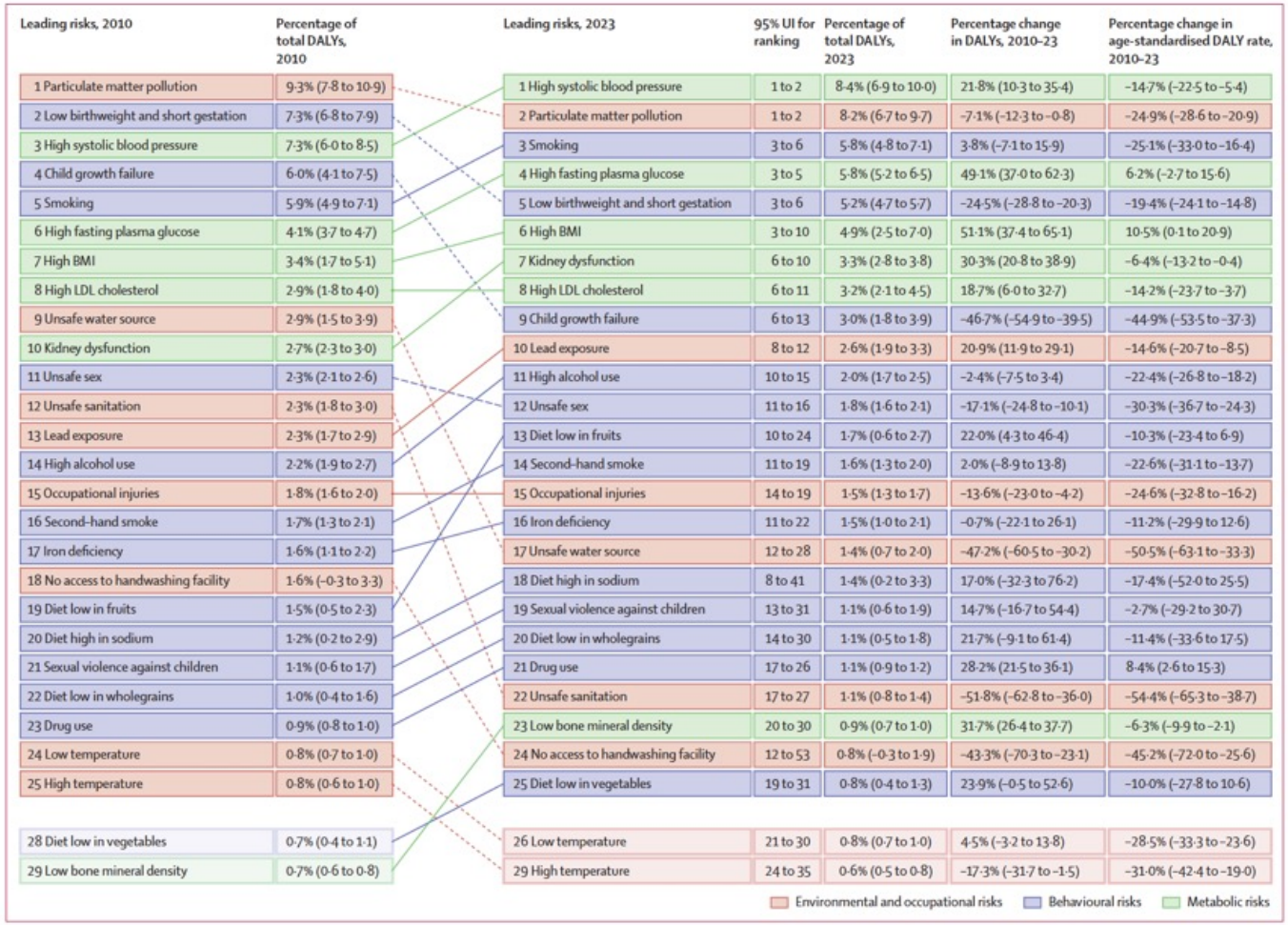

Figure 7: **Leading 25 GBD level 3 risk factors by attributable DALYs as a percentage of total DALY counts (2010 and 2023), and percentage change in attributable DALY counts and age-standardised DALY rates from 2010 to 2023**

Each column displays the top 25 risks in descending order for the specified year. Risk factors are connected by lines between time periods; solid lines represent an increase or lateral shift in ranking, and dashed lines represent a decrease in rank. Faded colours indicate that the cause is not within the top 25 causes of DALYs for that year. Data in parentheses are 95% UIs. DALY=disability-adjusted life-year. GBD=Global Burden of Diseases, Injuries, and Risk Factors Study. UI=uncertainty interval.

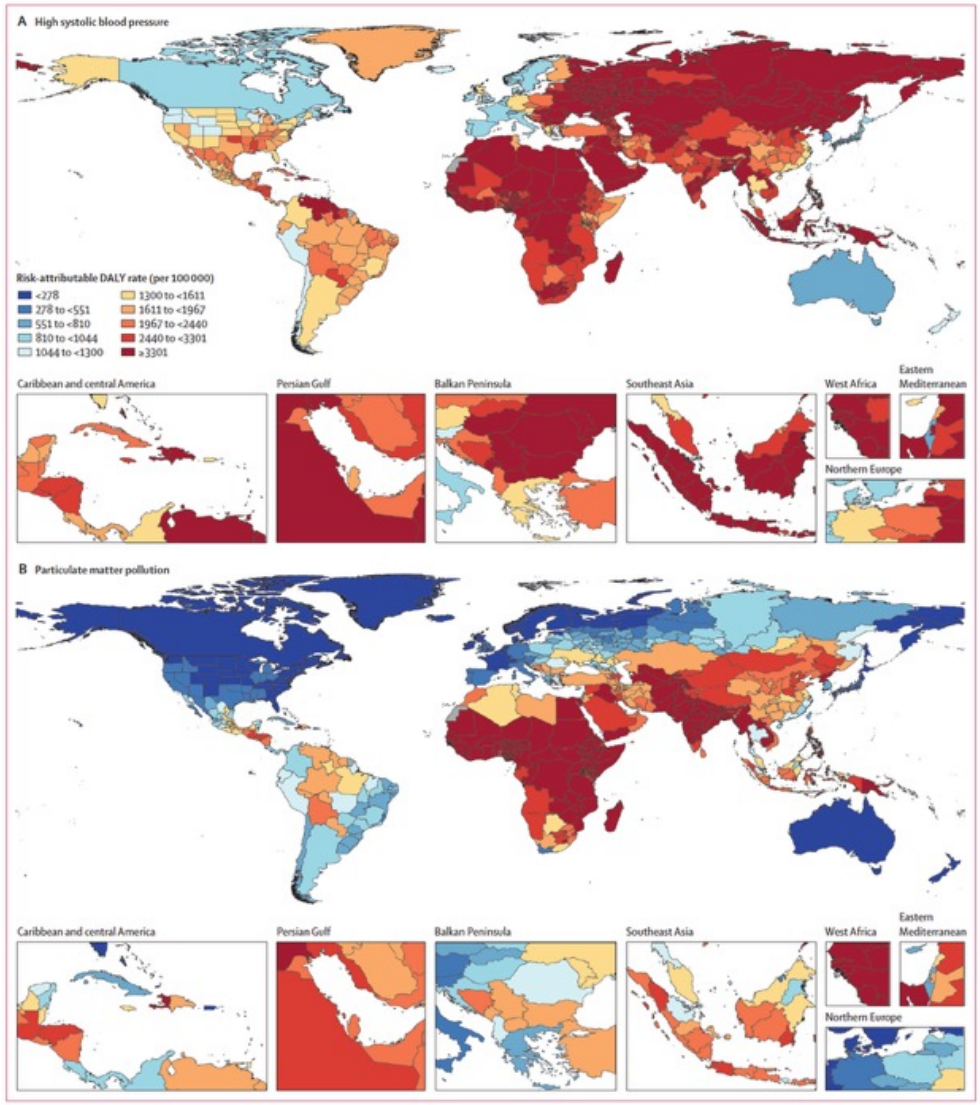

(Figure 8 continues on next page)

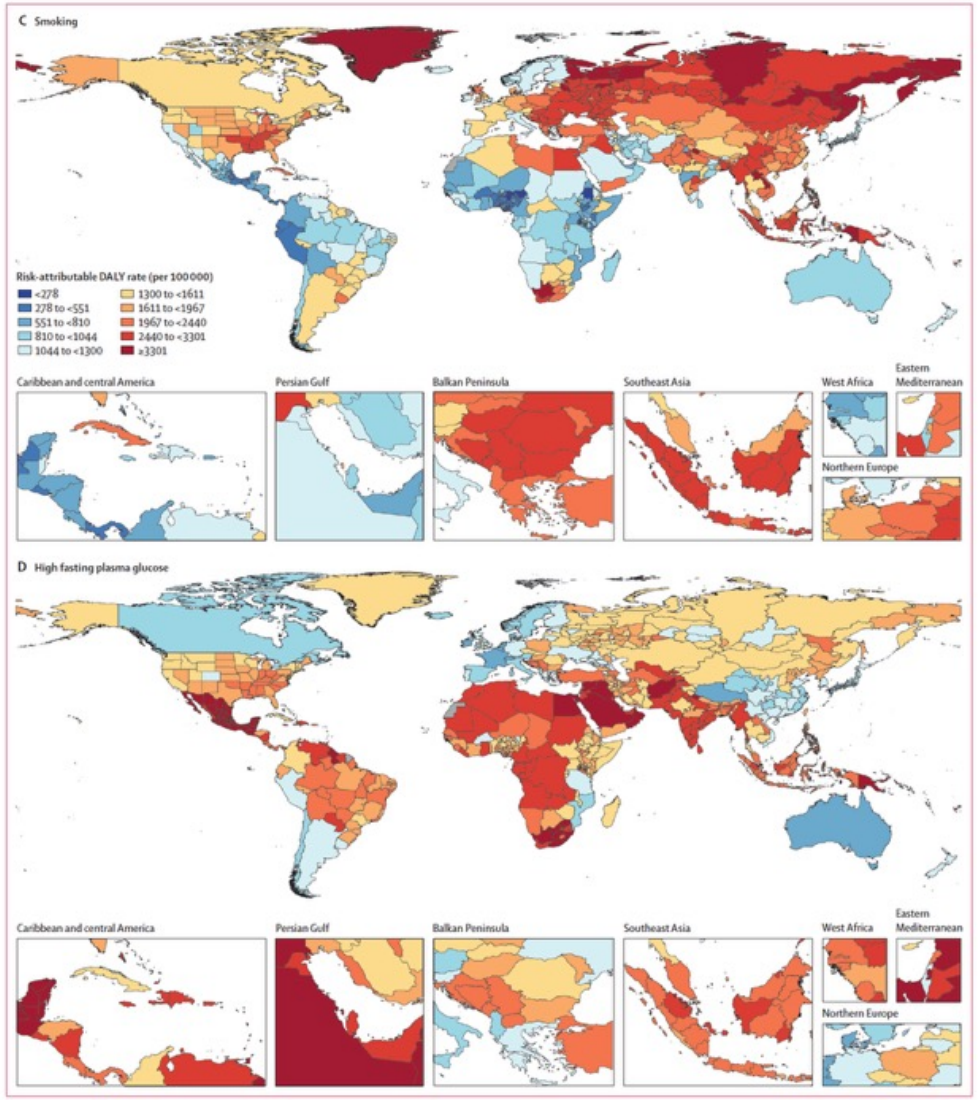

(Figure 8 continues on next page)

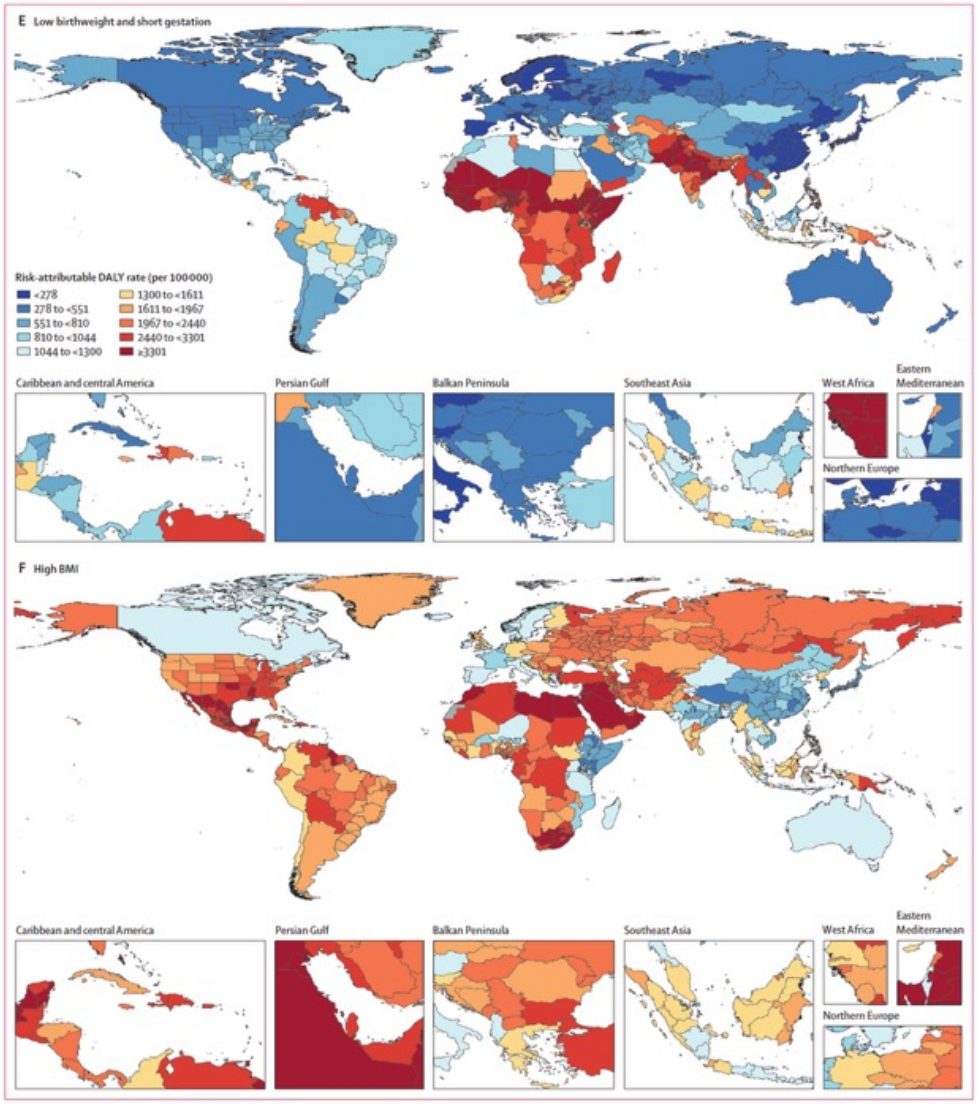

(Figure 8 continues on next page)

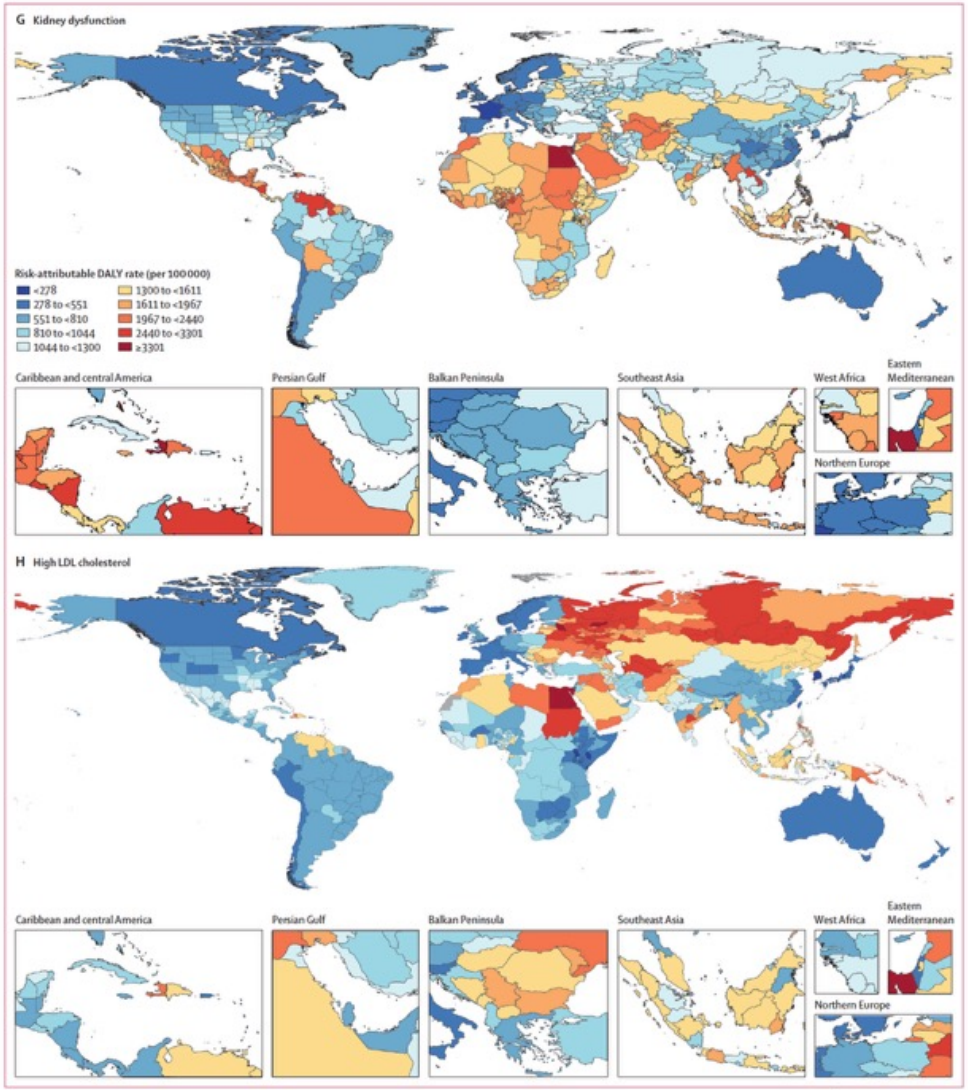

(Figure 8 continues on next page)

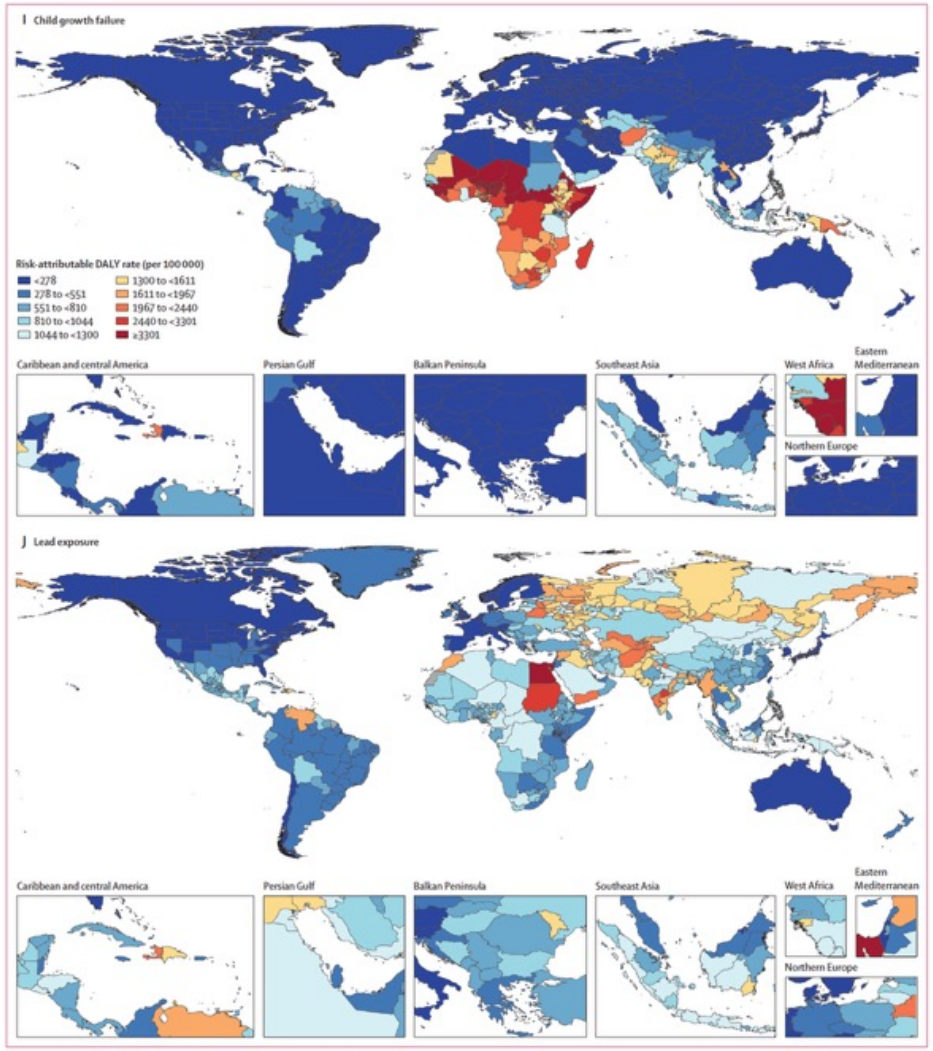

Figure 8: **Age-standardised DALY rate attributable to the ten leading GBD level 3 risk factors, ranked by percentage of total DALY counts, by location, 2023**
High systolic blood pressure (A), particulate matter pollution (B), smoking (C), high fasting plasma glucose (D), low birthweight and short gestation (E), high BMI (F), high LDL cholesterol (G), kidney dysfunction (H) child growth failure (I), and lead exposure (J). Dotted lines indicate disputed territories. DALY=disability-adjusted life-year. GBD=Global Burden of Diseases, Injuries, and Risk Factors Study.

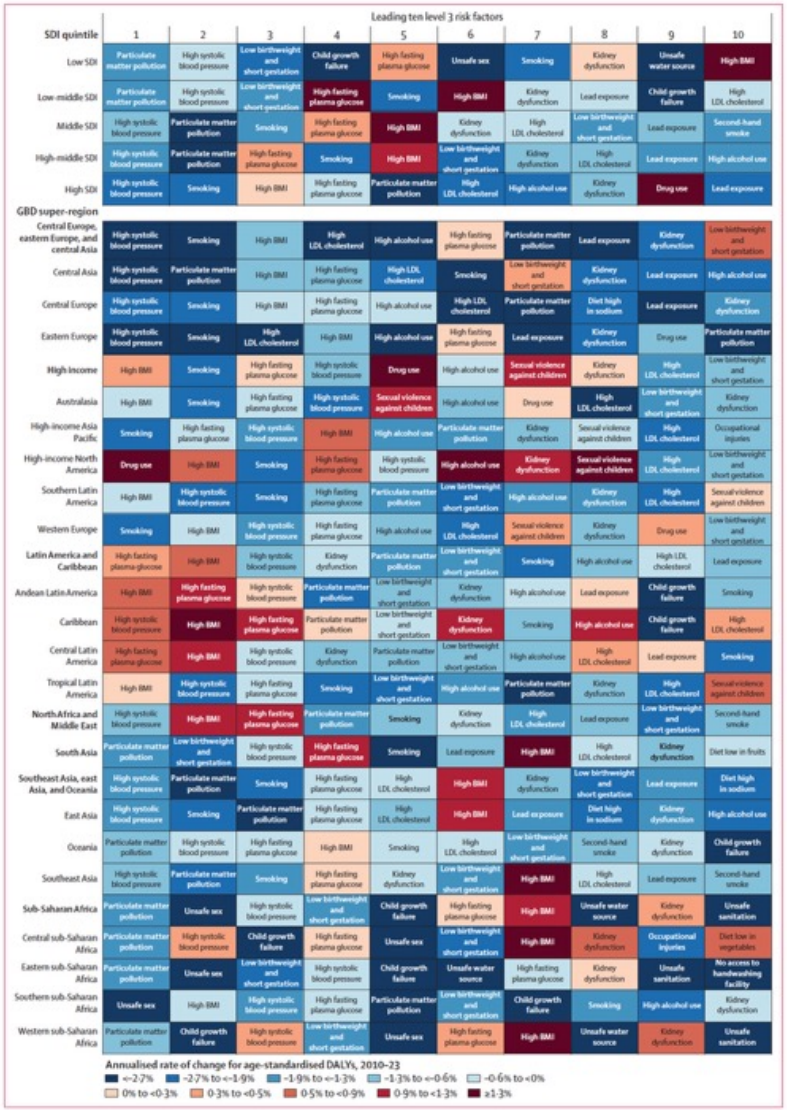

Figure 9: **Leading ten GBD level 3 risk factors for 2023 attributable age-standardised DALY rates by SDI quintile, GBD region and super-region, and annualised rate of change between 2010 and 2023**

For each region and super-region (in bold) and SDI quintile, level 3 risk factors are ranked by attributable age-standardised DALY rates from left (first) to right (tenth). DALY=disability-adjusted life-year. GBD=Global Burden of Diseases, Injuries, and Risk Factors Study. SDI=Socio-demographic Index.

Figure 10: **Annualised rate of change in age-standardised risk-attributable DALY rates by GBD level 1 risk, SDI quintile, and country or territory, 2010–23**
The black dashed lines depict the linear regression line. Country and territory points are categorised by GBD super-region. Selected countries and territories are labelled by International Organization for Standardization 3 codes. AFG=Afghanistan. AGO=Angola. ARM=Armenia. BFA=Burkina Faso. CAF=Central African Republic. CAN=Canada. CIV=Côte D'Ivoire. DOM=Dominican Republic. GBD=Global Burden of Diseases, Injuries, and Risk Factors Study. GMB=The Gambia. GUM=Guam. HTI=Haiti. KAZ=Kazakhstan. KGZ=Kyrgyzstan. LBN=Lebanon. LBY=Libya. MNG=Mongolia. NER=Niger. SDI=Socio-demographic Index. SLB=Solomon Islands. SOM=Somalia. SSD=South Sudan. SWZ=Eswatini. VEN=Venezuela. ZAF=South Africa. ZWE=Zimbabwe.

Research in context

Evidence before this study

Since its inception in the early 1990s, the Global Burden of Diseases, Injuries, and Risk Factors Study (GBD) has systematically quantified health and health loss across time, age, sex, location, and sociodemographic groups. GBD introduced and uses disability-adjusted life-years (DALYs) as a measure of disease burden that captures disability and premature mortality. DALYs have been widely adopted by WHO, the UN, and public health agencies to measure overall disease burden in a population. Previous research efforts, including WHO World Health Statistics and initiatives such as the NCD Risk Factor Collaboration and the Prospective Urban and Rural Epidemiological (PURE) study, have advanced understanding of specific diseases or risk factors and, like GBD, are continuously updated, making it possible to track progress towards the UN Sustainable Development Goals. GBD stands out for its comprehensive scope, wealth of data, and rigorous methodological provenance and updates, as well as its global coverage and commitment to reporting scientific findings free of political bias and the influence of special interests.

Added value of this study

GBD 2023 analysed 375 diseases and injuries and 88 modifiable risk factors, providing updated estimates of prevalence, incidence, years lived with disability (YLDs), years of life lost (YLLs), DALYs, and risk-attributable DALYs for 204 countries and territories from 1990 to 2023. Our estimates of burden improved on those from GBD 2021 by the inclusion of data from more than 35 000 new sources, with particularly notable increases in data used to estimate the burden of diseases such as ischaemic heart disease, chronic obstructive pulmonary disease, and tuberculosis. Analyses were extended to five new causes: ulcerative colitis; Crohn's disease; thyroid diseases; other endocrine, metabolic, blood, and immune disorders; and electrocution. "Other pandemic-related outcomes" was removed as a cause. Additionally, we began to transition our primary tool to model prevalence from disease modelling meta-regression version 2.1 (DisMod-MR 2.1) to disease modelling age-time (DisMod-AT), which more effectively captures temporal trends in data. GBD 2023 advanced risk factor analyses from previous GBD cycles, strengthening attributable burden estimates by conducting 85 new or updated systematic reviews and incorporating additional data from more than 16 000 new sources, particularly for intimate partner violence, lead exposure, high BMI, and high fasting plasma glucose. Based on new evidence or further specification of outcomes or mediation factors, 50 new risk–outcome pairs, such as the relationship between particulate matter pollution and dementia, were analysed; two pairs were excluded (child wasting and malaria, and high alcohol use and nasopharynx cancer) for not meeting inclusion criteria or for overlapping with other outcomes. In total, 676 risk–outcome pairs were analysed for GBD 2023. Methods were updated for specific risk factors, notably regarding estimation of burden attributable to lead exposure and revision of the theoretical minimum risk exposure level for diet high in trans fatty acids.

Implications of all the available evidence

This study reaffirms that the global epidemiological transition has continued up to 2023. Although the COVID-19 pandemic temporarily disrupted health trends, the long-term decline in burden due to communicable, maternal, neonatal, and nutritional (CMNN) diseases has continued, whereas absolute burden of NCDs has risen sharply, largely due to demographic changes. It is an opportune time to revisit these two patterns at the highest policy levels. First, acknowledging and celebrating the staggering success of reducing the impact of CMNN diseases worldwide is important, alongside warnings that progress is fragile. The threats of stagnation or resurgence do not recede simply because our global policy focus might shift. Second, there is an opportunity to make substantial progress in reducing the burden of NCDs across sociodemographic strata. Since our present analyses show that almost half of total disease burden is attributable to specific modifiable risk factors—with increasing contributions, especially in ageing populations, of metabolic risks (eg, high systolic blood pressure, smoking, lead exposure, and ambient particulate matter air pollution)—considerable progress can be made by addressing risk-attributable burden, although successful mitigation varies substantially across risk factors. Equitable scaling of implementation remains a challenge, requiring coordinated policy efforts, targeted prevention strategies, and strengthened health-care systems to mitigate disparities and improve population health outcomes.

Metal-Organic Frameworks (MOFs) are crystalline materials composed of metal ions or clusters connected by organic linker molecules, forming highly porous, three-dimensional structures. Their porous nature and huge surface area make them ideal for applications like gas storage, separation, catalysis, and drug delivery. By changing the metal and organic linker components, scientists can tune the pore size and properties to create a vast array of different MOFs with specialized functions.

Structure:

MOFs are hybrid materials made of inorganic "secondary building units" (metal clusters) connected to organic "linkers" (like carboxylates) to form extended networks.

Properties:

They are highly porous, have a very large surface area, and their pore size and shape can be adjusted.

Applications:

MOFs are used in a wide range of fields, including:

- **Gas storage**: Storing gases like hydrogen or methane.
- **Separation**: Separating different gases or liquids.
- **Catalysis**: Acting as catalysts for chemical reactions.
- **Sensing**: Detecting specific substances.
- **Drug delivery**: Delivering drugs within the body.

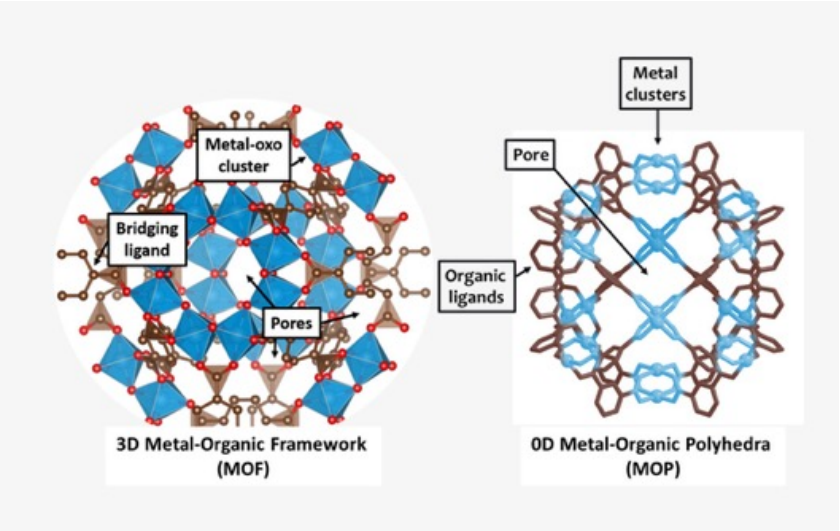

Architects of molecular cages win Chemistry Nobel

As early as the 18th century, people knew the pigment Prussian Blue had the mysterious ability to absorb and hold water. Its structure, deciphered much later, showed the compound was, in fact, a molecular cage: a cubic arrangement of iron ions joined by nitrile groups (carbon and nitrogen linked by a triple bond).

This year's Nobel Prize in Chemistry has gone to three researchers who pioneered modern versions of these porous structures by using organic molecules as struts to link up metal atoms. The Nobel-winning work, by Susumu Kitagawa of Kyoto University, Richard Robson of the University of Melbourne, and Omar Yaghi of the University of California (UC), Berkeley, led to metal-organic frameworks (MOFs) with large voids tailored to trap specific molecules, making them useful for storing gases such as hydrogen and methane, or soaking up water vapor or carbon dioxide out of the air. Some believe they even have the potential to deliver drugs or catalyze reactions.

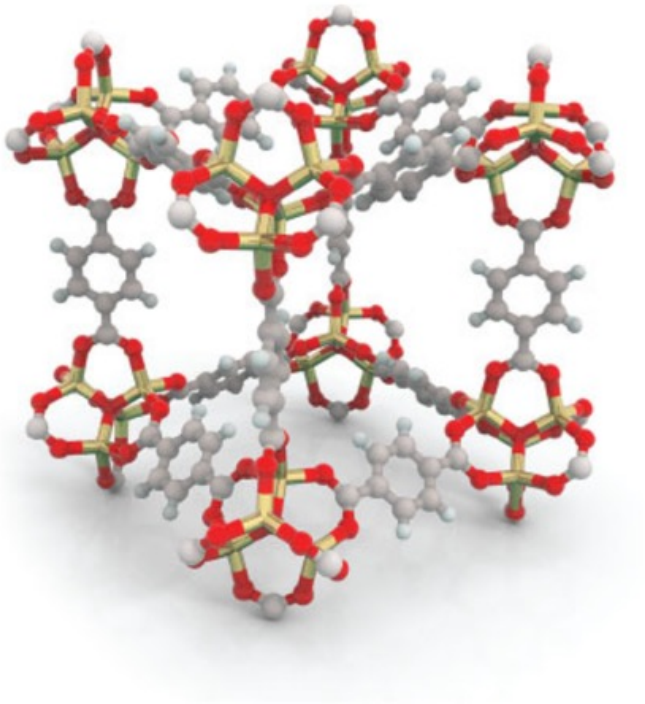

A couple grams of the material MOF-5 have the surface area of a football field. IMAGE: RAMON ANDRADE 3DCIENCIA/SCIENCE PHOTO LIBRARY

The initial breakthrough came from Robson in the 1980s. He created a tetrahedral molecule using nitrile groups to link up copper ions at each of the four vertices. Moreover, he was able to stack these molecules into a repeating crystalline structure with large cavities. “It was just amazing imagination that he had to devise, in fairly simple terms, this way of making his new class of materials,” says Brendan Abrahams, a longtime collaborator of Robson’s at Melbourne.

Robson's material was quite fragile and prone to collapse. But Kitagawa saw the potential. In the 1990s, despite meager funding, he made a thin 2D structure that could hold acetone molecules in its cavities. In 1997, he and his team succeeded in making a 3D crystal with cobalt, nickel, or zinc ions as the hubs. It was threaded with open channels, enabling it to absorb and release methane, nitrogen, and oxygen. And it was stable. "At first, everyone thought such structures would fall apart immediately—that was common sense," Kitagawa said last week at a press conference organized by Kyoto University. "But we proved that stable, robust frameworks could, in fact, be built this way.

In 1999, Yaghi, then at the University of Illinois Urbana-Champaign, revealed the work that would cement the status of metal-organic frameworks. Instead of linking up ions, Yaghi and his team used more complex metal clusters as the hubs. Their iconic material, known as MOF-5, was a cubic lattice with huge cavities. A couple grams of the material have the surface area of a football field.

WINNERS

SUSUMU KITAGAWA, Kyoto University

RICHARD ROBSON, University of Melbourne

OMAR YAGHI, University of California, Berkeley

The researchers also showed they could tailor the voids and their properties. By using longer or shorter organic linkers and exposing metal ions in the pore spaces, they could tune the materials to attract specific gases at mild pressures and release them as the pressure drops. The number of design possibilities is immense, Yaghi said last week at a press conference organized by UC Berkeley. “If you think it, you can make it.”

Today, researchers have conjured up tens of thousands of kinds of metal-organic frameworks, and dozens of companies are trying to commercialize their use. They have “huge importance for humanity,” says Wendy Lee Queen, an inorganic chemist at the Swiss Federal Institute of Technology, Lausanne.

Some companies are trying to use them to store methane fuels for cars, whereas others see potential for trapping hydrogen, a clean fuel that otherwise requires high pressures, cold temperatures, or large volumes to store.

Another application is to use the selectivity of the materials as a filter to soak up particular compounds. Yaghi’s group has spun off companies developing metal-organic frameworks to pull pure water out of thin air—even in desert environments. Other companies are testing the materials to extract carbon dioxide from industrial processes and power plants to reduce greenhouse gas emissions.

The materials could also be used to sequester toxic wastes—or simply to identify when they are present. Jing Li, an inorganic and materials chemist at Rutgers University, has experimented with using metalorganic frameworks to detect explosives and toxic vapors. Now, she is developing some that can separate mixes of hydrocarbons into various petrochemical products. Metalorganic frameworks could be more efficient than traditional approaches such as distillation, she says. “There has been tremendous progress.”

In theory, metal-organic frameworks could even be used as catalysts: Reagents could be implanted in the cavities, and reactions could progress through different steps as compounds pass through the corridors of the material. At the Kyoto press conference, Kitagawa said his dream was to use the materials not just to separate and capture the components of air—nitrogen, oxygen, water vapor, and carbon dioxide—but to convert them into useful products. “From these simple elements—C, H, O, N—we make proteins, food, and fuels,” he said. “Air, in that sense, is ‘invisible gold.’”

4 vaccines linked to a lower risk of dementia

The flu shot

An estimated 47 million to 82 million people in the United States — about 13 to 24 percent of all people — caught influenza, or the flu,

The shingles vaccine

The shingles vaccine has the strongest evidence for reducing the risk of dementia with multiple large-scale studies in the past two years corroborating the results of older studies.

The RSV vaccine

Respiratory syncytial virus, or RSV, is a common respiratory virus that can cause mild, cold-like symptoms in most people, but may cause severe infections in children as well as adults ages 65 and older. (The virus is the leading cause of hospitalization among American infants and causes an estimated 100 to 300 deaths in children under 5, and 6,000 to 10,000 deaths in people 65 or older, every year in the U.S.)

The Tdap vaccine

Several studies have reported that the vaccine against tetanus, diphtheria and pertussis (or whooping cough), or Tdap, is associated with a reduced risk of dementia.